Regulation of CFTR function and stability by phosphorylation and its membrane environment

by

Stephanie Chin

A thesis submitted in conformity with the requirements
for the degree of Doctor of Philosophy

Department of Biochemistry
University of Toronto

Regulation of CFTR function and stability by phosphorylation and its membrane environment

Stephanie Chin

Doctor of Philosophy

Department of Biochemistry
University of Toronto

2019

Abstract

Cystic Fibrosis is caused by mutations of the gene that codes for Cystic Fibrosis Transmembrane conductance Regulator (CFTR), an ATP-Binding Cassette anion channel. The major disease-causing mutation, deletion of phenylalanine at position 508 (F508del), results in misfolding, mistrafficking and loss of CFTR at the cell surface where CFTR normally functions to maintain proper hydration of epithelia. Protein kinase A (PKA) phosphorylation enhances CFTR function at the cell surface. However, not much is known regarding the structural consequences of full-length CFTR upon PKA phosphorylation. Towards this, I developed biophysical methods to study purified full-length CFTR and showed that PKA phosphorylation modifies its overall structure, possibly at the transmission interface between coupling helices and nucleotide binding domains. Channel function studies with disease-causing mutations at the transmission interface further support the role of transmission interface interactions for phosphorylation-mediated channel gating. Recent structural studies have found that PKA phosphorylation causes subtle changes in zebrafish CFTR structure. However, the channel remains closed. We propose that this may be due to the detergent environment of the protein. We developed a novel purification method that maintained CFTR: lipid interactions. We conducted ATPase and iodide efflux assays to show that purified CFTR associated with lipids resulted in significantly higher CFTR activity

than purified CFTR in detergent micelles. These experiments suggest involvement of lipids in regulating CFTR function. Potentiator drugs, like ivacaftor, enhance CFTR function at the cell surface. I conducted biochemical experiments to find that high concentrations of ivacaftor non-specifically destabilized F508del-CFTR and other membrane proteins. This non-specific destabilization of ivacaftor appears to be associated with its lipophilicity which disrupts the membrane. This further highlights the importance of lipids for stabilizing and modifying CFTR function in the lipid bilayer. In summary, CFTR function and stability are regulated by PKA phosphorylation and lipids of the membrane environment of CFTR.

Acknowledgments

Throughout my PhD journey, I am extremely fortunate to have met the many individuals listed below. Thank you so much for your guidance, support and positive energy throughout the years! I wish you all the best in your future endeavours!

Firstly, I would like to thank my supervisor, Dr. Christine Bear, for the many years of supervision that has helped me grow as a scientist. You were an amazing supervisor and it was a pleasure working in your laboratory to discover new things about the challenging CFTR protein. Your enthusiasm for science is infectious and has motivated me to work harder and smarter. Thank you for the many helpful scientific discussions on interpreting results and troubleshooting experiments. Thank you also for your readiness to help me with manuscripts, grant applications and job applications. Good luck with your journalism course and I look forward to reading and/or watching great things from you! Take care and don't forget to relax once in a while!

I would like to thank my supervisory committee members, Dr. Trevor Moraes and Dr. Oliver Ernst, for their suggestions, engaging questions and help throughout the years.

I am grateful that I had the privilege of working with Dr. Mohabir Ramjeesingh. I have learned a lot from you! I would like to thank you for all of your contributions and troubleshooting ideas throughout my research. Your wisdom and calm exterior have been instrumental for helping me to effectively deal with the obstacles in my life.

I would like to thank my really good friend and colleague, Yu-Sheng (Wilson) Wu. During the last two to three years of my PhD, you have helped me so much with readily offering to conduct experiments and tasks in the lab and offering me snacks when I'm extremely stressed and tired. Outside of the lab, I am also thankful for the enjoyable and funny moments that we have had! I'm glad that I have met you and I know that our friendship will last a really long time in which I will attempt to repay you back for your kindness. Thank you for all of the encouragement and motivation throughout the years. I know that you will have an awesome future ahead of you!

Next, I would like to thank another good friend and colleague, Maurita Hung, for her help and support over the years. Thank you for all of your illustrations for the presentations and

Table of Contents

List of Tables

List of Figures

List of Abbreviations

$\Delta\varepsilon$	Delta Epsilon
λ_{max}	Emission Wavelength Maxima
3D	Three-dimensional
ABC	ATP-Binding Cassette
AMPK	Adenosine Monophosphate-activated Protein Kinase
ATP	Adenosine triphosphate
B-factor	Temperature Factor
BMOE	Bismaleimidoethane
BtuCD	*Escherichia coli* vitamin B_{12} ABC transporter
cAMP	cyclic Adenosine Monophosphate
CF	Cystic Fibrosis
CFBE	CF Bronchial Epithelial
CFTR	Cystic Fibrosis Transmembrane conductance Regulator
CFTR$_{inh}$-172	CFTR specific inhibitor
CH	Coupling Helix
chCFTR	Chicken CFTR
CK2	Casein Kinase 2
C$_m$	Midpoint urea concentration
CNX	Calnexin
COP	Coat Protein
CRE	cAMP Response Element
Cryo-EM	Cryo-Electron Microscopy
C-terminal	carboxyl-terminal
Cys-less	CFTR variant lacking native cysteine residues
DDM	n-Dodecyl β-D-Maltoside
EC$_{50}$	Half maximal effective concentration
ECL	Extracellular Loop
ER	Endoplasmic Reticulum
ERAD	ER-Associated Degradation
F508del	Deletion of Phenylalanine at position 508
FDA	Food and Drug Administration
FEV$_1$	Forced Expiratory Volume in 1 second
FLIPR®	Fluorescence Imaging Plate Reader
F$_{max}$	Fluorescence Maxima
G551D	Glycine to Aspartic Acid at position 551
GPCR	G Protein-Coupled Receptors
GT	GripTite
GWAS	Genome Wide Association Study
hCFTR	Human CFTR
HEK	Human Embryonic Kidney
ICL	Intracellular Loop
K$_m$	Substrate concentration at half V_{max}
K$_{sv}$	Stern-Volmer Constant
LMNG	Lauryl Maltose Neopentyl Glycol
logP	Partition Coefficient

m value	Slope of the urea denaturation curve
MD	Molecular Dynamics
MRP	Multi-Drug Resistance Protein
MS	Mass Spectrometry
MSD	Membrane Spanning Domain
NATA	N-Acetyl-L-Tryptophanamide
NBD	Nucleotide Binding Domain
NDPK	Nucleoside Diphosphate Kinase
NHERF1	Na^+/H^+ Exchanger Regulatory Factor
NMR	Nuclear Magnetic Resonance
N-terminal	amino-terminal
P-	PKA phosphorylated
PC	Phosphatidylcholine
PDB	Protein Data Bank
PDE	Phosphodiesterase
PE	Phosphatidylethanol
PKA	Protein Kinase A
PKC	Protein Kinase C
PKG	Protein Kinase G
PS	Phosphatidylserine
pTIRF	polarized Total Internal Reflection Fluorescence
Pyk2	Proline-rich Tyrosine Kinase 2
R domain	Regulatory Domain
RE	Regulatory Extension
RI	Regulatory Insertion
RT	Retention Time
Sav1866	Multidrug transporter from *Staphylococcus aureus*
SCAM	Substituted Cysteine Accessibility Mutagenesis
SDS	Sodium Dodecyl Sulfate
SEC	Size Exclusion Chromatography
Sf9	Clonal isolate of *Spodoptera frugiperda* Sf21 insect cells
SLB	Supported Lipid Bilayer
SLC	Solute Carrier
SMALP	Styrene Maleic Acid co-polymer Lipid Particle
Src	Proto-oncogene tyrosine-protein kinase
SRCD	Synchrotron Radiation Circular Dichroism
SRM-MS	Selected Reaction Monitoring Mass Spectrometry
SS	Silver Stain
TLC	Thin-Layer Chromatography
TM	Transmembrane
V_{max}	Maximum velocity
Wt	Wildtype
zCFTR	Zebrafish CFTR

Chapter 1 Introduction

Portions of this chapter have been published in the following review article.

Stephanie Chin, Maurita Hung & Christine E. Bear. Current insights into the role of PKA phosphorylation in CFTR channel activity and the pharmacological rescue of cystic fibrosis disease-causing mutants. Cell. Mol. Life Sci. 2017 Jan;74(1):57-66. doi: 10.1007/s00018-016-2388-6. (PMID: 27722768).

Contributions:

Review was written by Stephanie Chin and C.E.B. and reviewed by all authors. M.H. generated the figures in the review that corresponds to Figure 1.8, Figure 1.11, Figure 1.12 and Figure 1.14 of this chapter.

1.1   Cystic Fibrosis

Cystic Fibrosis (CF) is the most common autosomal recessive genetic disease in which 1 in 3600 Canadian newborns (Canadian CF Registry, 2016) and 70,000 people worldwide are diagnosed with CF (CF Foundation Patient Registry, 2016). CF mainly affects the Caucasian population (for approximately 93% of all incidences) with some incidences of CF occurring in other racial populations (CF Foundation Patient Registry, 2016). CF is a multi-organ disease affecting the epithelia of certain organs [1]. The major organs affected by CF and the disease phenotypes of those organs are summarized in Table 1.1

Table 1.1: Summary of major CF affected organs and their clinical manifestations.

Organ	Clinical manifestation
Lungs, nose, sinuses	Bacterial infection, inflammation, respiratory obstruction [2, 3]
Sweat gland	Increased sweat chloride [4, 5]
Liver	CF-associated liver disease, cirrhosis [6]
Pancreas	Pancreatitis [7], exocrine pancreatic insufficiency [8], CF-related diabetes [9]
Intestine	Meconium ileus at birth [10], intestinal obstruction [11]
Reproductive tract	Congenital bilateral absence of van deferens, infertility in males [12]

Recently, the median age of survival of CF patients in Canada is 53.3 years which is the highest in the world (Canadian CF Registry, 2016). Despite the high median age of survival, CF patients experience pulmonary complications which is the main cause of mortality (Canadian CF Registry, 2016). These pulmonary complications include mucus accumulation, persistent bacterial infections with *Pseudomonas aeruginosa* as the most common bacterial infection in

patients (CF Foundation Patient Registry, 2016) and inflammation in the lungs [2, 3]. These complications contribute to reduced lung function as assessed by a significantly reduced forced expiratory volume in 1 second (FEV_1) which is a clinical measure of lung function [13-15].

The main underlying cause of CF is mutations within the *Cystic Fibrosis Transmembrane conductance Regulator* (*CFTR*) gene on chromosome 7 [16-19].

1.2   Cystic Fibrosis Transmembrane conductance Regulator

The *CFTR* gene encodes for CFTR which is an anion channel of the ATP-Binding Cassette (ABC) transporter superfamily [19, 20]. The CFTR channel is expressed on the apical membranes of epithelia of the major organs as previously listed in Table 1.1 [21].

1.2.1   Structure of CFTR

CFTR is a large membrane protein consisting of 1480 amino acids. At the membrane, CFTR has two membrane spanning domains (MSDs) with each MSD containing six transmembrane segment (TM) helices; for a total of 12 TMs in CFTR. There are six extracellular loops (ECLs) and four intracellular loops (ICLs) that connect certain TMs as illustrated in Figure 1.1 [22]. CFTR also has two nucleotide binding domains (NBDs) and a unique regulatory (R) domain [22]. Recent cryo-electron microscopy (EM) studies by the Chen group have solved the first structure of CFTR to an overall resolution of 3.7 angstroms (Å) [23]. This structure was of the full-length zebrafish CFTR (zCFTR) in the dephosphorylated, ATP-free ("closed") state [23]. Applying cryo-EM, the Chen group has also solved the full-length human CFTR (hCFTR) structure in the "closed" state to an overall resolution of 3.9 Å [24] and the full-length zCFTR structure in the protein kinase A (PKA) phosphorylated, ATP-bound state to an overall resolution of 3.4 Å [25]. This group expressed their CFTR constructs in the HEK293S GnTI⁻ suspension cell system that lacks complex N-glycans, solubilized the membrane pellet with Lauryl Maltose Neopentyl Glycol (LMNG), and then exchanged the detergent to digitonin during the purification of CFTR [23-25]. Interestingly, the zCFTR and hCFTR structures have revealed that CFTR contains a novel motif which is known as the lasso motif [23]. Based on the hCFTR structure, the domain boundaries of CFTR are as follows: lasso motif (residues 5-69), MSD1 that consists of TM1-6, ICL1-2, and ECL1-3 (residues 70-390), NBD1 (residues 391-644), R domain (residues 645-844), MSD2 that consists of TM7-12, ICL3-4, and ECL4-6 (residues 845-

1172), and NBD2 (residues 1207-1436). The structural boundaries as well as the topology of TMs, ECLs, ICLs and domains of CFTR are summarized in Figure 1.1.
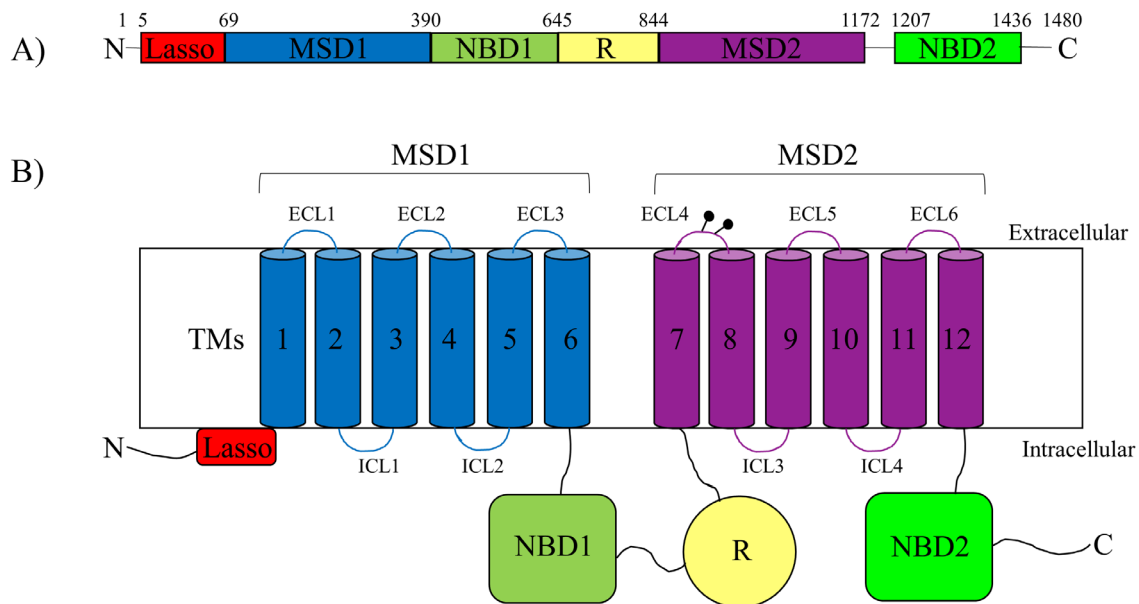
Figure 1.1: Structural boundaries and topology of hCFTR domains.
(**A**) Linear arrangement of CFTR from amino (N-) to carboxy (C-) terminal showing the amino acid residue numbers at domain boundaries based on the solved hCFTR structure in the "closed" state (PDB: 5UAK) [24]. (**B**) Schematic diagram of domain organization as well as TM, ECL and ICL topologies. The N-glycosylation sites (black circles) of ECL4 that gets glycosylated during biosynthesis of CFTR are also shown.

Based on amino acid substitution analysis and sequence alignment studies, two proteins that have a sequence conservation higher than 35-40% are most likely to be structurally similar [26, 27]. Regarding this, zCFTR has a 55% overall sequence identity to hCFTR [23]. In addition, zCFTR appeared to be functionally similar to hCFTR. zCFTR has an important role in fluid homeostasis in the gut tube development of zebrafish [28] and loss of zCFTR function resulted in pancreatic destruction in larval zebrafish which is a similar phenotype to CF-related pancreatic insufficiency [29]. Thus, it was not surprising that zCFTR resulted in a similar structure as hCFTR in the "closed" state. However, there is an additional helix that was solved in the intracellular space between TMs 9, 10 and 12 that is located between the two halves of the hCFTR structure which the Chen group claim to represent a peptide of the R domain [23, 24].

The similarities of the "closed" CFTR structures between the two species are shown in Figure 1.2.
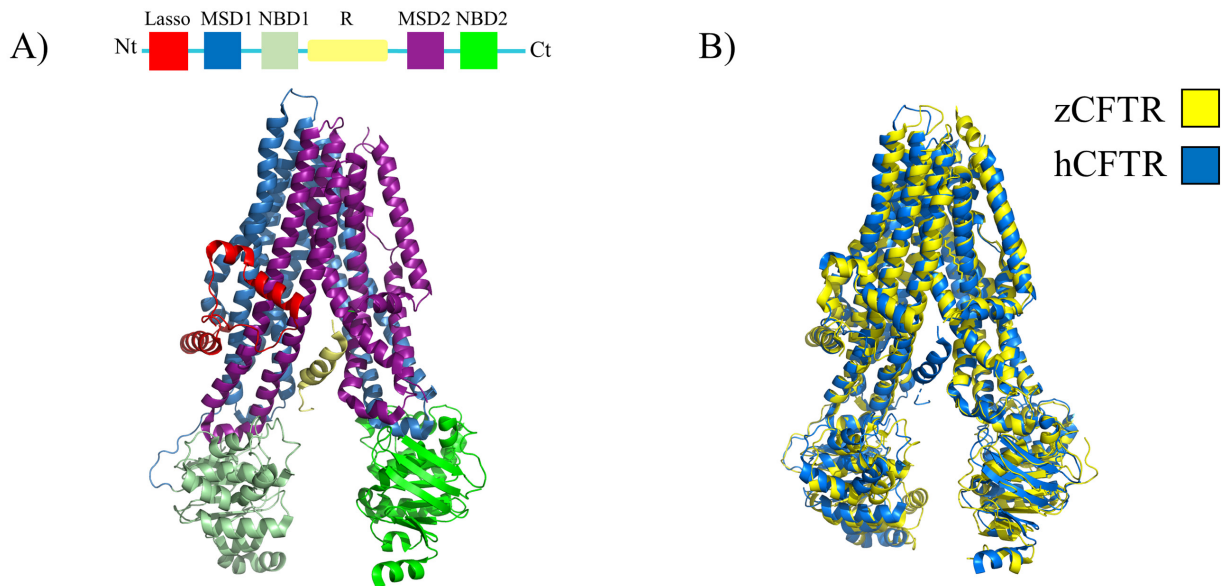
Figure 1.2: Structural comparison of CFTR structures from two species in the "closed" state which were solved by cryo-EM.
(**A**) Structure of hCFTR (PDB: 5UAK) solved by cryo-EM shows an additional helix between the MSDs that apparently represents a peptide of the R domain (yellow). (**B**) Overlaying zCFTR (yellow, PDB: 5UAR) with hCFTR (blue, PDB: 5UAK) structures shows that these two proteins are structurally similar to each other.

The three-dimensional (3D) structure of CFTR was previously generated using homology models based on a similar ABC multidrug transporter from *Staphylococcus aureus* known as Sav1866 [30-32]. Now, we have the actual 3D structures of zCFTR and hCFTR in the "closed" state as well as the structure of zCFTR in the PKA phosphorylated, ATP-bound state [23-25]. As shown in Figure 1.3, these structures, especially zCFTR in the PKA phosphorylated, ATP-bound state, resemble the 3D structure that was predicted by homology models using Sav1866 with some differences [23, 25, 30-32].
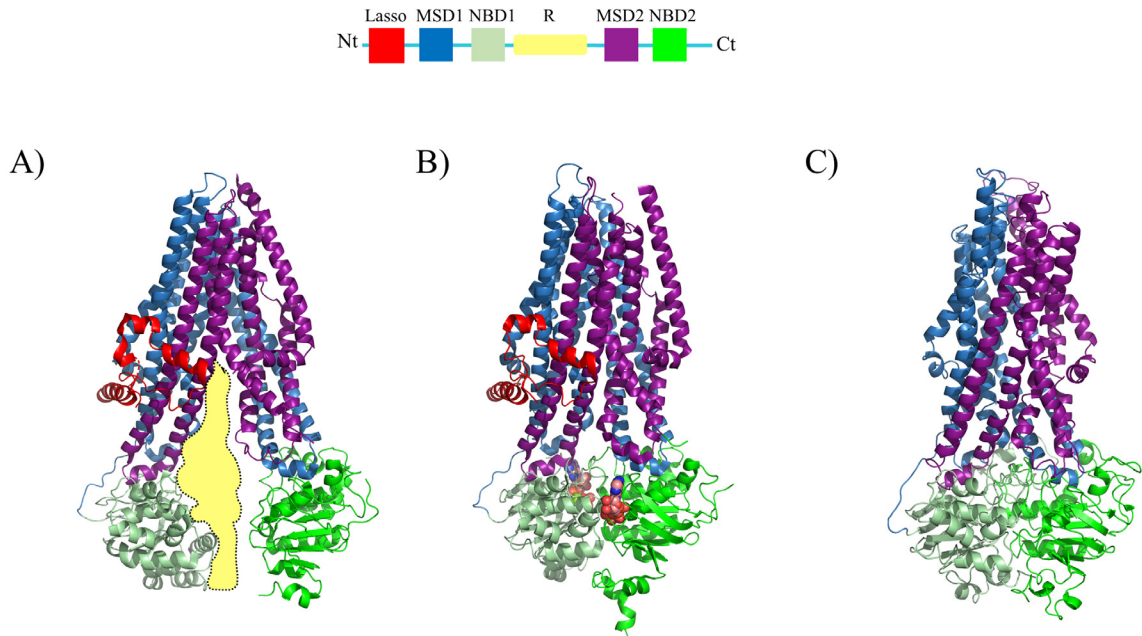
Figure 1.3: Structural comparison of zCFTR structures determined by cryo-EM to the CFTR homology model based on Sav1866.
Top: Domains were coloured as indicated on the linear arrangement of CFTR. (**A**) zCFTR structure in its "closed" state as determined by cryo-EM (PDB: 5UAR) [23]. The EM density that corresponds to the R domain could not be structurally resolved and is roughly illustrated as a yellow blob on the zCFTR structure. (**B**) zCFTR structure upon PKA phosphorylation and ATP binding as determined by cryo-EM (PDB: 5W81) [25]. Two molecules of magnesium ATP were captured in this structure as shown as spheres. The R domain moved away from the centre of the CFTR molecule but its relative location was not modeled on this structure by the Chen group. (**C**) CFTR homology structure with the R domain removed is based on a similar ABC transporter, Sav1866, which was forced to its "open" state through alignment of a chloride pathway through its "pore" [31].

However, certain regions like the R domain, parts of the NBDs and certain loop regions were not resolved in all 3 of the cryo-EM structures solved by the Chen group [23-25]. Despite the low resolution at those regions, these new structures provide the first good structural models for testing potential hypotheses.

Recent cryo-EM studies from the Riordan group have resulted in low resolution structures of chicken CFTR (chCFTR) with mutations at the NBDs that enhanced the thermal stability of the protein in both the "closed" and proposed "open" (PKA phosphorylated, ATP-bound) states to an overall resolution of 4.3 Å and 6.6 Å, respectively [33]. This group stably expressed the chCFTR

construct in the baby hamster kidney (BHK) suspension cell system that contained complex N-glycans, solubilized the membrane pellet with Decyl Maltose Neopentyl Glycol (DMNG), and exchanged the detergent to digitonin during the purification of chCFTR [33]. Despite the low resolution of these structures [33], they provide additional insights of the CFTR structure. For example, these studies have found a density at the proposed ECL4 location that may represent the large complex N-glycosylation sugars (N-glycans) [33] which are different from the smaller core N-glycans from the cryo-EM structures solved by the Chen group [23-25]. These large complex N-glycans appear to modify the CFTR structure which will be further discussed.

1.2.1.1 Lasso motif

The zCFTR and hCFTR structures determined by cryo-EM showed a unique feature of CFTR known as the lasso motif. The lasso motif comprises the first 40 residues of the N-terminus of CFTR [23-25]. Related to its name, this domain is shaped like a "lasso" that wraps around the middle of CFTR under the cell membrane [23-25, 34]. The Chen group speculate that this lasso motif may be important for CFTR trafficking and/or gating [23]. A recent review has found that the lasso motif also occurs in other similar ABC transporters and suggests that this motif may have a role in facilitating protein: protein interactions with CFTR [34, 35].

1.2.1.2 Pore lining regions of the MSDs

As previously described, each MSD consists of six TM helices that are embedded in the membrane (Figure 1.1). The MSDs are essential for the pore and selectivity filter for the transport of chloride/bicarbonate ions across the membrane. Previous studies of the pore have applied a technique known as substituted cysteine accessibility mutagenesis (SCAM) to determine the residues that line the pore [36]. SCAM analyses model the pore of CFTR as a wide outer vestibule, followed by a narrow region, a wide inner vestibule and a lateral pathway [36]. SCAM analyses have found that TM6, TM12, restricted regions of TM1 and TM11, and extreme ends of TM5 appear to line the pore [36]. TMs 3-6 also appear to contribute to the lateral pathway [36].

From the hCFTR structure in the "closed" state, it was found that TM4 and TM5 of MSD1 and TM10 and TM11 of MSD2 reach across the interface to pack against the other half of CFTR [24]. The pore of the hCFTR structure mostly agrees with previous SCAM studies [36]. The

hCFTR structure models the pore as a funnel shape which consists of: 1) a constricted region at the outer vestibule that consists of the extracellular regions of TM1, TM6, TM8 and TM12; and 2) a large inner vestibule that opens up to the cytosol between TM4 and TM6 [24]. In addition, TM8 was found to have a helical kink that breaks TM8 into 3 sections [24]. TM8 was also found to displace TM7 from the pore towards TM9 which may have a role in ion conductance and gating [24]. Interestingly, the Chen group has found a large amount of positively charged arginine and lysine residues that line the internal and external vestibules of the pore of their hCFTR structure [24]. The role of these positively charged residues was previously proposed by several studies to facilitate anion entry through the pore via electrostatic interactions [24, 36-39]. In addition, the residues that were extensively studied and suggested to form the selectivity filter, threonine at position 338 (T338) and phenylalanine at position 337 (F337) [36], were found to be located near the narrow region at the outer vestibule of the hCFTR structure as expected [24]. The features of the pore of CFTR are further illustrated on the cryo-EM structure of hCFTR in the "closed" state in Figure 1.4.
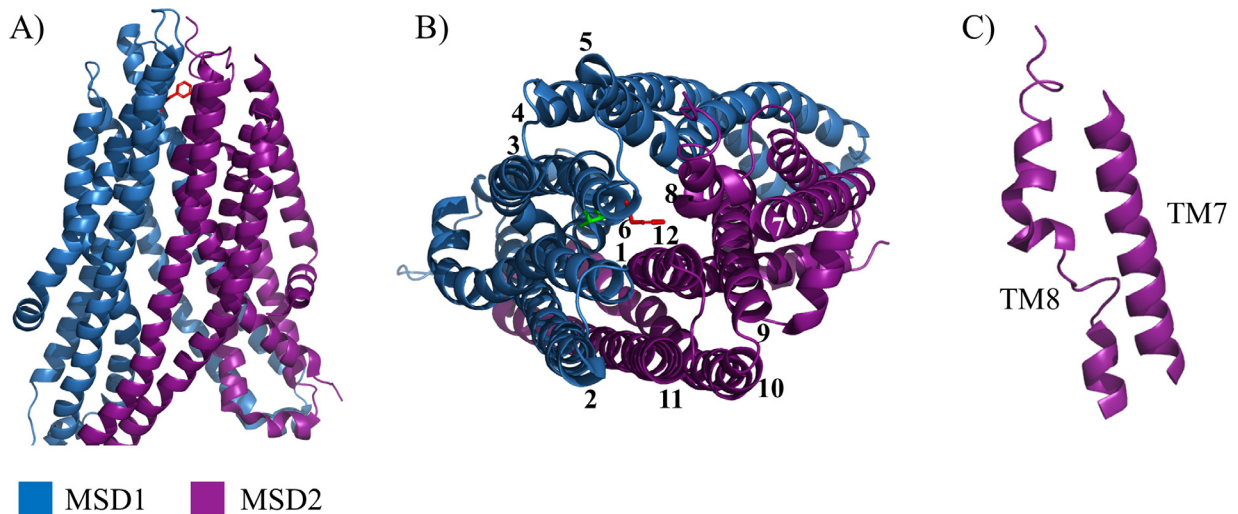
Figure 1.4: Cryo-EM structure of hCFTR in the "closed" state (PDB: 5UAK) showing the essential features of the pore.
(**A**) Side view of the TMs show that F337 (red) forms a cap at the top of the pore that corresponds with previous SCAM and electrophysiology studies. (**B**) Top view of the pore shows the TMs that line the pore and this also corresponds with previous SCAM and electrophysiology studies. F337 (red) can be seen facing the inner vestibule and T338 (green) appears near the extracellular side of the pore. (**C**) Zoom in of the iconic "kink" feature of TM8 shows that it appears to displace TM7 from the pore.

In the low resolution chCFTR structures with complex N-glycans, TM8 appeared extended [33] instead of kinked which was observed in the higher resolution structures with core N-glycans [23-25]. This different conformation of TM8 may be due to the pull of the complex N-glycans on ECL4 that is connected to TM8 which are absent from the higher resolution structures with core N-glycans [23-25, 33] (Figure 1.1). This extension of TM8 in the low resolution chCFTR structures with complex N-glycans revealed an extracellular vestibule that appears to be a plausible anion permeation pore that is formed by TMs 5, 6, 9, and 12 [33]. TM7 also appeared at a different location, near TM4 and TM5, from the higher resolution structures with core N-glycans [23-25, 33].

1.2.1.3 Loops and helices extending from the MSDs

CFTR contains alpha-helical regions known as the ICLs that extend from the MSDs. These ICLs contain coupling helices (CHs), alpha-helical regions that interact with the NBDs at an interface known as the transmission interface [40]. Cysteine cross-linking studies were traditionally applied to monitor the affinity of interactions at domain: domain interfaces of interest [41-46]. These studies apply a CFTR protein variant with its native cysteine residues replaced with other residues like alanine or leucine residues (cys-less) and then strategically engineering cysteine residues at interfaces of interest [41-46]. Interactions at these interfaces of interest were determined through the observation of a unique cross-linked band on an immunoblot [41-46]. Previous cysteine cross-linking studies that were originally designed based on CFTR homology models have found that CH1 from MSD1 and CH4 from MSD2 interacts with NBD1 at the transmission interface [30-32, 41-45]. These studies also found that CH2 from MSD1 and CH3 from MSD2 interacts with NBD2 at the transmission interface [30-32, 41-45]. The interactions at the transmission interface observed by cysteine cross-linking studies appear to coincide with the new CFTR structures and are illustrated with the hCFTR structure in the "closed" state in Figure 1.5.
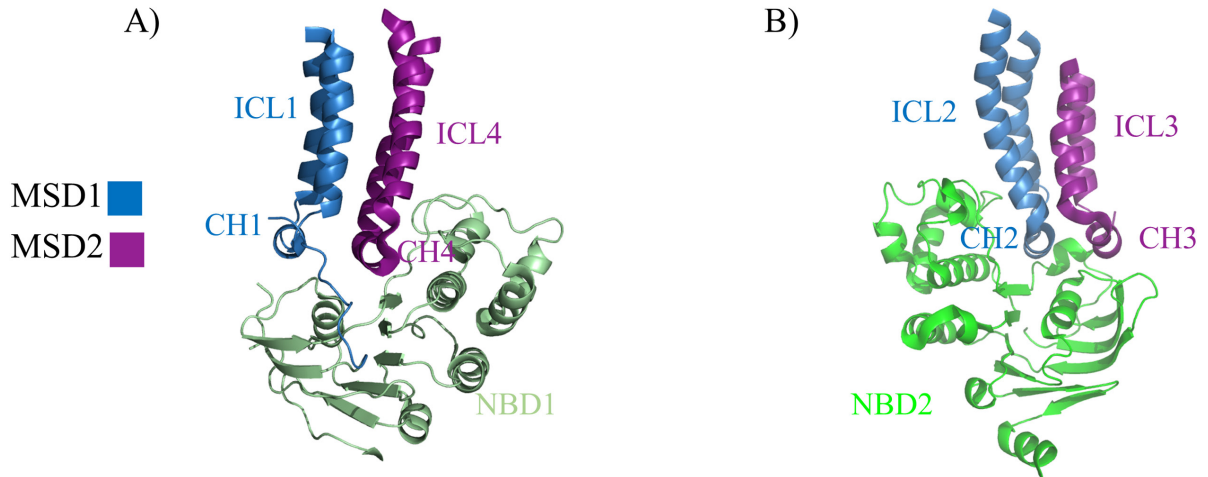
Figure 1.5: The transmission interface of hCFTR in the "closed" state (PDB: 5UAK).
(**A**) The transmission interface at the NBD1 side shows CH1 of ICL1 (MSD1) and CH4 of ICL4 (MSD2) interacts with NBD1. (**B**) The transmission interface at the NBD2 side shows CH2 of ICL2 (MSD1) and CH3 of ICL3 (MSD2) interacts with NBD2.

1.2.1.4 NBDs

Each NBD of CFTR consist of a Walker A motif, a Walker B motif and a unique signature motif that is also known as a C loop [47, 48]. The NBDs dimerize or interact at the NBD1: NBD2 interface to form two sites of ATP binding [48, 49]. The non-canonical site (Site 1) consists of Walker A and B motifs of NBD1 and the non-canonical signature motif (LSHGH) of NBD2 [50]. The canonical or catalytic site (Site 2) consists of Walker A and B motifs of NBD2 and the canonical signature motif (LSGGQ) of NBD1 [50]. Due to the differences in the signature motifs, these sites exhibit functional differences. Site 1 strongly binds and does not hydrolyze ATP whereas Site 2 binds and immediately hydrolyzes ATP [50]. The hydrolysis of ATP is also known as ATPase activity with Site 2 solely contributing to the ATPase activity of CFTR which was determined from our studies of purified CFTR [50-52]. The ATP binding sites at the NBDs are summarized in a schematic diagram presented in Figure 1.6.
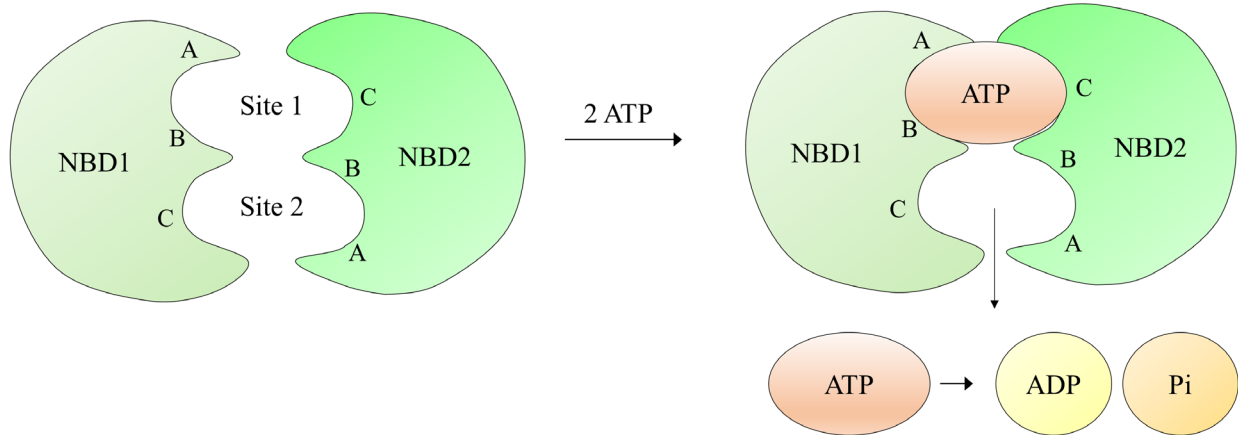
Figure 1.6: Schematic of NBDs and ATP binding sites.
Diagram summarizes the Walker A (A), Walker B (B), and signature motifs (C) that comprise the ATP binding sites at the NBDs. The consequences of ATP binding at each site are also shown.

1.2.1.5 Regulatory regions

CFTR also has unique regulatory regions that include the R domain (residue 631-849), the regulatory extension (RE, residues 638-673) [53] and the regulatory insertion (RI, consisting of residues 413-428 as reported by Lewis and colleagues [53] or consisting of residues 404-435 as reported by Aleksandrov and colleagues [46]). The R domain is a disordered region that is unique to CFTR and is essential for regulating CFTR channel gating [54, 55]. Despite its disordered state, the R domain still has a propensity to form alpha-helical structure as well as interact with the other domains of CFTR and other proteins [56-58]. The N-terminus of the R domain also constitutes an alpha-helical region known as the RE [53]. The RI is an alpha-helical region that is part of NBD1 as determined from the X-ray crystallography structure of isolated NBD1 [53]. Previous nuclear magnetic resonance (NMR) studies of the isolated NBD1 and regions of the R domain (residues 654-838) have found that in the "closed" state of CFTR, the RI and RE interact with NBD1 which prevents NBD1 from interacting with other domains such as NBD2 and the ICLs (ICL1 and ICL4) [56-59]. These interactions and the effect of phosphorylation on these interactions are illustrated below in Figure 1.8.

As previously shown in Figure 1.2, the R domain was found to be wedged between the two halves of the protein at the intracellular space and was found to interact with TM9, TM10 and

TM12 in the cryo-EM structures of hCFTR (as a resolved small peptide) and zCFTR (as an unresolved "blob" that was removed from the final structure) in the "closed" state [23, 24]. The location of the R domain wedge prevents NBD dimerization and consequently inhibits CFTR channel gating [23, 24]. This finding is consistent with the previous NMR studies on isolated domains described in this section [23, 24, 56-59]. Interestingly, the cryo-EM structures of both hCFTR and zCFTR in the "closed" state showed that there is an asymmetric opening at the NBD1: NBD2 interface, the NBDs at Site 1 are further apart than at Site 2, which may be caused by the R domain wedge [23, 24].

The low resolution chCFTR structure in the "closed" state also shows the R domain as unresolved [33]. However, this structure shows that the R domain was located between TM3 and TM4 [33]. This location is quite different from the higher resolution structures with core N-glycans, where the R domain was near TM9, TM10 and TM12 [23-25], and appears to be a plug to block the anion pathway at the intercellular vestibule between TM6 and TM12 in the "closed" state [33]. Interestingly, the R domain was found to interact with TM3, ICL1, the first ATP binding site of NBD1 and the RI [33]. The chCFTR structures also reveal the asymmetric opening at the NBD1: NBD2 interface [23-25, 33]. However, the NBDs appeared closer in the chCFTR structures (6 Å closer at Site 1 and 2 Å closer at Site 2) than in the higher resolution zCFTR and hCFTR structures in the "closed" state [23-25, 33].

1.2.1.6 Features that distinguish CFTR as a channel

Ion channels passively move ions across the membrane down their concentration gradients which causes changes in membrane potential [60]. On the other hand, pumps hydrolyze ATP to release energy in order to actively transport substrates across the membrane against their concentration gradients [60]. CFTR evolved to become the only anion channel of the ABC transporter superfamily. The main feature that distinguishes CFTR as an anion channel from the rest of the ABC transporters is the adaptation of a pore at the TMs that is open to both sides of the membrane which allows for an anion permeation pathway [61, 62]. In addition, structural comparisons of hCFTR and another ABC transporter, multidrug-resistance protein 1 (MRP1), have shown that the structures are quite similar except at TM7 and TM8 [24]. TM8 has a kink that separates TM8 into 3 segments and TM7 is displaced by TM8 in hCFTR compared to its location on MRP1 [24]. This unique feature of hCFTR is illustrated in Figure 1.4C. As

mentioned above, the pore of CFTR also contains positively charged residues that attract and facilitate anion movement through the channel. CFTR has two proposed gates that control the anion permeation pathway through its pore: 1) an ATP-dependent cytosolic gate that involves conformational changes induced by ATP-dependent dimerization of the NBDs and 2) an ATP-independent gate that likely involves subtle conformational changes in the TMs that constitute the selectivity of the pore [63, 64]. In addition, the anion permeation pathway of CFTR is regulated by phosphorylation of its unique R domain which will be discussed in the next section.

1.2.2   Regulation of CFTR channel activity by phosphorylation

CFTR channel activity is regulated by phosphorylation and dephosphorylation by protein kinases and phosphatases respectively. The CFTR protein harbours consensus sites for phosphorylation by multiple kinases including serine/threonine dependent kinases such as PKA, protein kinase C (PKC), protein kinase G (PKG), casein kinase 2 (CK2), adenosine monophosphate-activated protein kinase (AMPK), nucleoside diphosphate kinase (NDPK) and tyrosine kinases [65-70]. Dephosphorylation of serine/threonine residues in CFTR is mediated by phosphatases 2A/C [71].

PKC directly phosphorylates CFTR to partially activate the channel which reaches only 1-2% of CFTR activation by PKA [69]. PKC also enhances CFTR responses to PKA through a PKA-independent manner, possibly by inducing conformational changes of CFTR to enhance its response to PKA [69]. There are nine PKC consensus sites on CFTR that include two sites at NBD1 (T582 and T604) and seven sites at the R domain (S641, T682, S686, S707, S790, T791 and S809) [69, 70]. These PKC consensus sites have various functional roles. T582, T604 and S686 maintains the channel-competent state of CFTR and thus, are essential for CFTR activation by PKA, but not PKC [70]. Phosphorylation of S641 and especially of S686 are required for the partial activation of CFTR by PKC [70]. In contrast, the S641 and T682 sites are inhibitory for PKA- and PKC- dependent activation respectively [70].

Phosphorylation by tyrosine kinases was found to directly activate CFTR in a PKA- and PKC-independent manner [67]. The tyrosine kinases include proto-oncogene tyrosine-protein kinase (Src) [72] and proline-rich tyrosine kinase 2 (Pyk2) [73] in which Pyk2 forms a complex with Src to enhance its activity [74]. Src and Pyk2 were each capable of stimulating approximately 80% of CFTR channel stimulation by PKA [67]. The potential sites of CFTR activation by these tyrosine kinases include Y625 and Y627 which are located between NBD1 and the R domain

[66]. Src also reduces dephosphorylation of CFTR through inhibiting protein phosphatase 2A which enhances CFTR activation by PKA and PKC phosphorylation [74, 75].

CK2 is a ubiquitously expressed and constitutively active serine/threonine kinase that also regulates CFTR activity [76]. CK2 was found to phosphorylate CFTR at S422 [77] and T1471 [78]. Interestingly, a previous study has found that S511 could not be phosphorylated by CK2 unless the adjacent residue Y512 is phosphorylated by tyrosine kinase(s), such as spleen tyrosine kinase (SYK) [79], which alleviates the "block" on S511 for CK2 phosphorylation [77, 80].

PKG is a cGMP-dependent protein kinase in which it is activated through cGMP binding to its C-terminal nucleotide domain B [81]. Activated PKG was found to directly activate CFTR [82, 83]. The activation of CFTR by cyclic guanosine monophosphate (cGMP) was found to be approximately 87% of the activation of CFTR by cyclic adenosine monophosphate (cAMP) [84]. Previous studies have identified that V397 and L420 of CFTR as potential binding sites for cGMP [84] and that serine residues at positions 660, 700, 737, 768, 795 and 813 of CFTR can be phosphorylated by PKG [85].

In contrast, AMPK is a metabolic sensor to intracellular changes in AMP and ATP levels that inhibits CFTR activity [86-89]. The inhibition of CFTR by AMPK is caused by its phosphorylation at inhibitory PKA sites of CFTR which include S737 and S768 [90-92].

There are several isoforms of NDPK that include NDPK-A and NDPK-B [93]. Interestingly, the mechanisms of these two isoforms on CFTR channel regulation are different. NDPK-A was found to form a complex with AMPK and CFTR [94]. The catalytic activity of NDPK-A is dependent on autophosphorylation at its H118 and S120 residues, which is enhanced by AMPK, and this was found to be essential for AMPK-dependent CFTR inhibition [94]. In contrast, NDPK-B interacts with CFTR in a cAMP- and PKA-dependent manner and may be important for regulation of CFTR activity by PKA [95].

Therefore, the regulation of CFTR channel activity is dependent on the activity of the combination of various kinases and protein phosphatases. In addition, the site-specific propensity for phosphorylation will depend on the cellular localization of CFTR, accessibility of such phosphorylation sites to these enzymes in the context of the CFTR protein structure and its interaction with other binding partners.

1.2.2.1 PKA phosphorylation of CFTR

CFTR is regulated primarily by cAMP-dependent PKA phosphorylation [96-100]. Intracellular cAMP levels can be enhanced by a cAMP agonist such as forskolin which enhances PKA-dependent phosphorylation and consequently channel gating of CFTR [96-98]. This section describes the conformational changes and the functional consequences of CFTR upon PKA phosphorylation.

1.2.2.2 PKA phosphorylation sites on CFTR

There are ten PKA phosphorylation consensus sites on CFTR that include one site at the RI of NBD1 (S422), one site at the N-terminus of the R domain known as the RE (S660) and eight sites at the R domain (S670, S700, S712, S737, S753, S678, S795 and S813) [91, 92, 101-108]. The phosphorylation consensus sites are summarized in Figure 1.7. Previous radioactivity and mass spectrometry (MS) studies showed that in the inactive or resting state, certain phosphorylation sites (S660 of the RE along with S700, S712, S737, S768 and S795 on the R domain) exhibit low or basal levels of phosphorylation as shown in Figure 1.7A [91, 92, 101-108]. These studies also found that upon PKA activation, certain phosphorylation sites (S660, S700, S737, S768, S795 and S813) exhibit an increase in phosphorylation as shown in Figure 1.7B [91, 92, 101-108]. Unfortunately, these studies were unable to study the effect of phosphorylation at three phospho-sites (S422, S670, S753) due to sensitivity issues of the methods that were applied. In summary, the multiple sites exhibit variable degrees of PKA phosphorylation in which certain sites exhibit basal phosphorylation and only specific sites exhibit an increase in phosphorylation after PKA activation.
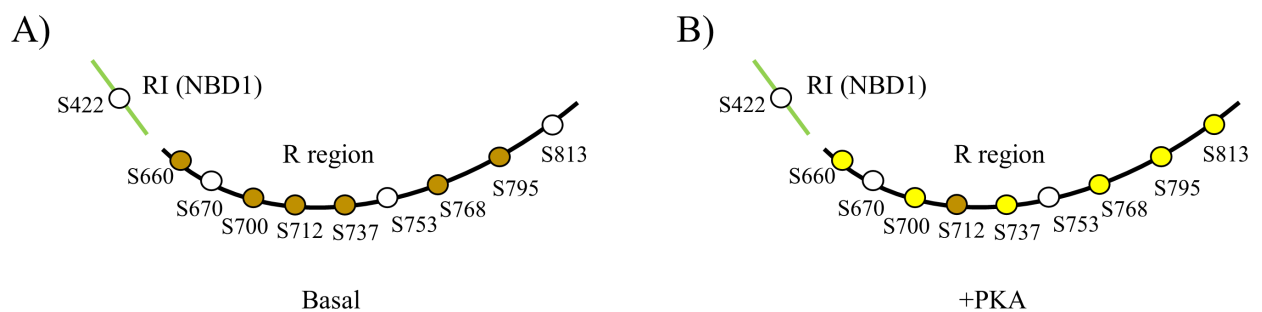
Figure 1.7: Summary of levels of phosphorylation at phosphorylation sites of intact CFTR. (**A**) Brown spheres indicate PKA sites (at Serine or S) that are basally phosphorylated in intact CFTR in resting cells. Empty circles indicate the PKA sites that are not phosphorylated. (**B**)

Yellow spheres indicate PKA sites that become more phosphorylated after PKA activation in full-length CFTR. *Note:* Levels of phosphorylation at S422, S670 and S753 sites could not be detected with radioactivity and MS.

1.2.2.3 Regulation of CFTR channel gating by PKA phosphorylation

PKA phosphorylation of CFTR is absolutely required for ATP-dependent gating [104, 105, 109]. After this necessary modification, ATP binds to the two ATP binding sites (Site 1 and Site 2) at the NBD1: NBD2 interface [48]. As previously mentioned, Site 1 does not hydrolyze ATP whereas Site 2 immediately hydrolyzes ATP [50]. ATP binding at both sites enhances NBD dimerization and leads to channel opening [110]. ATPase activity at Site 2 then destabilizes the NBD dimer and leads to channel closing [110].

Despite PKA phosphorylation being absolutely required for ATP-dependent gating, its mechanisms with regards to ATP binding or ATPase activity are not well understood. Previous patch clamp studies have found that PKA phosphorylation increased ATP affinity to one or both ATP binding sites [111]. On the other hand, ATPase activity studies on the purified protein in my laboratory have found that PKA phosphorylation increased ATP affinity to Site 2 [51]. However, ATPase activity studies on the purified protein by the Chen group have found that PKA phosphorylation significantly increased the turnover rate of ATP hydrolysis without increasing the ATP affinity [23, 24]. Clearly, more research is needed to determine the effect of PKA phosphorylation on ATP affinity of the purified CFTR protein.

Interestingly, PKA phosphorylation also appears to regulate ATP-independent gating through studies of the ATP-binding mutant (glycine to aspartic acid at position 551 or G551D) and the NBD2 deletion mutant (deletion of residues 1172-1480) [112]. The mechanism of this regulation remains unknown but it may involve allosteric intramolecular interactions of the R domain, MSDs and/or ICLs by phosphorylation [112] which will be further discussed.

1.2.2.4 PKA phosphorylation-dependent conformational changes for CFTR gating

EM studies have shown that full-length CFTR protein becomes more compact upon PKA phosphorylation, indicating that phosphorylation modifies intramolecular interactions of CFTR [113].

As previously mentioned, studies on isolated domains have claimed that the RE and RI interact with NBD1 in the inactive state of CFTR which prevents NBD1 from interacting with other domains of CFTR [56-59]. Previous NMR studies have found that PKA phosphorylation of S660 of RE and S422 of RI decreases the helical content of the RE and RI [56-59]. This in turn decreases the interaction of RE and RI with NBD1 which is proposed to allosterically increase interactions at the NBD1: NBD2 and NBD1: ICL(1 and 4) interfaces, respectively [56-59]. Interestingly, studies on CFTR in which the RI was removed enhanced the stability, processing and function of both wildtype (Wt-) and the major mutant, F508del-CFTR, which supports the claims from the NMR studies and also suggests that RI removal may contribute to restoring ICL4: NBD1 interactions [46].

Previous cysteine cross-linking studies have shown that phosphorylation enhances interactions at specific regions of the R domain and the N- and C-termini of the full-length CFTR [113-115]. *In vivo* cysteine cross-linking studies of the full-length CFTR protein have also shown that phosphorylation increases interactions at the NBD1: NBD2 interface, consistent with the claims of the NMR studies [49, 58]. The NBD1: NBD2 interactions are essential for formation of the ATP binding pockets, a prerequisite for CFTR channel gating [49, 58].

Cysteine cross-linking could not detect an enhanced interaction at the ICL: NBD interfaces upon PKA phosphorylation [30, 41-45]. The inability to detect modifications at the interfaces upon PKA phosphorylation with cysteine cross-linking may be due to the domains of those interfaces interacting independently from phosphorylation or the changes upon PKA phosphorylation may be too subtle to be detected by that assay [30]. Interestingly, locking the ICL4: NBD1 and ICL2: NBD2 "domain-swapping" interfaces via cysteine cross-linking prevented phosphorylation-dependent channel gating of CFTR [30, 41]. In addition, abolishing the ICL1: NBD1 interaction with an ICL1 peptide significantly reduced channel gating and ATPase activity of full-length CFTR [116]. Despite the inability to detect changes at the ICL: NBD interfaces upon

phosphorylation, dynamic interactions at those interfaces, as shown in Figure 1.8 [117], may be essential for phosphorylation-dependent channel gating.
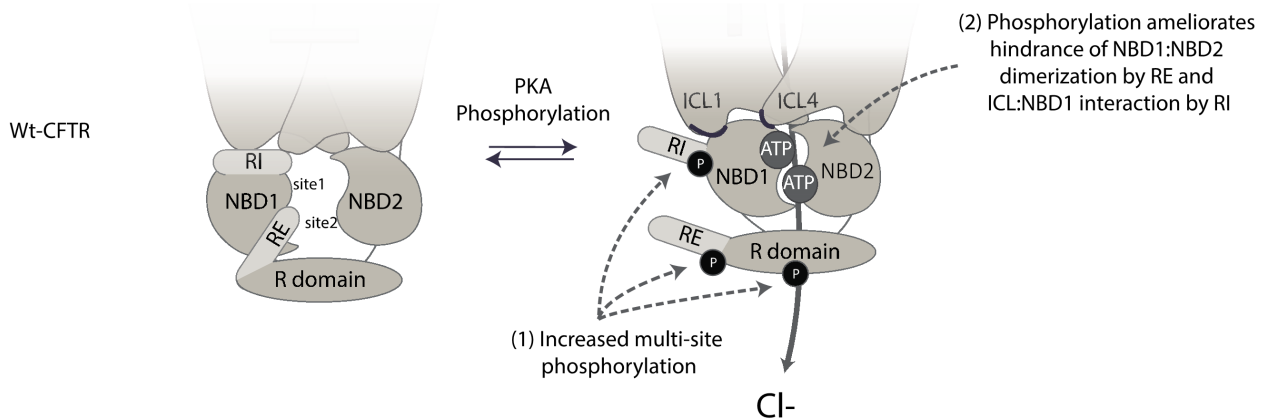
Figure 1.8: Phosphorylation-dependent conformational changes for CFTR gating.
In the basal phosphorylated state, the RI and RE interact with NBD1. Upon PKA phosphorylation, the RI and RE moves away from NBD1 which then allows for essential channel gating interactions at the NBD1: NBD2 and ICL(1 and 4): NBD1 interfaces. *Note:* This schematic does not depict the actual location of the R domain relative to the other CFTR domains.

In the context of the full-length protein, cryo-EM studies have found that PKA phosphorylation of zCFTR resulted in the R domain moving away from the space at the centre of CFTR between the TMs and the NBDs moving closer together [25]. There are also subtle conformational changes of the TMs near the pore, notably TM8 and TM7, which were suggested to be important for gating [25]. These findings are summarized in Figure 1.9 and support the NMR studies that suggest that PKA phosphorylation induces conformational changes of the R domain which then allows for essential interactions with NBD1 [56-59]. Surprisingly, the Chen group was unable to detect a chloride and water path out of the pore of the channel and the F337 residue that acts as the "cap" of the selectivity filter still appears to be in the "closed" conformation [25]. Thus, the structure of the channel still appears "closed" despite PKA phosphorylation and ATP binding [25].
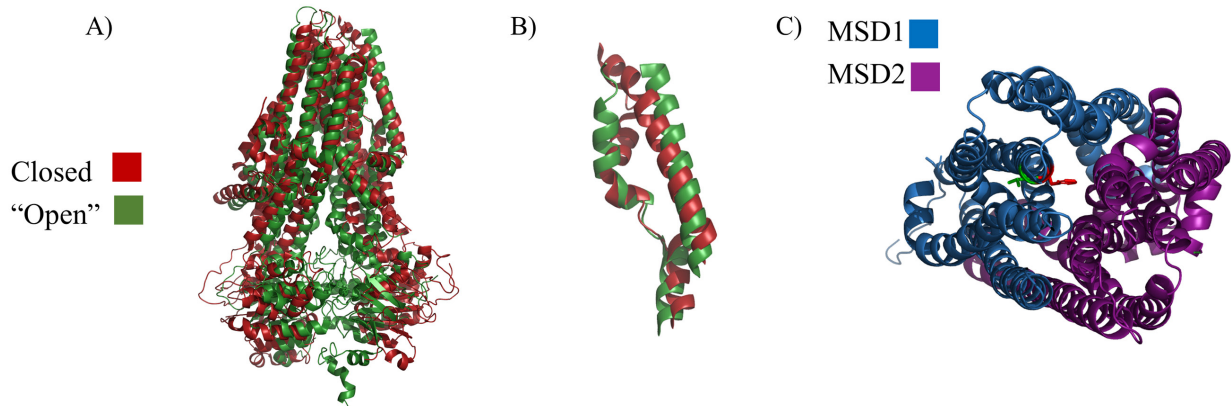
Figure 1.9: Conformational changes of zCFTR upon PKA phosphorylation and ATP binding.
(**A**) Comparison of zCFTR in the "closed" state (PDB: 5UAR, red) and in the PKA phosphorylated, ATP-bound state (PDB: 5W81, green). (**B**) Conformational changes of TM8 and TM7 upon PKA phosphorylation and ATP binding. (**C**) Top down view of the pore in the phosphorylated, ATP-bound state (PDB: 5W81) shows that F337 (red) still appears to "cap" down at the pore which may impede extracellular chloride efflux. F337 (red) and T338 (green) also appears to be in the relatively same conformation as in the "closed" conformation (Figure 1.4B).

Based on the low resolution chCFTR structures, PKA phosphorylation removes the R domain from its location at the "closed" state [33]. There also appears to be rigid and subtle movements of TM7 and TM8 in which the helices moved 2 Å from their original orientations at the "closed" state [33]. The change in the NBDs upon PKA phosphorylation was subtle unlike the significant change observed in the zCFTR structures [25, 33]. However, since the chCFTR structure in the PKA phosphorylated state is of low resolution, these structural changes of CFTR upon PKA phosphorylation remain unclear and more structural work is needed to validate these claims [33].

1.2.3 Biosynthetic pathway of CFTR in epithelial cells

CFTR traffics through its biosynthetic pathway to reach the cell surface of epithelial cells. CFTR is post-translationally modified by glycosylation at two N-glycosylation sites (N894 and N900) located at ECL4 (Figure 1.1) during different stages of its biosynthetic pathway [118]. The glycosylation states of CFTR, which can be observed on an immunoblot as differences in the molecular weight of the protein, provides information on the approximate localization of the protein. As shown in Figure 1.10A, the protein traffics in vesicles to the endoplasmic reticulum

(ER) where it is core glycosylated after its protein synthesis. From an immunoblot as shown in Figure 1.10B, the core glycosylated form of the protein is known as band *B* with a molecular weight of approximately 140-150 kDa. The protein then traffics to the Golgi where it is complex glycosylated. From an immunoblot as shown on Figure 1.10B, the complex glycosylated form of the protein is known as band *C* with a molecular weight of approximately 170-180 kDa.
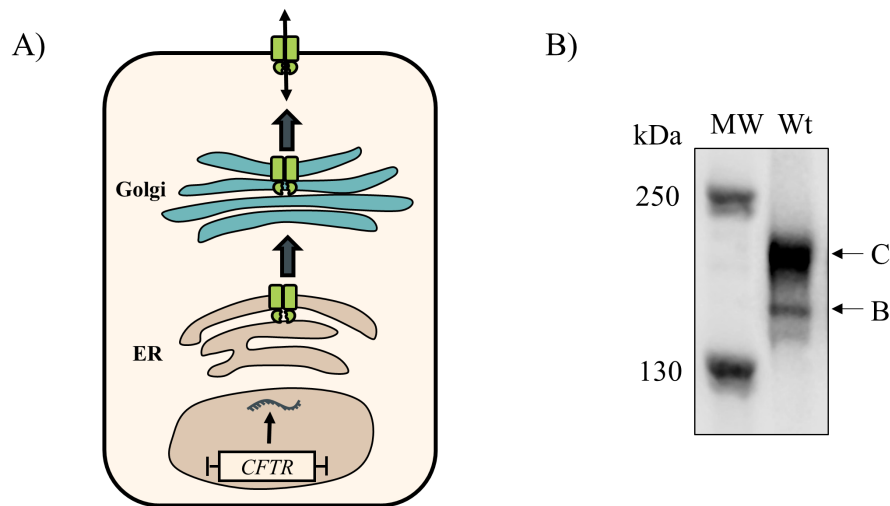
Figure 1.10: Biosynthetic pathway of CFTR in epithelial cells.
(**A**) Schematic of the biosynthetic pathway of Wt-CFTR shows that after protein synthesis, the protein traffics to the ER, the Golgi and consequently the cell surface where it functions as an anion channel. *Note:* Not shown for simplicity are the vesicles that CFTR traffics in throughout its biosynthetic pathway. (**B**) Representative immunoblot of Wt-CFTR has two bands: band *B* which is the core glycosylated form of the protein at the ER, and band *C* which is the complex glycosylated form of the protein at the Golgi and at the cell surface.

1.2.3.1 Biosynthesis of CFTR is modified by PKA phosphorylation

The *CFTR* gene has a cAMP response element (CRE) in the promoter region [119, 120]. PKA phosphorylation was found to enhance CFTR gene expression through activating the CRE of the *CFTR* gene and/or stabilizing the mRNA transcripts of CFTR [119, 120].

After the partially folded CFTR exits the ER, it interacts with β-coat protein (COP), a protein that is part of the COPI complex which is associated with ER retention [121, 122]. PKA phosphorylation was found to decrease the interaction of CFTR and β-COP and in turn increase the interaction of CFTR and 14-3-3, a protein that facilitates forward trafficking [121]. A

previous study applying fluorescence polarization of fluorescein isothiocyanate labeled R domain peptides has found that the interaction of CFTR and 14-3-3 is initiated by PKA phosphorylation of S768 of the R domain of CFTR. This phosphorylation-dependent interaction "anchors" CFTR to 14-3-3 which mediates the binding of the other sites (S712, S753, S795 and S813) of CFTR to 14-3-3 [123].

PKA phosphorylation was also found to increase CFTR abundance at the cell surface through two mechanisms. Firstly, PKA phosphorylation enhances interactions of CFTR, via its C-terminal PDZ domain, with cytoskeletal proteins that include Na^+/H^+ Exchanger Regulatory Factor (NHERF1), ezrin and actin which stabilizes CFTR and increases its residence time at the cell surface [124-127]. Interestingly, ezrin was found to shuttle PKA to CFTR which enhances the functional expression of the CFTR channel at the cell surface [128-130]. Secondly, PKA phosphorylation was found to increase CFTR cell residence time by enhancing recycling of CFTR in Rab11 positive endosomes as shown by fluorescence detection technology studies applying fluorogen activating proteins [131].

The effects of PKA phosphorylation on CFTR protein synthesis and trafficking are also summarized in Figure 1.11 [117].
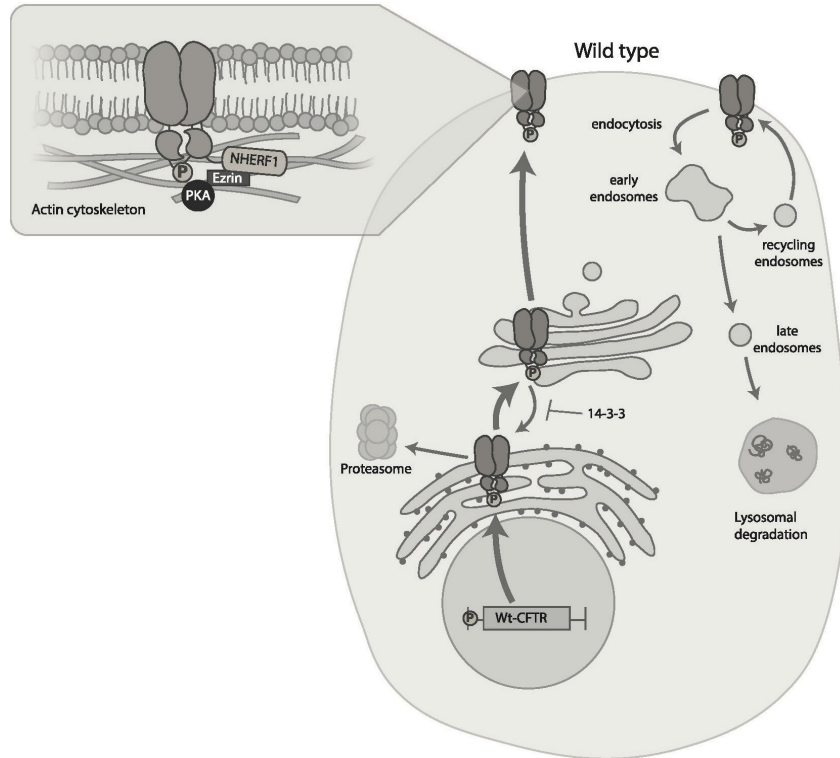
Figure 1.11: Summary of the effect of PKA phosphorylation on CFTR expression and trafficking through the biosynthetic pathway.
PKA phosphorylation has been shown to increase *CFTR* gene expression, facilitate forward trafficking of CFTR by enhancing interactions with 14-3-3, as well as increase protein cell surface time by stabilizing CFTR at the cell surface, enhancing interactions of the protein with the cytoskeletal scaffold proteins (NHERF1, ezrin, actin) and/or enhancing recycling of the protein.

1.2.4   Interactions of CFTR at the apical membrane

At the cell surface, previous studies have found that CFTR appears to be localized in lipid rafts [132]. Lipid rafts are microdomains that contain and require an abundant amount of cholesterol and lipids [132]. Previous studies have found that CFTR also interacts with other membrane proteins like the solute carrier (SLC) proteins at the apical membrane, possibly in lipid rafts, in a tissue-specific manner [133-135]. Studies have also found that CFTR interacts with cell surface scaffolding proteins that include NHERF1, ezrin and actin which helps stabilize the protein at the cell surface [128, 136]. The interaction of CFTR with the cell surface scaffolding proteins may also be involved in its localization in lipid rafts [132]. At the cell surface, CFTR is continually

removed and recycled via recycling endosomes in order to regulate the abundance of CFTR at the cell surface [131].

1.3 CF-causing mutations

There are currently more than 2000 known mutations identified in CFTR. These mutations are classified under six main classes based on their effects on the CFTR protein in the cell. These classes of mutations include: class I mutations that lead to defects in protein synthesis, class II mutations that lead to protein misfolding and misprocessing, class III mutations that affect channel regulation and gating, class IV mutations that affect channel conductance, class V mutations at the promoter and splicing mutations that affect its abundance without changing its conformation, and class VI mutations that destabilize the protein at the plasma membrane [137]. The two mutations that will be discussed in the subsequent sections include G551D and the major disease-causing mutation, F508del. The location of these mutations on the hCFTR structure is shown in Figure 1.12.
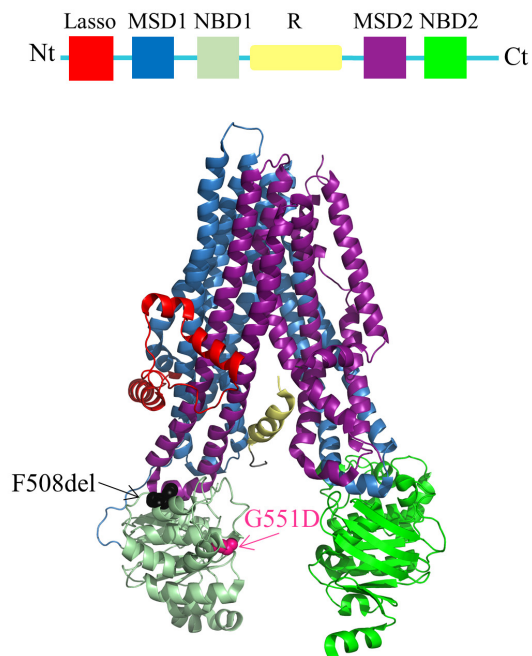
Figure 1.12: CF-causing mutations, G551D and F508del, on the hCFTR structure.
The locations of the major CF-causing mutations, G551D and F508del, are shown in pink and black spheres respectively on NBD1 of the hCFTR structure solved by cryo-EM (PDB: 5UAK).

1.3.1   G551D

G551D is the third most common CF-causing mutation that occurs in approximately 4% of CF patients (CF Foundation Patient Registry 2016). The G551D mutation occurs at the canonical signature motif, LSG(**G->D**)Q, at NBD1 which is part of Site 2 of the ATP binding sites [138]. This mutation results in defective channel gating but does not affect trafficking of the mutant protein to the cell surface [139]. Our iodide efflux studies with purified and reconstituted full-length G551D-CFTR protein show that the mutant displays defective phosphorylation- and ATP-dependent gating [140, 141]. The dysfunction of G551D-CFTR may be due to the mutation disrupting ATP binding at Site 2, as ATPase activity assays from my laboratory show that the G551D mutation significantly decreases the apparent affinity of CFTR for ATP [141]. However, it was reported that mutation of the G551 residue in NBD1 of a similar ABC transporter, human MRP1, does not affect ATP binding [142]. An alternative explanation for the defective CFTR gating is that the mutation may prevent conformational changes upon ATP binding at the NBD1: NBD2 interface [138]. However, additional studies must be conducted to test this hypothesis.

1.3.2   F508del

The major CF-causing mutation is F508del, which occurs in approximately 90% of CF patients (CF Foundation Patient Registry 2016). F508del is classified as a class II, III and VI mutation. The following sub-chapters explore the major defects of F508del-CFTR.

1.3.2.1 Intrinsic structural defects of F508del-CFTR

The F508del mutation causes various intrinsic defects of CFTR which lead to defects in folding, trafficking, cell surface stability and channel activity of CFTR.

Since the F508 residue is located at NBD1, previous studies have isolated NBD1 to study the effect of F508del on that domain [143, 144]. These studies on isolated NBD1 have found that the F508del mutation thermally destabilizes NBD1 [144]. Cysteine cross-linking studies have also found that F508del disrupts major interfaces of full-length CFTR such as ICL4: NBD1 [30, 41-43, 45, 46]. Previous studies have found that correction of NBD1 thermostability and interactions at the ICL4: NBD1 interface are both required for rescuing the F508del-CFTR protein with respects to assembly/folding and stability at the cell surface [145, 146].

1.3.2.2 Defects in folding, trafficking, cell surface stability and channel activity

The F508del mutation disrupts CFTR protein assembly and leads to misfolding [147]. The misfolded protein is retained in the ER where it is consequently removed by ER-associated degradation (ERAD) [148-150]. A small population of F508del-CFTR can escape ERAD and reach the Golgi [151, 152]. However, the mutant protein exhibits aberrant exposure of diarginine (RXR)-based ER retention motifs that is recognized and redirected back to the ER [151, 152]. An even smaller population of F508del-CFTR can reach the cell surface by evading those quality controls [153, 154]. However, the mutant protein exhibits conformational instability and defective channel function at the physiological temperature of 37°C [153, 154]. F508del-CFTR stability at the cell surface appears to be related to disrupted interactions of CFTR with the cytoskeleton proteins: NHERF1, ezrin and actin [128]. The intrinsically unstable protein at the cell surface is consequently removed by peripheral quality control and sent for lysosomal degradation [153]. The defects in F508del-CFTR biosynthesis and stability are summarized in Figure 1.13 [117].
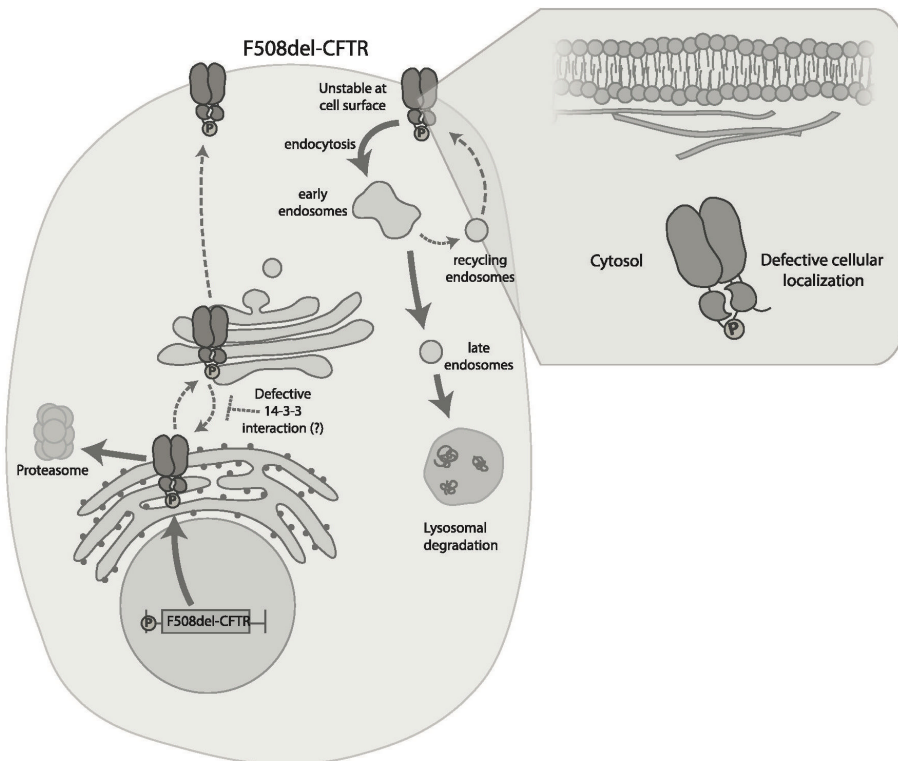
Figure 1.13: The effect of F508del mutation on CFTR trafficking and expression.

F508del-CFTR is misfolded which is targeted for proteasomal degradation. The small population of F508del-CFTR that can escape the ER has aberrant exposures of RXR motifs and possibly defective 14-3-3 interactions which prevents further trafficking to the Golgi. An even smaller population can reach the cell surface. However, the protein is unstable at the surface possibly due to defective interactions with the cytoskeletal scaffolding proteins. This unstable protein is then rapidly removed via endocytosis and sent to lysosomal degradation.

The defects in F508del-CFTR biosynthesis and stability results in the presence of only band *B* on the immunoblot compared to Wt-CFTR as shown in Figure 1.14.
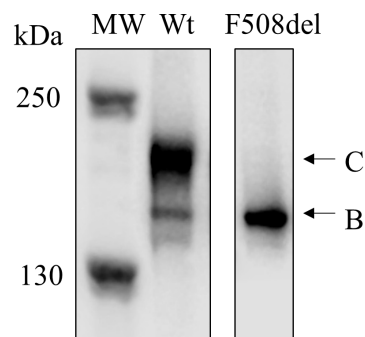
Figure 1.14: Consequence of F508del mutation on CFTR processing as detected by immunoblotting.
Wt-CFTR is expressed as mainly band *C* with some band *B* on the immunoblot. F508del-CFTR cannot reach the cell surface due to its defects and is only expressed as band *B* on the immunoblot.

1.3.2.3 Phosphorylation-dependent defects of F508del-CFTR

Previous studies in my laboratory applying selected reaction monitoring MS (SRM-MS) on purified full-length protein have found that F508del-CFTR exhibits reduced phosphorylation of S660 at the RE [101]. Additional phosphorylation sites may also exhibit defective phosphorylation. However, these could not be quantified by SRM [101]. The reduced phosphorylation of F508del-CFTR may contribute to disrupted intramolecular interactions between NBD1: NBD2 interface and/or between the transmission interface which is illustrated in Figure 1.15.
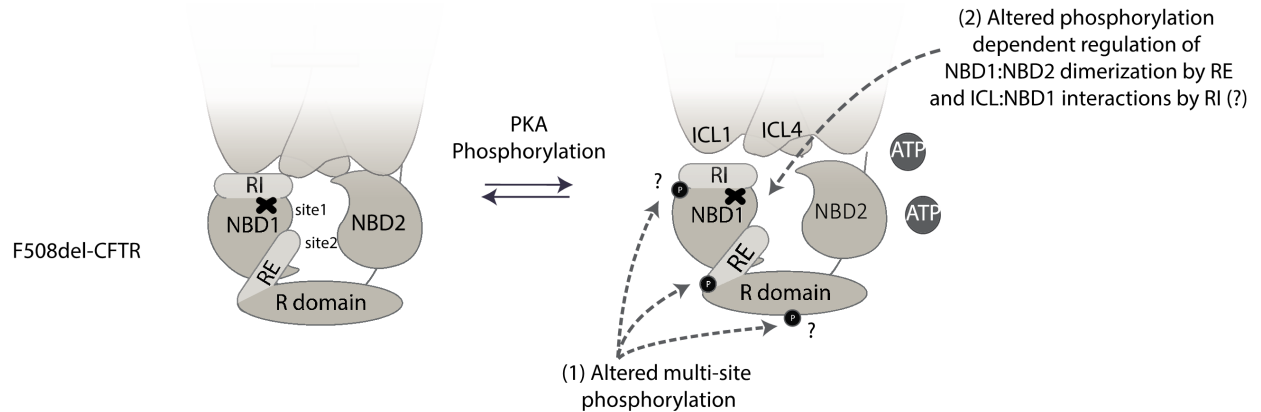
Figure 1.15: Summary of defective phosphorylation-dependent conformational changes of F508del-CFTR.
F508del-CFTR has altered levels of phosphorylation at multiple sites compared to Wt-CFTR which may result in altered phosphorylation-dependent interactions (i.e. NBD1: NBD2 and ICL: NBD1 interactions) and consequently altered phosphorylation-dependent regulation.

This claim was further supported by previous NMR studies on isolated F508del-NBD1 that have found that phosphorylation of the RI increased the interaction of the RI with the core of NBD1 which had a differing effect in Wt-NBD1 [57]. Furthermore, removal of the RI partially rescued interactions at ICL4: NBD1 and ICL2: NBD2 interfaces as well as F508del-CFTR channel activation [46]. Thus, this defect in phosphorylation may affect the processing/folding, stability and channel gating of F508del-CFTR.

The defective phosphorylation of F508del-CFTR may affect forward trafficking of the protein as it appears to be enhanced with the phosphorylation-dependent interaction of CFTR with 14-3-3 [121, 123, 133]. Unfortunately, this could not be validated as the phosphorylation sites involved in this interaction (S768 and S753) could not be studied due to the limitations of SRM-MS [101].

The defect in phosphorylation of F508del-CFTR may also affect the abundance of CFTR at the cell surface. F508del-CFTR stability at the cell surface appears to be reduced due to disrupted interactions of CFTR with the cytoskeleton proteins: NHERF1, ezrin and actin [128]. As previously mentioned, the interactions of CFTR and the cytoskeleton proteins appear to be phosphorylation-dependent and are essential for maintaining and stabilizing CFTR at the cell surface [128]. In addition, the small population of F508del-CFTR that manages to reach the cell

surface is sent to recycling endosomes [131]. However, the mutant protein exhibits defective phosphorylation-regulated exocytosis [131].

1.4 Food and Drug Administration (FDA) approved drugs for rescuing F508del defects

Drug discovery efforts that aimed to correct the defects caused by F508del resulted in a drug known as ORKAMBI® that has been recently FDA approved for F508del homozygous patients. ORKAMBI® is a combination of two drugs: a corrector compound known as lumacaftor or VX-809 and a previously FDA approved potentiator compound known as KALYDECO® (ivacaftor or VX-770). This section describes these two compounds and discusses their potential mechanisms of action towards restoring F508del defects as illustrated in Figure 1.16.
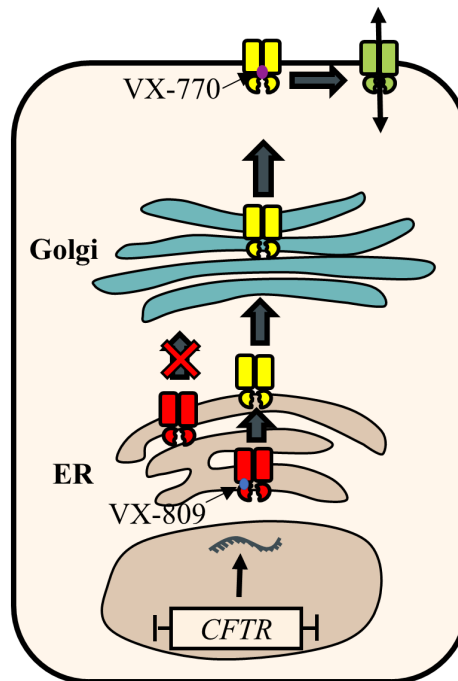
Figure 1.16: Proposed mechanisms of action of VX-809 and VX-770 on F508del-CFTR.
VX-809 (blue circle) binds directly to F508del-CFTR (in red), possibly at MSD1, which attempts to rescue the folding and forward trafficking of the protein (now in yellow). VX-770 (purple circle) binds directly to F508del-CFTR at an unknown site to potentiate or increase channel gating of the protein at the cell surface. The combination of VX-809 and VX-770 (ORKMABI®) aimed at correcting the folding and channel gating of the protein (from red to green).

1.4.1   Corrector compounds

Previous studies have shown that low temperature culture conditions (27°C) can enhance the amount of F508del-CFTR protein to the cell surface and partially restore its channel gating [154, 155]. Substantial efforts were made to discover small molecule compounds that recapitulate or have better effects compared to low temperature rescue. As previously mentioned, the corrector that has been combined in ORKAMBI® is known as VX-809.

1.4.1.1 VX-809

VX-809 is a corrector that partially rescues the folding and trafficking of F508del-CFTR to the cell surface as shown in Figure 1.16 [156]. Interestingly, studies have found that VX-809 was also able to maintain the channel opening of F508del-CFTR with increasing temperatures [145]. Previous studies applying truncation mutations and cell-based assays have found that VX-809 binds to MSD1 [157, 158]. Cysteine cross-linking has found that VX-809 allosterically restores the ICL4: NBD1 and ICL2: NBD2 interfaces [43, 45]. VX-809 may also have a role in stabilizing the mutant protein at the cell surface by enhancing its interactions with the cytoskeletal proteins [159].

1.4.2   Potentiator compounds

Potentiators are compounds that enhance channel gating of CFTR protein that has reached the cell surface. As previously mentioned, drug discovery efforts have resulted in the discovery of the first FDA approved potentiator compound known as VX-770. This compound was approved for a small population of CF patients with 36 missense gating mutations, such as G551D (Vertex Pharmaceuticals Incorporated 2018).

1.4.2.1 VX-770

VX-770 is a potentiator compound that enhances channel gating of CFTR protein that has reached the cell surface as shown in Figure 1.16. Previous studies have found that VX-770 enhances channel activity of G551D- and F508del-CFTR that has been rescued at the cell surface [160]. Studies from my laboratory and others have found that VX-770 potentiates CFTR in an ATP-independent manner [140, 161]. Single channel studies have suggested that VX-770 may bind to the TM regions of CFTR [161]. These studies also found that VX-770 shifts the equilibrium from the post-hydrolytic state to the pre-hydrolytic state to increase the opening time

of CFTR by permitting more ATP molecules to rebind to Site 2 [161]. Iodide efflux studies of purified and reconstituted full-length CFTR protein from my laboratory have found that VX-770 directly binds to the full-length protein and that this drug resulted in a two-fold increase in iodide efflux rate upon PKA phosphorylation [140]. This suggests that the VX-770 potentiation effect is phosphorylation-dependent [140]. On the other hand, a study from a different group has found that VX-770 can potentiate without the R domain which suggests that VX-770 may not act on the R domain [161]. Recent studies from my laboratory have shown that VX-770 can apparently "activate" CFTR prior to forskolin, which enhances cAMP levels via adenylyl cyclase and consequently enhances PKA phosphorylation of CFTR, and this effect is dependent on the basal phosphorylation of CFTR (Hung et al., manuscript in submission).

Recent studies have found that high or supra-pharmacological concentrations of VX-770 has a destabilizing effect on F508del- but not Wt- or G551D-CFTR [162, 163]. Thus, the destabilizing effect of VX-770 on F508del-CFTR may be one explanation as to why the ORKAMBI® drug had modest effects on the F508del homozygous patient population. However, not much is known of the mechanism of action of this destabilizing effect.

1.5   Genetic modifiers

Another explanation for the modest and variable effect of ORKAMBI® on patients with the same F508del homozygous genetic background may be due to modifier genes. Modifier genes are genes that modify the disease severity or pathology. A previous hypothesis-driven genome wide association study (GWAS) has found modifier genes, *SLC26A9* and *SLC6A14,* are associated with meconium ileus, an intestinal obstruction that occurs in approximately 15% of CF patients [164]. Previous studies applying multiple-phenotype analytic strategy has found that *SLC26A9* and *SLC6A14* have pleiotropic effects, in which one gene affects different phenotypes [165]. *SLC26A9* has a pleiotropic effect on meconium ileus and pancreatic impairment whereas *SLC6A14* has a pleiotropic effect on meconium ileus and lung disease upon bacterial infection [165]. Another GWAS has found that *SLC6A14* is associated with lung pathology in CF [166] and another study has found that *SLC26A9* modifies the airway response to CF therapeutic drugs such as VX-809 and VX-770 on CFTR protein expressed at the cell surface [167]. Thus, these genes appear to modify the CF phenotypes and response to CF drugs in the intestine and the lungs.

1.6 Alternative drug therapies that target PKA-dependent signaling

Since F508del-CFTR appears to have downstream effects from its phosphorylation defect, targeting PKA-dependent signaling may be an alternative drug therapy from ORKAMBI® towards rescuing trafficking, stability and function of F508del-CFTR.

Recent studies applying fluorescence polarization have found a drug that was produced by the fungus *Phomopsis amygdali*, fusicoccin-A, can significantly enhance binding of the pS753 epitope of the R domain of CFTR with 14-3-3 [123]. Due to the role of 14-3-3 in forward trafficking, this enhanced interaction can rescue forward trafficking of F508del-CFTR.

The stability of F508del-CFTR at the cell surface can be rescued by increasing phosphorylation-dependent interactions of the mutant protein with cytoskeletal proteins. Previous studies have found that phosphorylation of ezrin resulted in increased polymerization of actin and stability of F508del-CFTR at the surface of CF bronchial epithelial (CFBE) cells [159, 168]. Thus, drugs that can increase phosphorylation may stabilize F508del-CFTR at the cell surface.

Proximal phosphodiesterases (PDEs) regulates the concentration of cAMP in microdomains containing CFTR. Cyclic nucleotide PDE inhibitors that include RPL554, milrinone and rolipram were found to rescue the function of F508del-CFTR in CFBE cells [169]. Interestingly, these PDE inhibitors were found to significantly enhance the potentiation effect of VX-770 in CFBE cells which offers an alternative CF drug therapy [169]. cAMP concentrations near CFTR can also be regulated by another ABC transporter, MRP4, which has been shown to export cAMP out of the cell [170-173]. Previous studies inhibiting MRP4 with the drug MK-571 resulted in an increase in intracellular cAMP levels and enhanced Wt-CFTR function at the cell surface [173].

1.7 Thesis Rationale and Hypotheses

As previously mentioned, CF is caused by mutations of CFTR with the major disease-causing mutation, F508del, occurring in approximately 90% of CF patients. The FDA approved drug for F508del homozygous patients, ORKAMBI®, has modest and variable effects on lung function [174]. This calls for better drug therapies for the major CF patient population. In order for this to occur, we must better understand the CFTR structure and the conformational changes of CFTR

channel gating. This will then contribute to better understanding of the F508del defects as well as the mechanisms of drugs in the current (i.e. VX-770) and future markets.

Recent cryo-EM studies have solved 3 structures of CFTR: zCFTR and hCFTR in the "closed" state [23, 24] as well as zCFTR in the PKA phosphorylated, ATP-bound state [25]. Despite these structures providing novel insights on the CFTR structure, there are still important gaps in knowledge that must be filled:

1. There are certain regions of CFTR that remain unresolved like the R domain which is important for regulation of CFTR channel gating [23-25]. Thus, the interactions of the R domain with other domains of CFTR, which may be important for channel gating, remain unclear.

2. The structure of zCFTR upon PKA phosphorylation and ATP binding does not appear to be "open" [24]. Even though there are similarities in zCFTR and hCFTR in the "closed" state [24], the hCFTR in the PKA phosphorylated, ATP-bound state has yet to be solved and this structure may or may not be similar to zCFTR.

3. The protein is purified in detergent and thus, it remains unclear whether these structures reflect the actual conformational changes of CFTR at the lipid bilayer.

In this thesis, I explore the conformational changes of CFTR channel gating in the context of CFTR at the cell surface and attempt to fill the gaps of knowledge that were previously described. Specifically, I am interested in the modulations of CFTR at the cell surface by PKA phosphorylation, lipid interactions and the potentiator, VX-770.

As previously mentioned, PKA phosphorylation is an essential regulator of CFTR channel gating at the cell surface. Previous NMR studies on isolated NBD1 and regions of the R domain have provided some insights on the conformational changes of those CFTR domains upon PKA phosphorylation [56, 58, 59]. However, this may not reflect the full-length CFTR. Cryo-EM studies have also provided some insights on the conformational changes of CFTR upon PKA phosphorylation [25] but as previously mentioned, there are still gaps in knowledge on the exact conformational changes of CFTR upon PKA phosphorylation. The studies described in this thesis aim to provide more insights on the structural changes of hCFTR channel gating. Based on

the importance of the transmission interface for CFTR channel gating, I propose that PKA phosphorylation would enhance interactions at the transmission interface of full-length CFTR [40].

At the cell surface, CFTR is in the presence of lipids which may be important for its structure and function. Previous studies have shown that CFTR is also localized in lipid rafts that are rich in lipids and cholesterol which regulate CFTR confinement and dynamics at the cell surface [132, 175, 176]. However, the exact role of lipid interactions on CFTR structure and function is not well studied. In addition, the 3 cryo-EM structures that were solved in detergent micelles by the Chen group [23-25] are missing essential lipid: CFTR interactions and thus, may not reflect the conformational changes of CFTR channel gating at the cell surface. I propose that lipid interactions with CFTR are essential for CFTR channel activity and that the absence of these lipid: CFTR interactions would ultimately affect the conformation of the "open" state structure of CFTR. The studies described in this thesis may also provide a novel approach towards solving the CFTR structure in its native "open" state which can help to fill the gaps of knowledge presented in the current CFTR structures.

VX-770 was the first FDA approved therapy for CF patients with gating mutations that enhances CFTR channel gating at the cell surface [140, 156, 161]. Thus, it was surprising that micromolar concentrations of VX-770 have destabilizing effects on VX-809 rescued F508del-CFTR in *in vitro* experiments [162, 163, 177]. However, the mechanism of action of this destabilizing effect of micromolar concentrations of VX-770 is not known. Understanding the destabilizing effect of micromolar concentrations of VX-770 in the context of patient cells is important and helps drive the development of better drug therapies for CF patients. Based on previous observations in my laboratory, I propose that this destabilizing effect may be related to the lipophilicity of VX-770 on the lipid bilayer.

1.7.1 Thesis Organization

Chapter 2 investigates the effect of PKA phosphorylation on modifying the structure and intramolecular interfaces of CFTR. Applying newly developed biophysical methods, PKA phosphorylation was found to modify the secondary and tertiary structure of purified full-length Wt-CFTR. Based on the changes observed in the biophysical methods, I proposed that PKA phosphorylation modifies the transmission interface. Fluorescence-based assay of membrane

potential changes of disease-causing mutations at the transmission interface further support that transmission interface interactions are essential for phosphorylation-mediated channel gating of CFTR.

Chapter 3 investigates the effect of CFTR: lipid interactions on the channel function of purified full-length CFTR. A novel purification method using amphipol was found to retain CFTR: lipid interactions using a high-throughput phospholipid assay and lipid thin-layer chromatography. Applying ATPase and iodide efflux activity assays, we showed that this purified CFTR in amphipol exhibited significantly higher CFTR activity compared to purified CFTR in detergent that was applied in the cryo-EM studies by the Chen group. These results suggest that lipid interactions are essential for maintaining the channel competent structure and function of CFTR.

Chapter 4 investigates the mechanism of the previously reported *in vitro* destabilizing effect of supra-pharmacological concentrations of VX-770 on F508del-CFTR. Biochemical studies were employed to show that supra-pharmacological concentrations of VX-770 also destabilize the SLC membrane proteins, suggesting that the VX-770 destabilizing effect is non-specific. VX-770 analogs with varying degrees of lipophilicity were applied to find that the non-specific destabilizing effect of VX-770 is correlated with the lipophilicity of the drug. Applying polarized internal reflection fluorescence microscopy studies, we further show that supra-pharmacological concentrations of VX-770, and not its less lipophilic analog, increased the fluidity of the lipid bilayer and reorganized the lipid bilayer.

Chapter 5 summarizes the insights of these modulations on CFTR structure and function at the cell surface that were thoroughly discussed in Chapters 2-4. Lessons that were learned from certain experiments and the future directions of these studies are also discussed in this chapter.

Chapter 2 PKA phosphorylation modifies interactions at the transmission interface of CFTR

Contributions:

Study was designed by Stephanie Chin and C.E.B. based on discussions with the other authors mentioned in the research article above. S.C. generated and analyzed all the data presented in this chapter with the help from all the authors. D.Y. assisted in the design and performance of mutagenesis studies and channel activity measurements. A.J.M. contributed to design, performance, and analysis of synchrotron radiation circular dichroism (SRCD) studies. P.D.W.E. contributed to the development of CFTR purification methods and interpretation of intrinsic fluorescence studies. S.V.M. contributed to the design and performance of mutagenesis studies. B.A.W. provided advice regarding the performance of SRCD and oversaw analysis of results. Manuscript was written by S.C. and C.E.B. with input from all the authors.

2.1 Summary

CFTR is a multi-domain membrane protein that functions as a phosphorylation-regulated anion channel at the cell surface. Phosphorylation, predominantly by PKA, of the R domain of CFTR is absolutely required for its regulated channel activity [104, 105, 109]. As previously mentioned, the CFTR interface between the two cytosolic NBDs and CHs (conferred by ICLs extending from MSDs) has been referred to as a transmission interface [40]. The transmission interface is thought to be critical for the regulated channel activity of CFTR [40]. However, it was unclear if phosphorylation modifies the transmission interface. Towards this, we first studied purified full-length Wt-CFTR protein using spectroscopic techniques, which included synchrotron radiation circular dichroism (SRCD) and intrinsic tryptophan fluorescence, to determine the consequences of PKA-mediated phosphorylation on the overall structure of full-length CFTR. SRCD spectroscopy confirmed that purified full-length Wt-CFTR from my laboratory is properly folded and is structurally responsive to PKA phosphorylation with an increase in alpha-helical structure. Intrinsic tryptophan fluorescence studies of CFTR showed that PKA phosphorylation modified urea-mediated unfolding and reduced iodide-mediated quenching of purified Wt-CFTR protein. Based on the properties of the transmission interface, our biophysical studies on purified full-length Wt-CFTR suggests that PKA phosphorylation may be modifying the transmission interface. To specifically probe this interface, we then employed *in vivo* cysteine cross-linking studies with a cell permeable cross-linker at the NBD1 side of the transmission interface (CH4: NBD1 and CH1: NBD1). However, we did not observe phosphorylation-mediated changes at those interfaces which was consistent with previous studies [30, 41]. I propose that this may be due to the inability of cysteine cross-linking studies to capture subtle and dynamic interactions of CFTR at the cell surface. Importantly, we have found that the rate of phosphorylation-dependent channel activation was compromised by the introduction of disease-causing mutations of the residues in either of the two CHs (CH1 and CH4) that are predicted to interact with NBD1 at the interface. Together, these results suggest that PKA phosphorylation modifies the transmission interface of CFTR and that this modification facilitates CFTR channel activation.

2.2 Introduction

CF is caused by mutations of a unique ABC channel, CFTR, which is a multi-domain protein that functions as a phosphorylation-regulated anion channel at the cell surface. As previously

mentioned, CFTR consists of two NBDs, two MSDs, a unique R domain and a newly defined lasso motif. The interface between the NBDs and MSDs of CFTR is an alpha-helical region consisting of ICLs and CHs [30]. The CHs interact with the NBDs at an interface which has been referred to as the transmission interface [40]. The transmission interface of CFTR was proposed to relay the conformational changes of the NBDs, upon ATP binding and hydrolysis, to the MSDs for channel opening or closing [178, 179]. Previous studies have found that the major CF-causing mutation, F508del, disrupts the transmission interface (i.e. at CH4: NBD1 and CH1: NBD1), which may result in its defective channel gating, and supports the importance of the transmission interface for channel gating [145, 146, 180].

Our understanding of the molecular basis for PKA phosphorylation-dependent regulation of CFTR channel activation has evolved considerably and we have gained greater insight into its complexity. The phosphorylation-regulated R domain of CFTR is a flexible, disordered region that undergoes dynamic interactions with other CFTR domains [54, 56]. PKA phosphorylation of the R domain is thought to alter multiple interactions with other CFTR domains, with certain interactions becoming weaker [56] and other interactions acquiring higher affinities [113, 181]. The regulation of domain: domain interactions has been studied using isolated domains and in chemical cross-linking studies of a full-length cys-less variant, with its native cysteine residues replaced, of CFTR protein with strategically inserted cysteine pairs at interfaces of interest. For example, studies of isolated CFTR domains suggest that PKA phosphorylation of the phospho-regulated insertion within NBD1 (the RI) decreases its interaction with the core of NBD1 and this in turn, acts allosterically to promote interaction between CH1 of ICL1 and NBD1 at the transmission interface [56, 58]. *In vivo* cysteine cross-linking studies using a cell permeable cross-linker, bismaleimidoethane (BMOE), of a full-length cys-less variant Wt-CFTR protein showed that phosphorylation enhanced NBD1: NBD2 dimerization [30, 41]. Studies of the consequences of strategic single site mutations at the NBD1: NBD2 interface also supported the importance of this phosphorylation-regulated interface in channel activation [49, 110]. In contrast to the above predictions based on isolated domains, chemical cross-linking studies of full-length cys-less variants of Wt-CFTR using cell impermeable cross-linkers on membrane vesicles failed to show modification of the interaction between the CHs and the NBDs by phosphorylation [30, 41]. These findings do not support the previous hypothesis that this transmission interface between the pore and catalytic domains is regulated by phosphorylation.

On the other hand, the previous hypothesis was supported by a recent study that showed that an isolated peptide derived from ICL1 disrupted phosphorylation-dependent activation of full-length CFTR [116].

Hence, there is considerable uncertainty regarding the regulation of the transmission interface by PKA phosphorylation, highlighting the need to develop novel approaches for its study in the context of the full-length protein. The goal of this study was to employ biophysical approaches, SRCD and intrinsic tryptophan fluorescence, that would permit insight into dynamic conformational changes caused by PKA phosphorylation in the purified full-length Wt-CFTR protein. We then specifically probed the CH: NBD1 interfaces of the transmission interface as there appears to be a gap between ICL1 and NBD1 from the "closed" and PKA phosphorylated, ATP-bound zCFTR structures which is consistent with CH1 being dynamic and regulated by phosphorylation. Towards this, we applied the *in vivo* cysteine cross-linking studies with a cell permeable cross-linker (BMOE), that have previously found that phosphorylation enhanced NBD1: NBD2 dimerization [49], to determine whether we can observe an *in vivo* modification of CH: NBD1 interfaces by phosphorylation that the other cysteine cross-linking studies were unable to detect with their methods [30, 41]. Further, the relative importance of the CHs in phosphorylation-dependent channel activation was probed in comparative functional studies of disease-causing mutations at the CH: NBD1 interfaces.

2.3   Materials and Methods

2.3.1   Purification of full-length Wt-CFTR

Full-length Wt-CFTR with a C-terminal polyhistidine (His$_{10}$) tag was overexpressed in *Sf9* cells and crude membranes were prepared as previously described [140]. Crude membranes were solubilized by 2% *fos*-choline 14 (Anatrace, Maumee, OH). CFTR was purified via affinity to Ni-NTA column and exchanged to n-Dodecyl β-D-maltoside (DDM, BioShop Canada Ltd., Burlington, Ontario, Canada) detergent micelles. The purified protein sample was run on a 4-12% SDS-acrylamide gel and developed by the silver stain method.

2.3.2   SRCD spectroscopy

Full-length CFTR protein was purified in buffer (20 mM sodium phosphate, 25 mM sodium chloride, 1 mM DDM, pH 7.2). The protein sample was split into two conditions: non-PKA

phosphorylated and PKA phosphorylated CFTR. In the PKA phosphorylated condition, purified CFTR was phosphorylated with 200 nM PKA (New England Biolabs Ltd., Ipswich, MA) and 5 mM Mg-ATP (Sigma, St. Louis, MO) in buffer (20 mM sodium phosphate, 25 mM sodium chloride, 1 mM DDM, pH 7.2) on the Ni-NTA column (Qiagen, Hilden, Germany) as previously described [140]. PKA (38 kDa) was effectively washed out of the PKA phosphorylated sample with buffer (20 mM sodium phosphate, 25 mM sodium chloride, 1 mM DDM, pH 7.2) and a centrifugal filter with a cutoff of 100 kDa (Merck Millipore Ltd., Tullagreen, Ireland) as previously described [140]. The non-PKA phosphorylated sample was also washed the same way as the PKA phosphorylated CFTR sample. SRCD spectra were obtained at the ISA synchrotron (Aarhus, Denmark) using a 0.1 mm pathlength sealed Suprasil (Hellma Analytics, Müllheim, Germany) quartz cuvette. For each spectrum, a stepsize of 1 nm and an averaging time of 2 s were used. In each case, three replicate scans of the sample were subtracted from three scans of the baseline (20 mM sodium phosphate, 25 mM sodium chloride, 1 mM DDM, pH 7.2) and the net spectrum calibrated to a spectrum of camphorsulfonic acid (Sigma) measured prior to data collection [182]. Two sample loadings, each with three replicate scans, were conducted for each condition (non-PKA and PKA phosphorylated). Delta epsilon (Δε) curves were scaled as previously described [183]. All processing was carried out using the CDTool software [184]. Differences were identified from error bars (indicating reproducibility levels) at all wavelengths, set at 1 s.d.

2.3.3   Intrinsic tryptophan fluorescence

Purified full-length Wt-CFTR was concentrated to concentrations between 50 and 70 µg/ml as determined by the NanoDrop 2000 (1 Abs ≈ 1 mg/ml, ThermoFisher) in buffer (25 mM HEPES, 25 mM sodium chloride, 1 mM DDM, pH 7.2). Protein sample was split into two conditions: non-PKA phosphorylated and PKA phosphorylated as previously described. Intrinsic tryptophan fluorescence studies of the purified protein were conducted on the Photon Technology International QM80 spectrofluorimeter (HORIBA Scientific, Edison, NJ) with bandwidths of 2 nm for both excitation and emission and using a 10 x 2 mm quartz cuvette (Hellma Analytics). Fluorescence traces were corrected for dilution, inner filter effect, scattering and background (via subtraction of the buffer fluorescence trace).

2.3.4 Urea denaturation studies

Samples of 130 µl were then incubated at each urea concentration for 10 min at room temperature. Tryptophan residues were excited at 290 nm and emission scans were run from 300 to 400 nm. The maximum emission wavelength (λ_{max}) at each urea concentration was determined and plotted against the urea concentration with GraphPad Prism (version 6.0c). Sigmoidal curves of emission wavelength maxima (λ_{max}) were fitted to the following equation using GraphPad Prism:

$$f(C) = (exp(-m*(C_m-C)/RT)/(1+exp(-m*(C_m-C)/RT)))$$

where "m" is the "m" value or slope of the urea denaturation curve, C is the individual urea concentration and C_m is the midpoint urea concentration [185]. 3 µM of N-acetyl-L-tryptophanamide (NATA, Sigma) was used as a control in which all the tryptophan residues were exposed to the solvent environment.

2.3.5 Quenching studies

Purified CFTR samples were titrated with 2 µl titrations of 2.5 M stock concentrations of acrylamide, potassium iodide or cesium chloride quenchers dissolved in buffer (25 mM HEPES, 25 mM sodium chloride, 1 mM DDM, pH 7.2). Fluorescence intensity at each quencher concentration was taken over a 20 s interval by excitation at 290 nm and emission at 322 nm. Fluorescence intensities were averaged over the 20 s interval and corrected for background. Values of initial fluorescence intensity of purified CFTR without quenchers (F_0) over fluorescence intensity at each quencher concentration (F) were plotted at each quencher concentration ([Q]). This plot known as a Stern-Volmer plot generates a linear regression using GraphPad Prism with the following equation:

$$F_0/F = 1 + K_{sv}[Q]$$

The Stern-Volmer constant (K_{sv}) was determined as the slope of each linear regression.

2.3.6 Generation and expression of mutants

The full-length cys-less Wt-CFTR constructs with V510C at NBD1 and A1067C at CH4 on separate plasmids and on the same plasmid (V510C/A1067C) were kindly provided by Dr. David

Clarke (Toronto, Ontario, Canada) [42]. To probe the CH1: NBD1 interface, primers of R170C (Forward: 5'-CTT TAA AGC TGT CAA GCT GTG TTC TAG ATA AAA TAA G-3' and reverse: 5'-CTT ATT TTA TCT AGA ACA CAG CTT GAC AGC TTT AAA G-3'), W401C (Forward: 5'-GTA ACA GCC TTC TGT GAG GAG GGA TTT GG-3' and reverse: 5'-CCA AAT CCC TCC TCA CAG AAG GCT GTT AC-3') and E476C (Forward: 5'-GAT TAT GGG AGA ACT GTG TCC TTC AGA GGG TAA AAT TAA G-3' and reverse: 5'-CTT AAT TTT ACC CTC TGA AGG ACA CAG TTC TCC CAT AAT C-3') were designed to generate single and double cysteine mutants on the cys-less Wt-CFTR cDNA template that was kindly provided by Dr. David Clarke [42]. Primers of disease-causing loop mutants, R170G (Forward: 5'-GAC TTT AAA GCT GTC AAG CGG TGT TCT AGA TAA AAT AAG-3' and reverse: 5'-CTT ATT TTA TCT AGA ACA CCG CTT GAC AGC TTT AAA GTC-3') and A1067T (Forward: 5'-GGA CAC TTC GTA CCT TCG GAC GG-3' and reverse: 5'-CCG TCC GAA GGT ACG AAG TGT CC-3'), were generated on full-length human Wt-CFTR cDNA (pcDNA3.1). Mutations were generated using the KAPA HiFi HotStart PCR Kit (KAPA Biosystems, Woburn, MA) and plasmid DNA was generated with the QIAprep Spin Miniprep Kit (Qiagen). Mutations were confirmed with DNA sequencing (TCAG, Toronto, Ontario, Canada). Plasmid DNA of mutants were transfected using Polyfect Transfection Reagent (Qiagen) in human embryonic kidney (HEK)-293 GripTite (GT) cells kindly provided by Dr. Daniela Rotin (Toronto, Ontario, Canada). Transfected cells were then temperature rescued at 27°C for 24 h.

2.3.7   FLIPR® membrane potential assay

The following steps of the fluorescence imaging plate reader (FLIPR®) assay were conducted at 27°C. Cells were loaded with 0.5 mg/ml FLIPR® membrane potential dye (Molecular Devices, Sunnyvale, CA) in sodium gluconate buffer (140 mM sodium gluconate, 0.5 mM potassium gluconate, 2 mM calcium gluconate, 2 mM magnesium gluconate, 10 mM HEPES, 12 mM sodium bicarbonate, pH 7.4) for 45 min. Fluorescence was recorded at excitation of 530 nm and emission of 560 nm on the fluorescence plate reader (SpectraMax i3X, Molecular Devices). Baseline fluorescence was read for 5 min and stimulation of CFTR activity by 10 µM forskolin (Sigma) was read for up to 15 min. The maximum peak of activation and the maximum rate during the first 5 min of forskolin stimulation, which was determined by linear regression with GraphPad Prism, were analyzed.

2.3.8   Cysteine cross-linking

Cells transfected with cys-less Wt-CFTR constructs were pre-treated with the cAMP agonists, 10 μM forskolin and 100 μM 3-Isobutyl-1-methylxanthine (Sigma), or vehicle (DMSO) for 30 min at 27°C. 50 μM BMOE (Life Technologies, Rockford, IL) in Dulbecco's modified Eagle's medium media (DMEM, Wisent, St-Bruno, Quebec, Canada) was added to HEK-293 GT cells transfected with the cys-less Wt constructs for 1 h on ice as previously described [49]. Transfected HEK-293 GT cells were lysed with radioimmunoprecipitation assay buffer (50 mM Tris-Base, 150 mM sodium chloride, 1 mM EDTA, 1% (v/v) Triton X-100, 0.1% (v/v) SDS, 1X protease inhibitor cocktail (AMRESCO, Cleveland, OH), pH 7.4). Protein samples were run on 6% Tris-Glycine sodium dodecyl sulfate (SDS) gels (Life Technologies, Carlsbad, CA) and transferred onto nitrocellulose paper. Immunoblots were probed for total CFTR protein with hCFTR NBD2 specific (amino acid 1204-1211) IgG2b mAb596 antibody (1:1000, University of North Carolina at Chapel Hill, Chapel Hill, NC, code: A4) overnight at 4°C and horseradish peroxidase-conjugated goat anti-mouse IgG secondary antibody (1:2000, Pierce, Rockford, IL) for 1 h at room temperature. Immunoblots were probed for phosphorylated CFTR protein with phosphorylation-sensitive (anti-Ser813, quenched by PKA phosphorylation) IgG1 mAb217 antibody (1:1000, University of North Carolina at Chapel Hill, code: A3) overnight at 4°C and horseradish peroxidase-conjugated goat anti-mouse IgG secondary antibody (1:2000, Pierce) for 1 h at room temperature. The specificities of these primary antibodies on CFTR epitopes were previously described [41, 107, 186]. Protein loading was normalized with the calnexin-specific rabbit pAb (1:10000, Sigma, cat. no.: C4731) primary antibody overnight at 4°C and horseradish peroxidase–conjugated goat anti-rabbit IgG secondary antibody (1:10000, Pierce) for 1 h at room temperature. Blots were exposed with Amersham enhanced chemiluminescent reagent (GE Healthcare Life Sciences, Mississauga, Ontario, Canada) on the Li-Cor Odyssey Fc (LI-COR Biosciences, Lincoln, NE) in a linear range of exposure. Normalized densitometry of immunoblot bands to total protein signal were analyzed with ImageJ 1.48v [187].

2.3.9   Expression and function of disease-causing loop mutants

Immunoblotting of disease-causing loop mutants were performed as previously mentioned with the exception that the immunoblots were probed with hCFTR NBD2 IgG2b mAb596 antibody (1:2000, University of North Carolina, code: A4) overnight at 4°C and horseradish peroxidase-

conjugated goat anti-mouse IgG secondary antibody (1:4000, Pierce) for 1 h at room temperature. The half maximal effective concentration (EC_{50}) values of phosphorylation-dependent channel activation of Wt, R170G and A1067T were determined by activating the channel with various forskolin concentrations (i.e. 0, 0.08, 0.16, 0.31, 0.63, 1.25, 2.5, 5 and 10 µM) and normalizing the maximum peak of activation to no forskolin control in the FLIPR® membrane potential assay. Curves were fit with the dose-response–stimulation log (agonist) versus response (three parameters) fit in GraphPad Prism. Slopes of activation within 4.5 min after 0.6 µM forskolin (the forskolin concentration closest to all the EC_{50} values of Wt and the disease-causing mutants) were determined by linear regression on GraphPad Prism.

2.3.10 Bioinformatics

The locations of CH residues, R170 and A1067, were identified from the Dalton-Kalid homology model [31] using the molecular graphics package, PyMOL (53). The secondary structure predictions of Wt-CFTR and the mutants (R170G, A1067T and R170G+A1067T) were conducted using the I-TASSER server [188-191]. The ResQ algorithm of I-TASSER generated the B-factor values by taking into account the changes in local structural assembly along with the sequence and structural profiles (30-33). These values were then normalized based on the z-scores [188-191].

2.4 Results

2.4.1 Purified full-length Wt-CFTR is properly folded and its structure is modified by PKA phosphorylation

Full-length Wt-CFTR was purified following expression in *Sf9* membranes as previously described [140]. Briefly, CFTR was extracted using the detergent, *fos*-choline 14, and CFTR (bearing a polyhistidine tag) was partially purified by virtue of the affinity of this tag to the Ni-NTA resin [140]. *Fos*-choline 14 was replaced with DDM and the protein: detergent complex was eluted from the affinity matrix [140]. The purified protein was treated with 200 nM PKA and 5 mM Mg-ATP on the Ni-NTA column to enable extensive washing as described [140] and phosphorylation at multiple consensus sites was confirmed previously using SRM-MS [101]. Applying this method [140], I was successful in purifying full-length Wt-CFTR as shown by the single, silver-stained protein band running at the expected molecular weight of approximately 140-150 kDa for the core-glycosylated form (band *B*) of CFTR expressed in *Sf9* cells (Figure

2.1A). In a subset of our experiments, we confirmed that the purified full-length Wt-CFTR is functional as a phosphorylation and ATP-regulated anion channel upon reconstitution in proteoliposomes using our previously published iodide efflux protocols [140, 192].

SRCD spectroscopy was used to examine Wt-CFTR. The spectra ressembled that of a protein with a high helical content as expected with negative peaks at 209 and 222 nm, and a positive peak at 192 nm (Figure 2.1B). Furthermore, comparison of the spectra of non-PKA phosphorylated Wt-CFTR and PKA phosphorylated Wt-CFTR indicated a subtle yet significant increase in the peak at 192 nm, which corresponds to an increase in helical structure content (Figure 2.1B). Indeed, the ratio of the magnitudes of the 192 and 222 nm peaks increased from 1.74 in the non-PKA phosphorylated state to 1.86 after PKA phosphorylation, a clear indication that the shapes of the curves are different and that the observed differences do not simply arise from different magnitudes of the spectra [193]. Previous NMR and CD spectroscopy studies on the isolated NBD1 and the R region (residues 654-838) have found that phosphorylation decreased the helical content of those isolated domains [56, 194]. Thus, the increase in helical structure upon PKA phosphorylation observed by SRCD in the full-length Wt-CFTR is likely due to allosteric effects induced by phosphorylation of the RI and R region [30, 31].
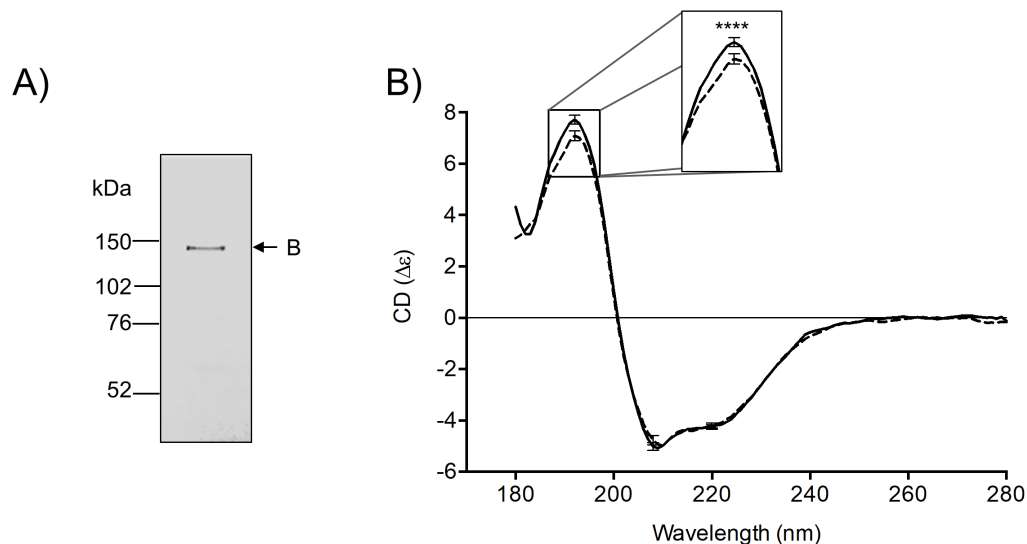
Figure 2.1: Purified full-length Wt-CFTR is properly folded and PKA phosphorylation modifies its secondary structure.
(**A**) Silver stained gel shows the purity of the full-length WT-CFTR and that it runs at its expected molecular weight of around 140–150 kDa in its core-glycosylated state (band *B*), the only form of CFTR that is expressed in the *Sf9* expression system. (**B**) The scaled Δε SRCD

spectra show that purified full-length Wt-CFTR is mostly α-helical with characteristic negative peaks at 209 and 222 nm and a positive peak at 192 nm. SRCD spectra for untreated purified full-length Wt-CFTR in DDM micelles (*hashed line*) and PKA-phosphorylated CFTR (*solid line*) are shown. *Error bars* indicate ± 1 S.D. between a total of six spectra from three replicate scans of two aliquots of sample from the same purification. The *inset* shows that phosphorylation significantly increases the peak at 192 nm (****, $p < 0.0001$, t test) relative to that at 222 nm.

Previous intrinsic tryptophan fluorescence studies of the *Escherichia coli* vitamin B_{12} ABC transporter, BtuCD, have shown that the interface between the CHs conferred by the MSD subunits (BtuC) and the NBD subunits (BtuD) was sensitive to urea-mediated unfolding [195, 196]. During the time of these studies, the CFTR structures solved by cryo-EM [23-25] were not published so I applied the CFTR homology model based on the structure of Sav1866 that was generated by Dalton and colleagues [31] to predict the localization of the tryptophans on CFTR. According to the CFTR homology model [31], the tryptophans endogenous to CFTR reside at the membrane: solvent interface and at the transmission (CH: NBD) interface (Figure 2.2A and B).
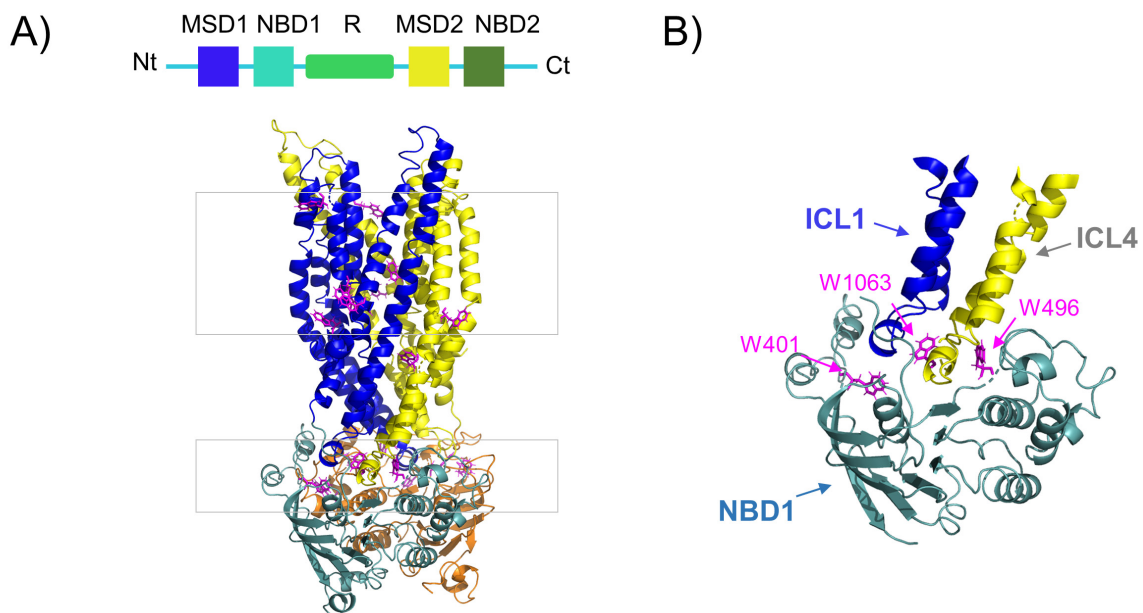
Figure 2.2: Localization of tryptophans on the CFTR homology model suggests that intrinsic tryptophan fluorescence can be applied to probe whether PKA phosphorylation modifies the transmission interface.
(**A**) *Top:* linear arrangement of CFTR domains from N- to C-terminal end which shows the MSD1 in blue, NBD1 in teal, R domain in green, MSD2 in yellow and NBD2 in orange. *Bottom:* The tryptophans on a CFTR homology model based on a bacterial transporter, Sav1866 [31], are

shown as pink sticks and are mostly located at the membrane: solvent interface (with the membrane indicated by a rectangle) and CH: NBD interface, i.e. the transmission interface (indicated by a distinct rectangle below the membrane). The R domain is omitted from this homology model of CFTR. (**B**) Close-up view of the transmission interface with NBD1 of the CFTR homology model [31] as this interface has been studied extensively with regard to its role in channel activation. This shows that the transmission interface contains the CHs of the ICLs and NBD1 with multiple tryptophans (i.e. 401, 496 and 1063) shown as pink sticks which are located at the interface between NBD1 (teal) and ICL1 (blue) or ICL4 (yellow).

Thus, I was prompted to determine whether measurements of intrinsic tryptophan fluorescence of purified full-length Wt-CFTR could reveal phosphorylation-associated changes in urea-mediated unfolding. DDM solubilized full-length Wt-CFTR exhibited a decrease in fluorescence intensity (Figure 2.3A inset) and a red shift in λ_{max} with increasing concentrations of urea, from its initial wavelength of 322 nm to its final wavelength of 332 nm (Figure 2.3A and B). The decrease in fluorescence intensity and red shift in the λ_{max} reported the change in the chemical environment of the tryptophans upon urea-induced unfolding of the protein. Interestingly, this red shift did not reach the λ_{max} of 355 nm observed in a NATA sample of free soluble tryptophan analogues (Figure 2.3A), suggesting that urea failed to completely unfold CFTR. Hence, akin to the previous SRCD experiments, intrinsic tryptophan fluorescence studies also demonstrated that the purified protein is properly folded in DDM micelles.

PKA phosphorylation shifted the concentration dependence for urea-induced unfolding to the right, from a C_m of approximately 2.8 M in the non-PKA phosphorylated sample to a C_m of approximately 4.0 M in the PKA phosphorylated sample (Figure 2.3B). In addition, the slope of the transition known as the "m" value was lower in the PKA phosphorylated condition: the "m" value was 0.8 kcal/mol·M^{-1} in non-PKA phosphorylated Wt-CFTR compared to 0.6 kcal/mol·M^{-1} in PKA phosphorylated Wt-CFTR (Figure 2.3B). These findings suggest that PKA phosphorylation protected the chemical environment of endogenous tryptophans from urea-induced unfolding at either the membrane: solvent interface or at the CH: NBD interface (Figure 2.2A and B*)*.
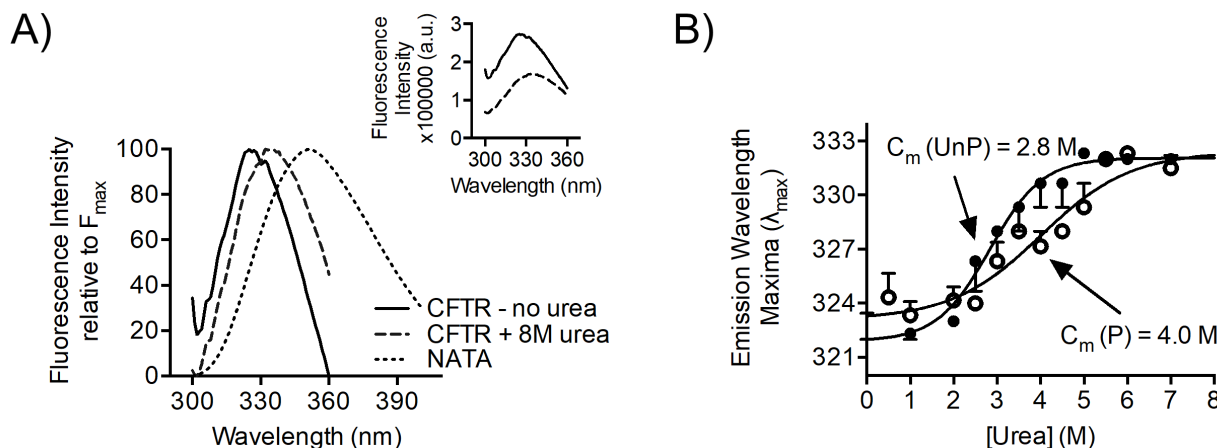
Figure 2.3: PKA phosphorylation modifies urea-mediated unfolding of purified full-length Wt-CFTR protein.
(**A**) Representative intrinsic tryptophan fluorescence readouts of PKA phosphorylated full-length Wt-CFTR prior to and after urea denaturation that were normalized to fluorescence maxima (F_{max}). The intrinsic tryptophan fluorescence of PKA phosphorylated full-length Wt-CFTR (solid line) exhibits a red shift in emission wavelength maxima (λ_{max}) upon treatment with the final concentration of 8 M urea (dashed line). CFTR was not completely denatured by 8 M urea as the trace did not completely overlap with the NATA trace (dotted line) in which all tryptophans are exposed to the solvent. *Inset:* Raw fluorescence intensity of untreated purified full-length Wt-CFTR protein (solid line) and treated protein with 8 M urea (dashed line) shows that urea shifts the λ_{max} and decreases the fluorescence intensity of purified CFTR. (**B**) Comparing the red shift in λ_{max} across urea concentrations of PKA phosphorylated (open circles) and non-PKA phosphorylated (closed circles) full-length CFTR shows that the PKA phosphorylated Wt-CFTR is less susceptible to urea denaturation compared to non-PKA phosphorylated CFTR. These two denaturation curves are significantly different: non-PKA phosphorylated Wt-CFTR has a C_m of 2.8 M urea whereas PKA phosphorylated Wt-CFTR has a C_m of 4.0 M urea. The "m" value or slope of unfolding was also lower in the PKA phosphorylated sample in which the "m" value was 0.8 kcal/mol·M^{-1} in the non-PKA phosphorylated Wt-CFTR compared to 0.6 kcal/mol·M^{-1} in the PKA phosphorylated Wt-CFTR. Error bars indicate +/- 1 SD between replicate samples (n = 5 biological replicates and n = 5 technical replicates, p = 0.0057, Two-way ANOVA).

In order to determine whether the intrinsic tryptophan fluorescence measurements reported the effect of PKA phosphorylation on the membrane: solvent interface or on the transmission interface, fluorescence quenching studies were conducted to probe the environment of the tryptophans that were responsible for the intrinsic tryptophan fluorescence of purified full-length Wt-CFTR. Quenchers of different polarity and charge were tested which include: polar and uncharged acrylamide, negatively charged iodide, and positively charged cesium salt. As expected, NATA was readily quenched by all quenchers with high K_{sv} values (Table 2.1) as the tryptophan analogues were completely exposed to the solvent and were therefore highly

accessible to the quenchers. In contrast, tryptophans intrinsic to full-length Wt-CFTR were relatively resistant to quenching with significantly lower K_{sv} values compared to NATA as expected for a properly folded protein (Table 2.1). Interestingly, all quenchers reduced the intrinsic tryptophan fluorescence of purified full-length Wt-CFTR in a linear fashion suggesting that only one cluster of tryptophans was reported for each quencher of this assay (Figure 2.4A-C). Quenching with polar and uncharged acrylamide was not affected by the phosphorylation status of CFTR (Figure 2.4A). I propose that acrylamide quenching may be reporting the membrane: solvent interface due to its difficulty to diffuse across the membrane [197]. In contrast, quenching with charged quenchers, iodide and cesium, were dependent on its phosphorylation status (Figure 2.4B and C). PKA phosphorylation of purified CFTR led to a lower K_{sv} value upon quenching with negatively charged iodide whereas it led to a higher K_{sv} value upon quenching with positively charged cesium (Table 2.1). Based on their properties, the charged quenchers may be reporting the cluster of tryptophans at the cytosol. In addition, the negative charge conferred by phosphorylation may have modulated the propensity of the reporting tryptophans to be quenched by aqueous, charged agents. Interestingly, there is a phosphorylation site, pS422 on the RI (which Lewis and colleagues report it as residues 413-428 [53] whereas Aleksandrov and colleagues report it as residues 404-435 [46]) of NBD1, which is proximal to the ICL: NBD1 interface [56, 58, 59, 198]. Previous NMR studies have suggested that phosphorylation at pS422 enhanced interactions at the ICL1: NBD1 and ICL4: NBD1 interfaces [56, 58, 59]. Based on these results, I propose that PKA phosphorylation may be modifying the electrostatic environment of the transmission interface as there are multiple tryptophans (including residues 401, 496 and 1063) residing in proximity to the putative transmission interface consisting of CH1, CH4 and NBD1 (Figure 2.2B) which may be reported in the intrinsic tryptophan fluorescence studies.

A)   B)   C)
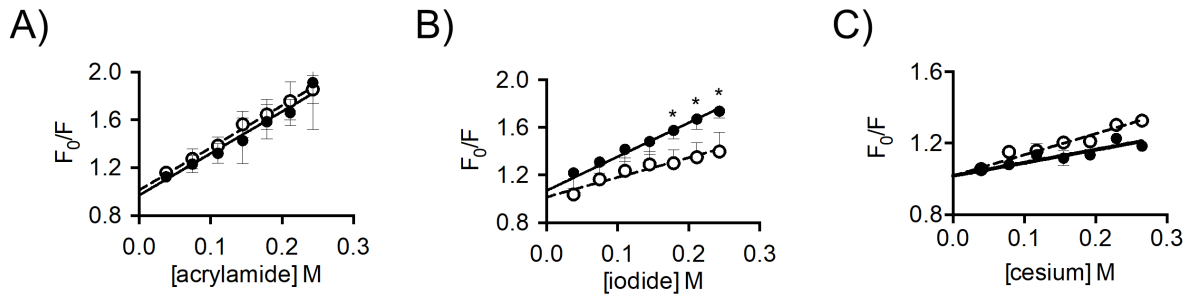
Figure 2.4: PKA phosphorylation modifies the tertiary structure of purified full-length Wt-CFTR, possibly within an electrostatic region.
(**A-C**) Stern-Volmer plots of tryptophan quenching of purified full-length non-PKA phosphorylated (closed circles) and PKA phosphorylated (open circles) Wt-CFTR at the major intrinsic tryptophan fluorescence peak, obtained from excitation at 290 nm and emission at 322 nm, were generated. Quenching with (**A**) acrylamide shows no difference upon PKA phosphorylation (n = 3 biological replicates and n = 3 technical replicates, $p > 0.05$, multiple t tests using the Holm-Sidak method). Quenching with (**B**) negatively charged iodide was significantly reduced upon PKA phosphorylation at high iodide concentrations starting at 0.18 M iodide (n = 3 biological replicates and n = 3 technical replicates, $*p < 0.005$, Multiple t tests using the Holm-Sidak method). (**C**) Interestingly, quenching of purified full-length non-PKA-phosphorylated (closed circles) and PKA-phosphorylated (open circles) WT-CFTR with positively charged cesium (n = 3 biological replicates and n = 3 technical replicates) showed an opposite quenching effect from iodide upon PKA phosphorylation, suggesting that phosphorylation modifies an electrostatic environment of the protein. Error bars indicate +/- 1 SD between replicate samples.

Table 2.1: K$_{sv}$ constants of intrinsic tryptophan fluorescence quenching studies of NATA, non-PKA and PKA phosphorylated Wt-CFTR.
Summary of the K$_{sv}$ values of NATA, non-PKA phosphorylated and PKA phosphorylated Wt-CFTR with the quenchers: acrylamide, iodide and cesium. The K$_{sv}$ values of all quenchers were significantly higher in the NATA sample compared to purified full-length Wt-CFTR. The K$_{sv}$ values of non-PKA phosphorylated and PKA phosphorylated Wt-CFTR with acrylamide were not different outside the range of error whereas the K$_{sv}$ values with iodide and cesium were different outside the range of error. Based on these results, I propose that intrinsic tryptophan fluorescence may be reporting the tryptophans at the transmission interface.

Sample	K$_{sv}$ (M^{-1})		
	Acrylamide	Iodide	Cesium
NATA	23.57 ± 2.66	15.81 ± 0.54	3.58 ± 0.10
Non-PKA phosphorylated CFTR	3.49 ± 0.41	2.85 ± 0.22	0.73 ± 0.22
PKA phosphorylated CFTR	3.53 ± 0.22	1.89 ± 0.34	1.18 ± 0.38

After the hCFTR structure in the "closed" state was published [24], I was interested to determine whether the localizations of the tryptophans on the native protein structure (Figure 2.5) were similar to that on the CFTR homology model (Figure 2.2). I have found that the tryptophans were also localized at the membrane: solvent and transmission interfaces which were similar to that on the CFTR homology model (Figure 2.2). This further supported that my intrinsic tryptophan fluorescence studies reported PKA phosphorylation-mediated modification of the transmission interface of the full-length CFTR protein structure.
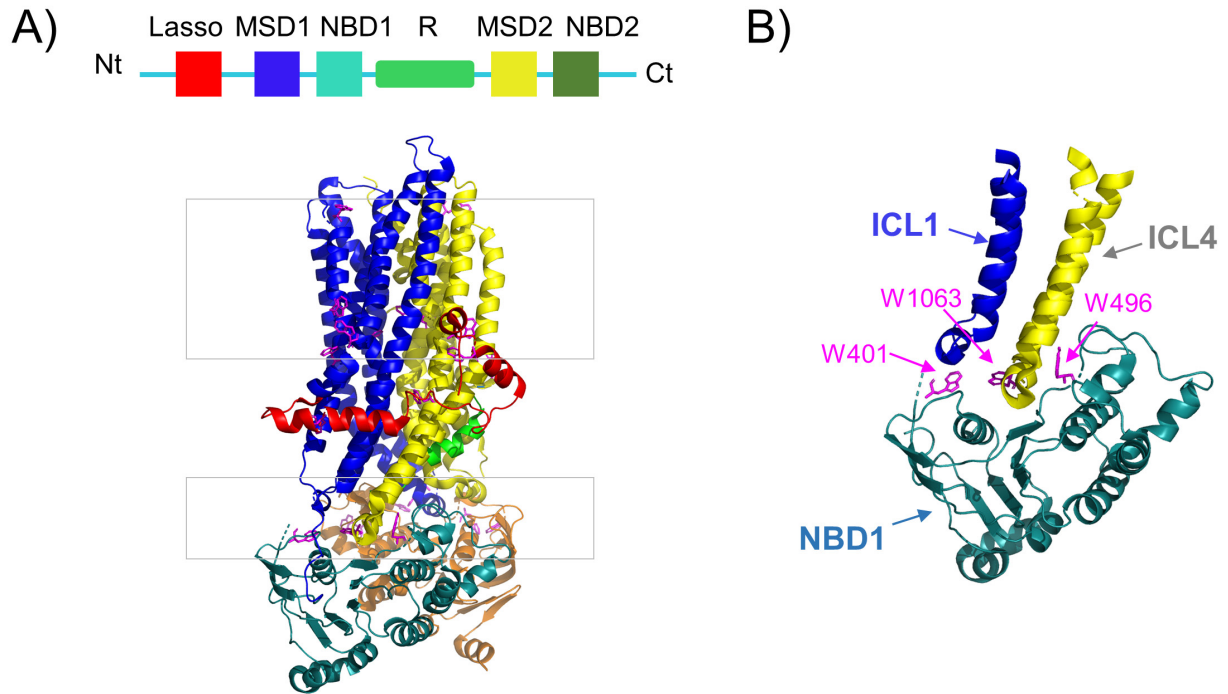
Figure 2.5: Localization of tryptophans on hCFTR structure in the "closed" state (PDB: 5UAK) was quite similar to the predictions based on the CFTR homology model.
(**A**) *Top:* linear arrangement of CFTR domains from N- to C-terminal end which shows the lasso motif in red, MSD1 in blue, NBD1 in teal, R domain in green, MSD2 in yellow and NBD2 in orange. *Bottom:* The tryptophans on hCFTR structure in the "closed" state [24], are shown as pink sticks and are mostly located at the membrane: solvent interface (with the membrane indicated by a rectangle) and CH: NBD interface, i.e. the transmission interface (indicated by a distinct rectangle below the membrane). (**B**) Close-up view of the transmission interface with NBD1 of the hCFTR structure in the "closed" state [24], as this interface has been studied extensively with regard to its role in channel activation. This shows that the transmission interface contains the CHs of the ICLs and NBD1 with multiple tryptophans (i.e. 401, 496 and 1063) shown as pink sticks which are located at the interface between NBD1 (teal) and ICL1 (blue) or ICL4 (yellow).

2.4.2 Cysteine cross-linking studies using a membrane permeable sulphydryl modifying reagent confirmed a physical interaction between CH4 of ICL4 and NBD1

Previous studies investigating phosphorylation-dependent changes in the affinity of the CHs and NBD1 used chemical cross-linking of cysteine pairs introduced on opposing surfaces of NBD1 and CH1 or CH4 (Figure 2.5A); cysteine pairs were introduced at positions previously shown to

reside at these domain: domain interfaces in a cys-less CFTR construct [30, 41]. These cross-linkers were long and membrane impermeable, necessitating the application of these sulphydryl reagents to inside-out membrane vesicles [30, 41]. In the current work, I was prompted to determine if phosphorylation-dependent changes in cysteine cross-linking could be detected using the short (8 Å) and membrane permeable maleimide reagent, BMOE, as this was previously successful in capturing phosphorylation-dependent changes of the NBD1: NBD2 interface in full-length cys-less CFTR [49].

Firstly, I confirmed that the cysteine mutants were expressed at the cell surface in HEK-293 GT cells as shown by the presence of complex-glycosylated form of the protein (band *C*) in the immunoblot (Figure 2.6A). In addition, CFTR activation of the cysteine mutants was studied using the membrane potential plate reader assay: FLIPR® [199]. As shown in Figure 2.6B, all of the cysteine mutants were functionally expressed as cAMP-activated conductances. Interestingly, the overall rate of activation was significantly reduced in V510C/A1067C cys-less CFTR (Figure 2.6C). This defect could reflect a disulphide bond formation for the pair of cysteines introduced at CH4 and NBD1 which could account for attenuation of channel activity by modifying important dynamic conformational changes as previously suggested [30, 41].
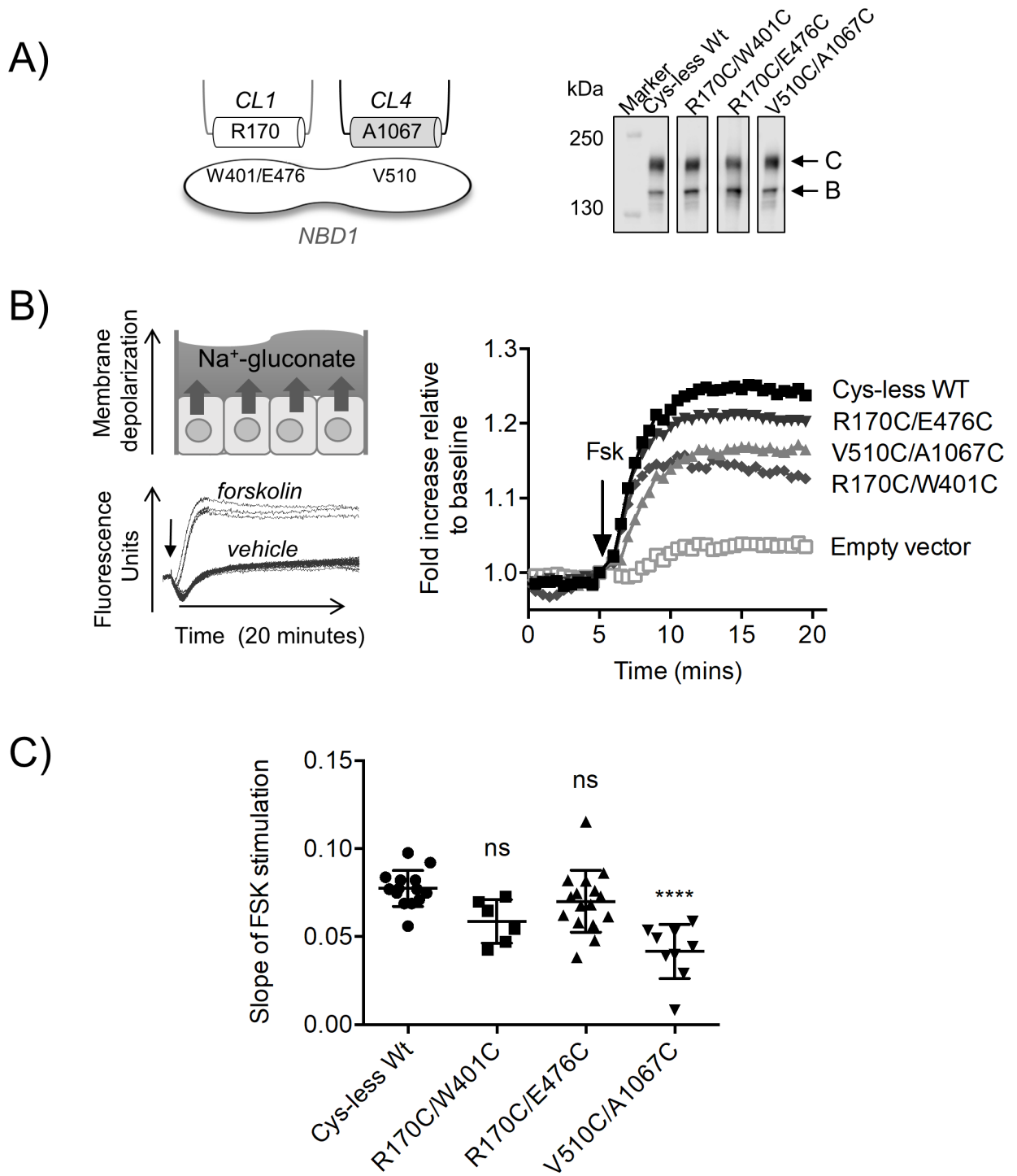
Figure 2.6: Cys-less CFTR mutants are functionally competent and introduction of V510C/A1067C at the CH4: NBD1 interface affects phosphorylation-dependent channel activity.

(**A**) *Left:* A cartoon showing the location of the residues predicted to interact at the transmission interface: V510 on NBD1 and A1067 on CH4 at the CH4: NBD1 interface and R170 on CH1 and W401/E476 on NBD1 at the CH1: NBD1 interface. Cysteine pairs were generated at those

residues to investigate interactions at those interfaces with cysteine cross-linking studies. *Right:* Immunoblot shows that the cys-less Wt-CFTR mutants were expressed at the ER as core-glycosylated protein (represented by band *B*) and at the cell surface as complex-glycosylated protein (represented by band *C*). (**B**) *Left:* Cartoon of the basis of the FLIPR® response of transiently transfected HEK-293 GT cells in sodium (Na$^+$) gluconate buffer. Activation of CFTR channel by forskolin leads to membrane depolarization of the cells which corresponds to a significant increase in fluorescence intensity compared to vehicle. *Right:* CFTR mutants were stimulated with the cAMP agonist, forskolin (Fsk, 10µM), after 5 min of baseline reading. Cys-less Wt along with V510C/A1067C, R170C/W401C and R170C/E476C cys-less Wt-CFTR channels were found to retain partial channel activity after forskolin stimulation in the FLIPR® assay. The empty vector was transfected in HEK-293 GT cells as a negative control. (**C**) The initial slope within the first 3 min of forskolin stimulation was significantly lower in V510C/A1067C whereas R170C/W401C and R170C/E476C did not have a significantly different rate compared to cys-less Wt. Error bars indicate +/- 1 SD between replicate samples (n = 9 biological replicates and n = 3 technical replicates, $p < 0.0001$ between cys-less Wt and V510C/A1067C, One-way ANOVA).

As in previous studies by Mense and colleagues, we studied cross-linking of cysteine pairs in cys-less CFTR using a cell permeable maleimide cross-linker, BMOE [49]. Previous studies have shown that V510C on NBD1 and A1067C on CH4 were in close proximity and could be cross-linked with a methane-thiosulfonate reagent in membrane vesicles [41, 42]. Thus, I studied those substitutions to confirm the efficacy of BMOE in capturing such interactions in intact cells. A unique molecular weight band (band *X*) above 250 kDa only appeared with BMOE treatment of cells expressing cys-less CFTR bearing two cysteines in the same protein (V510C/A1067C) (Figure 2.7A) and not in cells expressing cys-less CFTR with single cysteines (V510C or A1067C) or co-expressing single cysteines from different cys-less CFTR constructs (V510C+A1067C) (Figure 2.7A). This finding confirmed that the membrane permeable cross-linker, BMOE, can effectively cross-link interacting residues within CFTR.

Previous studies have suggested that R170 of CH1 interacts with residues of NBD1 (i.e. 402, 403 or 407) [30, 145]. From my intrinsic tryptophan fluorescence studies, W401 was a residue of interest that may be in close proximity to the transmission interface (Figure 2.2B and Figure 2.5B). Thus, the R170C/W401C mutant was generated to study the predicted interaction of those residues at the CH1: NBD1 interface. Band *X* was not detected upon BMOE addition to cells expressing R170C/W401C, single cysteine mutants (R170C or W401C) or co-expressing single cysteines from different cys-less CFTR constructs (R170C+W401C) (Figure 2.7B). We have

also applied these studies on a different site of NBD1 (by engineering a cysteine at E476), which was also predicted to interact with R170 of CH1 [145], to further interrogate the CH1: NBD1 interface. Addition of BMOE to cells expressing R170C/E476C also failed to confer the appearance of the unique cross-linked band in SDS analyses (Figure 2.7B). We did detect a modest increase in the apparent mass of band *B* of R170C/W401C and R170C/E476C cys-less CFTR after treatment with BMOE (Figure 2.7B). However, we also observed a similar shift in CFTR protein bearing only one cysteine, such as R170C (Figure 2.7B). I suggest that this change in mass does not represent cross-linking, rather a change in conformation induced by BMOE modification of a single cysteine. Hence, the membrane permeable sulphydryl reagent, BMOE, was successful in capturing CH4: NBD1 but not CH1: NBD1 interactions in this study.
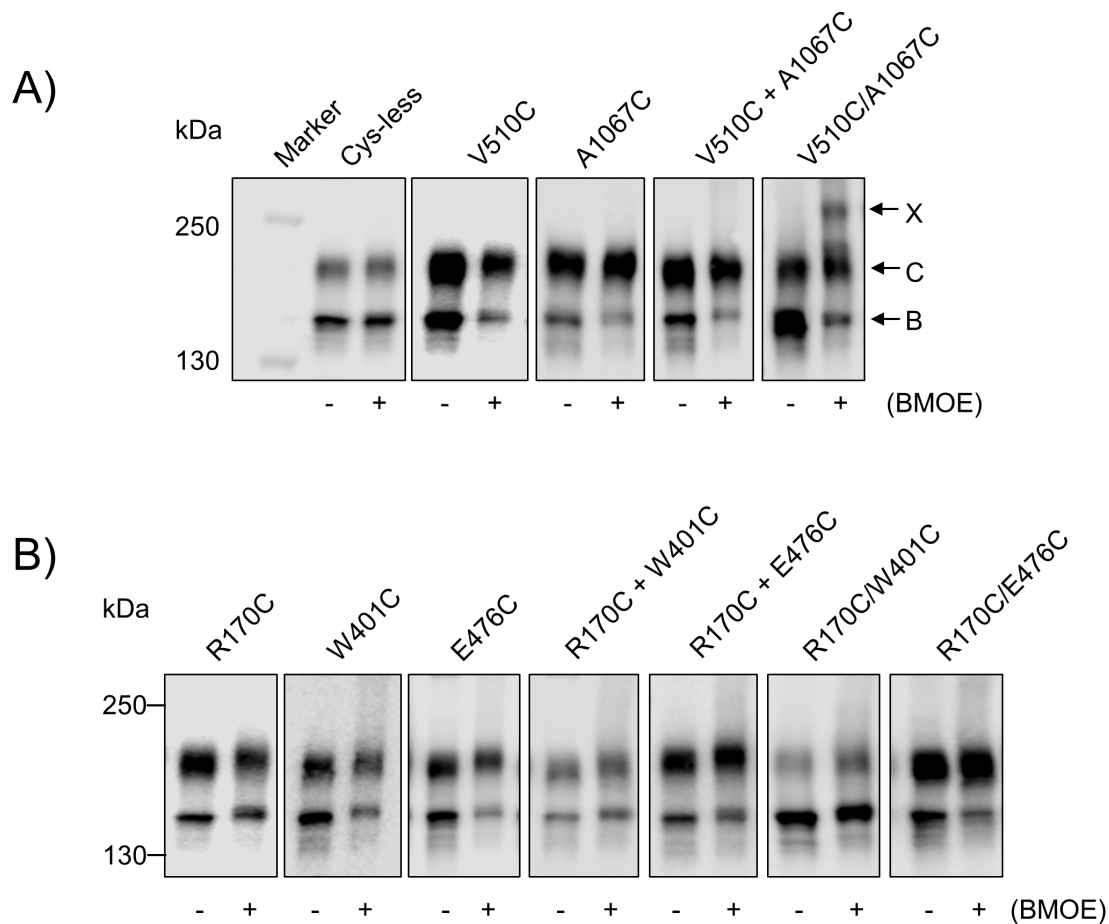
Figure 2.7: Cysteine cross-linking was observed at CH4: NBD1 but not CH1: NBD1.
(**A**) Immunoblot of cys-less variants of Wt-CFTR with cysteines engineered at the CH4: NBD1 interface. Negative controls that included cys-less Wt-CFTR (cys-less), single cysteine mutants (V510C, A1067C), and co-transfected single cysteine mutants on different plasmids (V510C+A1067C) were treated with (+) and without (-) BMOE for 1 h at 27°C. No additional

bands except for bands representing the core-glycosylated protein (band *B*) and complex-glycosylated protein (band *C*) were found from the negative controls. A higher molecular weight band above 250 kDa which corresponds to the cross-linked product of band *C* of the protein (band *X*) was only present upon treatment with BMOE on the construct expressing V510C and A1067C within the same CFTR protein (V510C/A1067C). (**B**) Immunoblot of cys-less variants of Wt-CFTR with cysteines engineered at the CH1: NBD1 interface. Single cysteine mutants (R170C, W401C, E476C) and co-transfected single cysteine mutants on different plasmids (R170C+W401C, R170C+E476C), and constructs expressing both cysteines on the same CFTR protein (R170C/W401C, R170C/E476C) were treated with (+) and without (-) BMOE for 1 h at 27°C. No additional bands except for bands representing the core-glycosylated protein (band *B*) and complex-glycosylated protein (band *C*) were found in all the conditions. This suggests that BMOE was able to capture the interaction of the cysteine pairs at the CH4: NBD1 interface but not at the CH1: NBD1 interface.

I then applied cysteine cross-linking studies to test my hypothesis that PKA phosphorylation modifies the CH: NBD1 interfaces. I could only test the effect of phosphorylation on the CH4: NBD1 interface as we could not detect cysteine cross-linking at the CH1: NBD1 interface as previously shown (Figure 2.7B). Phosphorylation has been shown to significantly enhance both band *B* and band *C* of Wt-CFTR over time [121]. To address this effect, I acutely treated the V510C/A1067C protein with cAMP agonists, forskolin and 3-isobutyl-1-methylxanthine (IBMX), for 30 minutes and conducted cysteine cross-linking on ice. I did not detect a change in the relative abundance of band *X* between V510C and A1067C after PKA-mediated phosphorylation (Figure 2.8A and B). In separate experiments, we also showed that band *X* did not appear in studies of R170C/(W410C or E476C) after phosphorylation with the cAMP agonists (Figure 2.8C). Together, these chemical cross-linking results were consistent with previous studies that suggest that chemical cross-linking may not be a sufficiently sensitive approach to detect subtle interactions mediated by PKA phosphorylation at the CH1: NBD1 interfaces [30, 41]. Alternatively, it may be necessary to introduce cysteines at different positions in the cys-less CFTR protein in order to monitor phosphorylation-dependent changes in domain: domain affinity. For example, Corradi and colleagues predicted that the interaction between the X-loop of NBD1 and CH4 may change with phosphorylation and initiation of the gating cycle of CFTR [40].
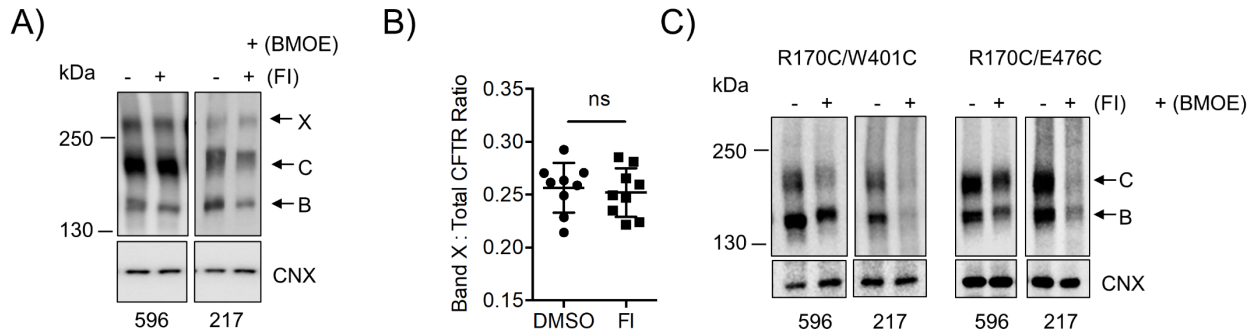
Figure 2.8: Interaction at CH4: NBD1 appears to be phosphorylation-independent. (**A**) Immunoblot shows that cross-linked V510C/A1067C was efficiently phosphorylated as shown by a decrease in signal following Fsk/IBMX (FI) treatment with detection by a phosphorylation-sensitive antibody, 217 (anti-S813 of hCFTR), compared to the non-phosphorylation sensitive CFTR antibody, 596 (epitope on NBD2 of hCFTR). Calnexin (CNX) was used as a loading control (n = 3 biological replicates and n = 3 technical replicates). (**B**) Densitometry analysis of band *X* to total CFTR ratio showed no significant difference between the cysteine cross-linking of DMSO and FI pre-treatment of V510C/A1067C. Error bars indicate +/- 1 SD between replicate samples (n = 9 biological replicates and n = 3 technical replicates, p = 0.7538, Paired t-test). (**C**) Immunoblot of R170C/(W401C/E476C) pre-treated with DMSO or FI and then treated with BMOE. Both R170C/W401C and R170C/E476C were efficiently phosphorylated as shown by a decrease in signal following FI treatment with detection by a phosphorylation-sensitive antibody, 217, compared to the non-phosphorylation sensitive CFTR antibody, 596. Calnexin (CNX) was used as a loading control (n = 3 biological replicates and n = 3 technical replicates). Immunoblot shows that only band *B* and *C* were present in non-PKA and PKA phosphorylated R170C/W401C and R170C/E476C cys-less Wt-CFTR.

2.4.3 Disease-causing mutations in the CHs of ICL1 and ICL4 attenuate the rate of CFTR channel activation

Multiple disease-causing mutations have been identified in the CHs of ICL1 and ICL4, including R170G and A1067T, respectively [137]. Both R170G and A1067T were shown to impair the biosynthetic maturation of the CFTR protein [145, 200] which we were able to recapitulate in this study (Figure 2.9). These findings support the hypothesis that both CHs are important for CFTR assembly.
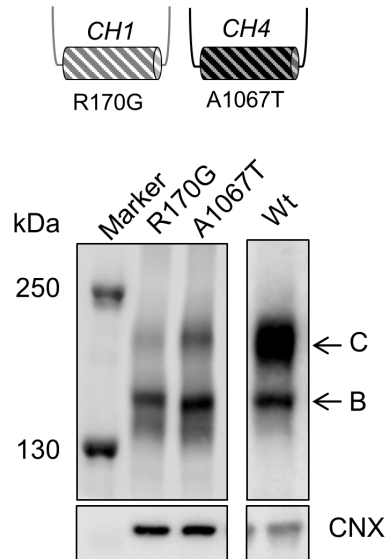
Figure 2.9: Disease-causing mutations at CH1 and CH4 impair biosynthetic maturation of CFTR.
Immunoblot shows that the abundance of complex-glycosylated protein (band *C*) compared to core-glycosylated protein (band *B*) of the disease-causing loop mutants was significantly lower than Wt-CFTR. Calnexin (CNX) was used as a loading control.

In order to determine if these helix-disrupting mutations also impair phosphorylation-regulated channel activity, we compared their forskolin sensitivity and kinetics of channel activation relative to the Wt-CFTR protein. Given the lower steady-state levels of mature CFTR protein exhibited by R170G and A1067T (Figure 2.9B), it was not surprising to find that the peak of forskolin-mediated channel activity measured using the FLIPR® assay was reduced for both mutant proteins relative to Wt-CFTR (Figure 2.10A). However, the dose response for forskolin-dependent activation was similar for the two mutants and Wt-CFTR protein (Figure 2.10B). This result suggests that these mutants do not exhibit a defect in forskolin-mediated phosphorylation per se. On the other hand, the rates of activation with forskolin (added at 0.6 μM, the forskolin concentration closest to the EC_{50} of all the constructs) were significantly attenuated relative to the Wt-CFTR protein for both CH mutants (Figure 2.10C). I interpret these findings to suggest that both CHs are required for phosphorylation-dependent activation of the channel gate.
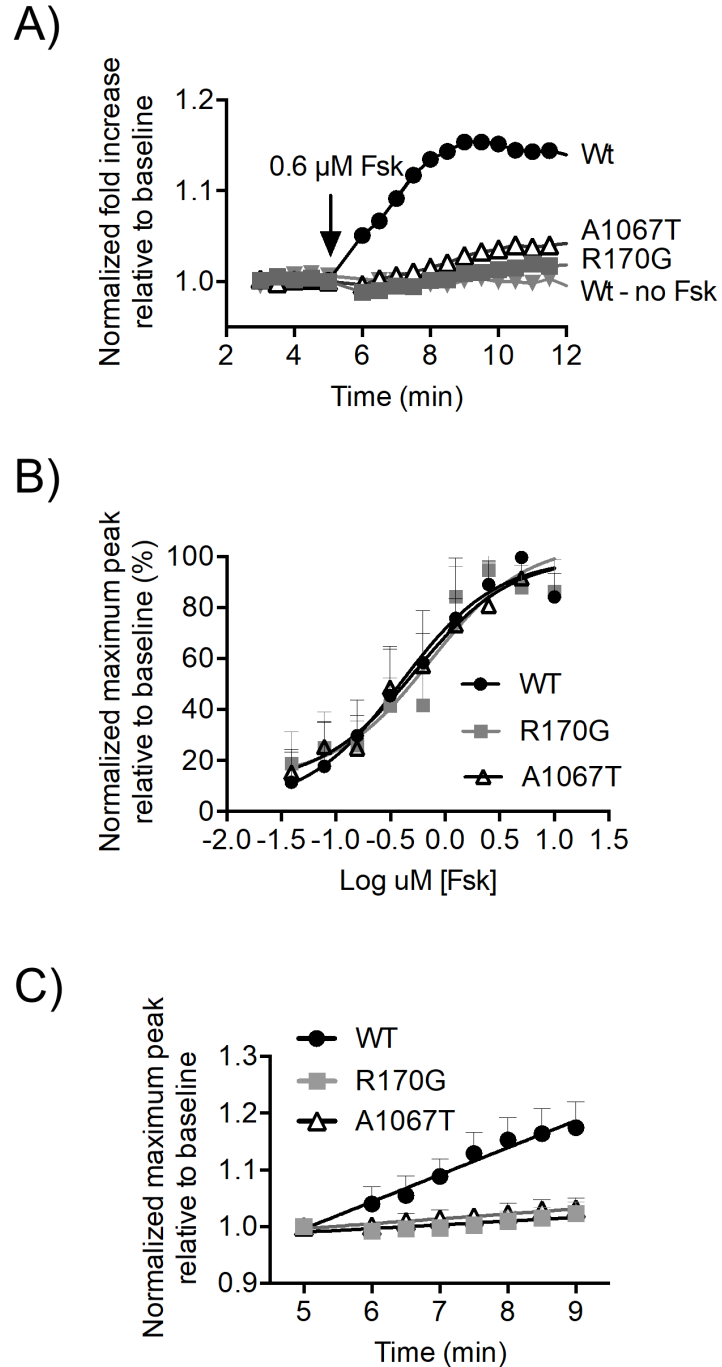
Figure 2.10: PKA-dependent channel activation is affected by disease-causing mutations at CH1 and CH4.
(**A**) Representative FLIPR® traces of Wt-CFTR (Wt) and disease-causing ICL mutants, R170G on CH1 and A1067T on CH4, stimulated with 0.6 μM forskolin (Fsk) were normalized to unstimulated (Wt – no Fsk) traces. (**B**) The maximum peak at each forskolin concentration was normalized to the unstimulated trace and highest forskolin stimulation (10 μM) to generate the forskolin dose-response curves. The EC_{50} values were quite similar: 0.40 μM for Wt, 0.73 μM for R170G and 0.54 μM for A1067T. Error bars indicate +/- 1 SD between replicate samples (n = 12 biological replicates and n = 4 technical replicates). (**C**) From these calculated EC_{50} values,

the closest forskolin concentration from our assay to these EC_{50} values was 0.6 μM. The initial slopes of activation within 4.5 min of forskolin stimulation with 0.6 μM forskolin were then compared. At 0.6 μM, the slopes of activation of the disease-causing ICL mutants were significantly lower than Wt: the slope of activation for Wt was 0.048 ± 0.002 whereas the slope of activation for R170G was 0.007 ± 0.001 and for A1067T was 0.009 ± 0.001. Error bars indicate +/- 1 SD between replicate samples (n = 12 biological replicates and n = 4 technical replicates).

I used a structure prediction method called I-TASSER [188-191] to test my prediction that both of the mutations in CH1 and CH4 are disruptive to the transmission interface comprising NBD1. I-TASSER modeled the full-length CFTR sequence by generating and clustering structural simulations with the SPICKER program and then aligning the TM region to similar PDB structures of ABC transporters which include P-glycoprotein, TM-0287, Atm1, PCAT1 and MsbA [188-191]. I generated separate models of the full-length protein bearing R170G, A1067T or both mutations (R170G+A1067T) for comparison. In Figure 2.11, I show the change in the normalized temperature factor (B-factor), an indication of protein flexibility, at all of the residues of the full-length mutant CFTR proteins relative to the Wt protein (excluding the R region as it is extremely flexible and can mask the effect of other structured regions of CFTR). The B-factor values were generated by an algorithm in I-TASSER known as ResQ which takes into account the changes in local structural assembly along with the sequence and structural profiles and then these values were normalized based on the z-scores [201]. Interestingly, the models for all of the three mutant proteins exhibited the largest change in B-factor in regions other than the CHs. Rather, the largest change for both mutants was detected at the amino-terminal region of the RI (residues 405-407) of NBD1 (Figure 2.11). These models suggest that both of these disease-causing mutations in CH1 or CH4 act allosterically to induce similar defects in the conformational stability of NBD1. Together with channel activity studies, this modeling supports the role of the transmission interface in mediating phosphorylation-dependent activation.
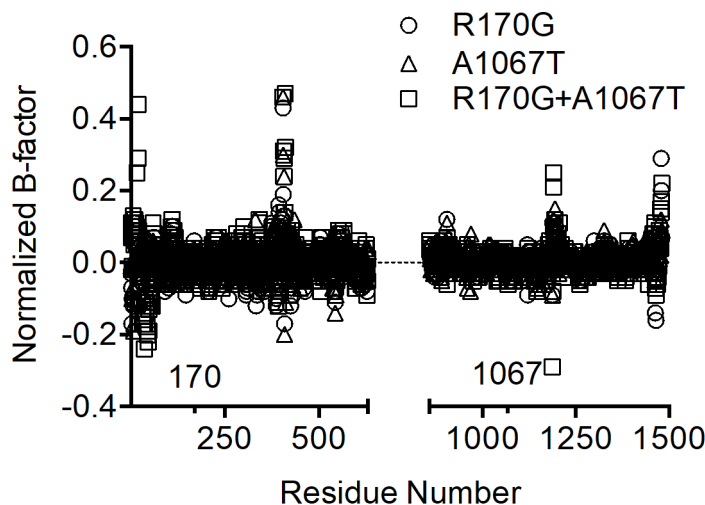
Figure 2.11: Flexibility of NBD1 is affected by disease-causing mutations at CH1 and CH4.
Normalized B-factor values, which represent protein flexibility, of the residues of R170G (circles) and A1067T (triangles) and both mutations, R170G+A1067T (squares) were determined by the protein structure prediction server, I-TASSER [188-191], and subtracted from Wt. Interestingly, the disease-causing mutations (arrows showing residue numbers of the mutations) did not affect the B-factor of the CHs but significantly increased the B-factor at the amino-terminal region of the RI (residues 405-407) of NBD1.

2.5 Discussion

The molecular mechanisms underlying the activation of CFTR channel function by PKA-dependent phosphorylation, ATP binding and hydrolysis remain poorly understood. Hypothetical models for CFTR channel activation have been developed on the basis of patch clamp studies [202-204], cross-linking studies of cysteine-substituted CFTR in cellular membranes [41, 43, 49] and biophysical studies of isolated domains [56, 58]. In this work, the first spectroscopic studies of purified full-length CFTR together with cell-based studies of disease-causing mutants support the importance of inter-domain interactions between the MSDs and NBDs in phosphorylation-dependent channel activation. These findings provide a molecular framework which is important for advancing our understanding of regulated CFTR channel gating, the defects caused by CF-causing mutations and potentially the mechanism-of-action of small molecule modulators of CFTR channel function.

Although the interaction between the MSDs and NBDs of other ABC proteins (i.e. solute transporters) is thought to form a structural conduit important for regulating transport function

[44, 205, 206], previous chemical cross-linking studies failed to detect a change in the proximity of these domains in CFTR, a unique ABC channel protein, after phosphorylation, a necessary trigger for channel activity [30, 41]. The present studies monitoring intrinsic tryptophan fluorescence in the purified full-length CFTR protein are the first to provide evidence supporting a model wherein phosphorylation modifies the affinity for coupling between the MSDs and NBDs of CFTR. Intrinsic tryptophan fluorescence studies showed that the propensity for urea-induced unfolding and fluorescence quenching by potassium iodide was reduced in the purified and highly PKA phosphorylated CFTR protein relative to the basally phosphorylated protein. The water-accessible junction between the ICLs extending from the MSDs and the NBDs harbours multiple tryptophans and constitutes the region most likely to be modified by phosphorylation. The inability to detect changes in steady-state chemical cross-linking in our current work and previous studies [30, 41] support the claim that the CHs are always in close physical proximity to the NBDs in both the basally and highly phosphorylated CFTR protein. Our findings suggest that the affinity of this interaction is increased with phosphorylation.

The importance of the transmission interface involving NBD1 (conferred by both CH1 and CH4) was substantiated in cell-based studies showing altered phosphorylation-dependent channel activation for two disease-causing mutations localized in these helices. Interestingly, rather than altering the sensitivity for the agonist of phosphorylation (forskolin), these mutations attenuated the kinetics of phosphorylation-dependent activation which implicates a defect in a secondary conformational change necessary of channel opening. Together, these data support a model wherein the interaction between the MSDs and NBDs of CFTR are modified by phosphorylation, and disruption of this transmission interface alters the kinetics of long-range conformational changes vital for channel opening.

These studies are relevant to our understanding of the impact of the major mutant, F508del, on CFTR channel function. As previously mentioned, this mutation is located in NBD1 at the interface where CH4 binds and is known to disrupt CFTR assembly, biosynthetic processing, and phosphorylation-dependent channel gating [145, 146, 180]. Relevant to the current work, it was previously reported that the rate of phosphorylation-dependent channel activation is attenuated in F508del-CFTR [207, 208], a similar phenotype that I have described for the disease-causing mutations in CH1 (R170G) and CH4 (A1067T). Given our finding that both interfaces (constituted by CH1 and CH4) contribute to normal channel activation by phosphorylation, I

hypothesize that small molecule stabilizers of the ICL1: NBD1 interface may augment the efficacy of modulators that partially rescue the defect in the ICL4: NBD1 interface caused by F508del. This concept was tested in part by Ehrhardt and colleagues [116] as they developed activators and inhibitors of CFTR channel activity by screening for enhancers or disruptors of the interaction of NBD1 with peptides derived from ICL1. In future studies, we would include the CH region of the ICL1 peptides that was absent in the peptides tested by Ehrhardt and colleagues [116] as our study shows that this region will be particularly effective in identifying modulators of phosphorylation-dependent activation in Wt-CFTR and potentially F508del-CFTR.

As previously mentioned in this chapter, the zCFTR structures in the "closed" and "open" states were recently solved by cryo-EM [23, 25]. Thus, I was interested in whether I could observe modifications of the interactions at the transmission interface upon PKA phosphorylation with these cryo-EM structures [23, 25]. As shown on Figure 2.12, there were subtle changes in the distances between the residues of the CH1: NBD1 and CH4: NBD1 interfaces that were previously interrogated in the cysteine cross-linking studies.
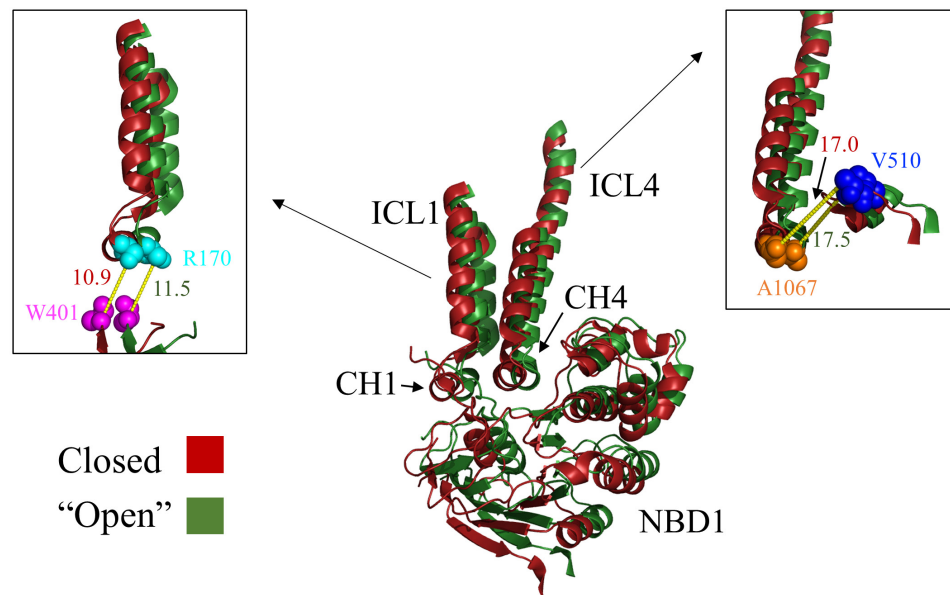
Figure 2.12: Analysis of transmission interface at NBD1 of zCFTR in the "closed" and "open" states.
Left inset: Zoom in of CH1: NBD1 interface with residues previously studied in cysteine cross-linking studies (R170 in light blue on CH1 and W401 in pink on NBD1). There is a subtle change in the distance between the residues; 10.9 Å in the "closed" state versus 11.5 Å in the "open" state. *Right inset*: Zoom in of CH4: NBD1 interface with residues previously studied in cysteine cross-linking studies (A1067 in orange on CH1 and V510 in dark blue on NBD1). There

is a subtle change in the distance between the residues; 17.0 Å in the "closed" state versus 17.5 Å in the "open" state.

However, the zCFTR structure in the "open" state does not appear to be "open" and hence the degree of the interactions at the transmission interface upon PKA phosphorylation may not be fully represented by these structures [23, 25]. I propose that this structure may not be fully "open" due to detergent environment of the protein. In addition, the recent cryo-EM structure of chCFTR upon PKA phosphorylation was of low resolution and the conformational changes remain unclear [33]. Towards this aim, we have developed a novel purification method that can purify the protein with its native lipids which is described in the next chapter.

Chapter 3 Lipid interactions modulate CFTR function

The content of this chapter is in preparation for a research article as follows.

Stephanie Chin, Mohabir Ramjeesingh, Maurita Hung, June Ereño-Oreba, Hong Cui, Jean-Philippe Julien & Christine E. Bear. Lipid associations protect the channel competent and drug responsive CFTR protein.

Contributions:

Study was designed by Stephanie Chin and C.E.B. based on discussions with the other authors mentioned in the research article above. S.C. generated and analyzed all the data presented in this chapter with the help from all the authors. M.R. assisted in optimization of the novel purification method, ATPase assay, lipid thin-layer chromatography and amino acid quantification of CFTR standard. M.H. assisted in optimization of the novel purification method. J.E.-O. conducted transfections of CFTR in HEK-293F cells in suspension and conducted size exclusion chromatography of purified protein. H.C. conducted transfections of CFTR in HEK-293F cells. J-P.J assisted with optimization of novel purification method and suggestions for improvement of assays. Manuscript was written by S.C. and C.E.B. with input from all the authors.

3.1 Summary

Despite impressive progress in determining the structure of the full-length ABC protein, CFTR, by cryo-EM, questions remain regarding the molecular mechanisms underlying its activity as an anion channel. In biological membranes, PKA phosphorylation of CFTR stimulates its ATPase activity and channel opening. Surprisingly, the cryo-EM structure of the PKA phosphorylated zCFTR protein in detergent micelles failed to reveal an open path for anion conduction [25]. Given the important role for lipids in modifying related members of the ABC superfamily, I hypothesized that lipid interactions critical for stabilizing the functional protein were stripped during purification of the phosphorylated zCFTR. In order to preserve CFTR: lipid interactions, we have developed and applied a novel detergent-free purification protocol that effectively purifies functional hCFTR with an amphipathic polymer known as amphipol A8-35 that has been previously shown to extract membrane proteins with its lipids [209, 210]. Applying a fluorescence-based phospholipid assay, we found that detergent extracted hCFTR retained fewer phospholipid molecules than hCFTR extracted using the amphipathic polymer: amphipol A8-35. Lipid thin-layer chromatography (TLC) further showed that purified hCFTR extracted in amphipol contained lipids that include phosphatidylcholine (PC) and phosphatidylethanol (PE) as well as cholesterol. Importantly, CFTR: lipid complexes extracted with amphipol exhibited significantly greater ATPase and enhanced functional reconstitution in liposomes as anion channels than did CFTR-detergent complexes. Interestingly, we have also found that re-introducing brain phosphatidylserine (PS) and PE/brain PS/egg PC/cholesterol (5:2:1:1 ratio by weight) lipids back to CFTR-detergent complexes partially rescued the ATPase activity of the purified CFTR. However, this does not reach the level of ATPase activity of purified hCFTR in amphipol which indicates that retaining specific lipid association to CFTR since the beginning of the purification better preserves CFTR activity. Importantly, I found that the fraction of CFTR molecules that exhibited activity as anion channels could be potentiated by the first Cystic Fibrosis drug, ivacaftor, and the potentiation by ivacaftor was significantly greater in the amphipol preparation than in the detergent preparation following reconstitution into liposomes. Hence, our understanding of the conformational changes that underlie channel opening will require studies of CFTR in the context of associated lipids.

3.2   Introduction

CF is caused by mutations of the *CFTR* gene that codes for the anion channel, CFTR [17, 18, 98]. As previously mentioned, CFTR channel activity and anion conduction through its membrane pore is regulated by PKA phosphorylation of its R domain as well as ATP binding and hydrolysis to its NBDs [48, 50, 104, 105, 109, 110]. Biochemical and electrophysiological studies support a model where phosphorylation promotes dissociation of the R domain from an inhibitory location at the interface of the NBDs to facilitate their dimerization and ATPase activity at the catalytic site formed by the Walker A and Walker B motifs conferred by NBD2 and the Walker C in NBD1 [48, 50, 52, 56, 57, 59, 211-215]. This model predicts that the NBDs of the unphosphorylated and nonconductive form of CFTR will be dissociated whereas the NBDs will be dimerized in the phosphorylated and conductive form of the protein.

Recently, three structures of CFTR have been determined using cryo-EM with resolutions of 3.4 – 3.9 Å [23-25]. These structures include the unphosphorylated, ATP-free and phosphorylated, ATP-bound forms of the zCFTR protein and the unphosphorylated, ATP-free form of the hCFTR protein [23-25]. Comparison of zCFTR structures show major conformational changes upon PKA phosphorylation and ATP binding that are consistent with the molecular mechanism proposed for opening of the conduction pore through human CFTR. Such changes included the loss of stable R domain interactions at the cleft between the two MSD-NBD halves of the CFTR molecule and tighter association of the NBDs [23, 25]. There were also subtle conformational changes at the TMs, notably at TM8 and TM12, upon PKA phosphorylation and ATP binding [25]. These structures suggest that both TM8 and TM12 helices rotated from their original orientation by approximately 50º and participated in novel interactions [25]. TM8 moved away from TM5 and TM7 to form new interactions with TM1, and TM12 formed new interactions with TM1 and TM2 [25]. Despite these conformational changes, the structure of phosphorylated zCFTR did not reveal a pathway for anion conduction [25]. Hence, factors required to stabilize the open conduction pathway may be lacking in the CFTR protein studied by cryo-EM.

Recent studies have shown that ABC transporters specifically bind to lipids and these lipid: protein interactions are structurally important. Phospholipids and cholesterol are bound to ABCG2 in a recent cryo-EM structure [216, 217] and conformers of MsbA solved in lipid

containing nanodiscs differ from those determined in detergent micelles [218]. Furthermore, lipid interactions are known to modify the activity of several ABC transporters including: P-glycoprotein [219, 220], ABCG1 [221], LmrA [222] and MsbA [223, 224]. In fact, the addition of lipids was found to stabilize CFTR after its purification in detergent and modulate its ATPase activity [225, 226]. Hence, I hypothesized that the conductance-competent form of phosphorylated, ATP-bound CFTR protein is stabilized through lipid interactions. To test this idea, we developed a novel method to purify CFTR in a detergent-free environment. We confirmed that CFTR extracted from mammalian membranes, using the amphipol A8-35, retains associated lipids and exhibits enhanced ATPase activity and channel function relative to the detergent purified protein.

3.3   Materials and Methods

3.3.1   Generation of FLAG-CFTR-HIS construct

N-terminal DYKDDDDK (FLAG) tag was introduced on the CFTR-His construct (with a C-terminal 10x His-tag) on the plasmid DNA containing WT-CFTR cDNA (in pcDNA3.1) as the template using the KAPA HiFi HotStart Ready Mix (KAPA Biosystems, Wilmington, MA), primers (Forward: 5'- GAG ATG GAT TAT AAA GAT GAT GAT G -3', Reverse: 5'- CAT CAT CAT CTT TAT AAT CCA TCT C -3') and polymerase chain reaction. The construct was validated by DNA sequencing (TCAG, Toronto, Ontario Canada) and amplified by transformation and plasmid maxi-prep (Qiagen, Hilden, Germany). High-quality (260/280 nm ratio of 1.8 and higher) plasmid DNA was concentrated to a final concentration of 1 μg/μl.

3.3.2   Transfection of FLAG-CFTR-His in HEK-293F cells in suspension

The FLAG-CFTR-His construct was transiently transfected in HEK293F (Thermo Fisher Scientific) suspension cell line capable of complex N-glycosylation. DNA at 50 μg was mixed in a 1:1 ratio with transfection reagent FectoPRO® (Polyplus, Berkeley, CA) and added to each 200 ml suspension culture at 0.8 x 10^6 cells per ml, as previously described [227, 228]. Cells were grown at 37°C shaking at 180 rpm with 8% CO_2 for 24 h. The next day, cells were treated with 10 mM sodium butyrate (Sigma-Aldrich, St. Louis, MO) at 37°C shaking for 24 h.

3.3.3   Generation of crude membranes

HEK293F cells transfected with FLAG-CFTR-His were collected and spun down at 6000 rpm at 4°C for 30 min. Fresh or frozen cell pellet generated from a 600 ml cell suspension was resuspended in 40 ml of phosphate-buffered saline (PBS, Wisent Inc., Saint-Jean Baptiste, Quebec, Canada) containing one tablet of cOmplete, EDTA free protease inhibitor (Roche, Mannheim, Germany). The cells were lysed using Emulsiflex C3 high pressure homogenizer (Avestin, Ottawa, Ontario, Canada) with at least 5 passages during the lysing process. Cell debris were spun down at 1000g at 4°C for 15 min. The supernatant from this spin was further spun down at 100,000g at 4°C for 2 h. The pelleted crude membrane was resuspended in 20 ml of PBS containing 0.1 mM DDM (BioShop, Burlington, ON, Canada) and protease inhibitor (Roche). Syringes with 21G and 27G needles (BD, Franklin Lakes, NJ) were used to disaggregate the pellet. The DDM treated membranes were incubated on ice for 10 min. Any heavy particulate matter that came down were discarded before spinning the membrane suspension at 100,000g at 4°C for 2 h. The extracted crude membrane pellet was again resuspended with the aid of the syringe and previously described needles in 20 ml of 25 mM HEPES, 100 mM NaCl buffer with protease inhibitor (Roche) and then aliquoted. Total protein concentration of the crude membranes was determined by Bradford assay [229] and presence of CFTR was confirmed by immunoblotting.

3.3.4   Purification of FLAG-CFTR-His in amphipol or detergent

Crude membranes were solubilized to a final concentration of 2 mg/ml with 1% LMNG (Anatrace, Maumee, OH) and 0.2% cholesterol hemisuccinate (Anatrace) in buffer A (20 mM Tris-HCl pH 7.5, 2 mM $MgCl_2$, 200 mM NaCl, 20% glycerol, and 2 mM DTT, with protease

inhibitor, Roche) as previously described [23-25] or with 3% (w/v) amphipol A8-35 (Anatrace) in buffer B (25 mM HEPES pH 8, 100 mM NaCl with protease inhibitor, Roche) at 4°C for 2 h with shaking. Insoluble fractions were removed by ultracentrifugation at 45,000 rpm at 4°C for 1 h. Anti-FLAG® M2 magnetic beads (Sigma-Aldrich) were washed with corresponding buffers (buffer A with 0.025% LMNG or buffer B with 0.025% amphipol) using a magnetic rack (New England Biolabs, Ipswich, MA) for a total of 3 times. Soluble fractions were incubated with anti-FLAG® M2 magnetic beads at 4°C overnight with shaking. Unbound proteins were removed the next day with a magnetic rack (New England Biolabs) and anti-FLAG® M2 magnetic beads (Sigma-Aldrich) were washed 5 times with corresponding buffers. If phosphorylation is required, the anti-FLAG® M2 magnetic beads (Sigma-Aldrich) were treated with a phosphorylation cocktail (10,000 U of PKA (New England Biolabs) and 5 mM Mg-ATP (Sigma-Aldrich) in buffer A with 0.025% LMNG or buffer B with 0.025% amphipol) at room temperature for 1 h with shaking. The phosphorylation cocktail was removed by magnetic rack and the anti-FLAG® M2 magnetic beads were washed again for 5 times with the corresponding buffers. FLAG-CFTR-His protein was eluted with 200 μg/ml FLAG® peptide (DYKDDDDK, Sigma-Aldrich) in buffer A with 0.025% LMNG or buffer B with 0.025% amphipol using the magnetic rack after 45 min incubation with shaking at 4°C. Purified protein at 500 μl was loaded in Superose 6 Increase 10/300 column (GE Healthcare, Chicago, IL) to further characterize the protein. Purity of purified CFTR was determined by densitometry of the CFTR bands compared to other bands present on the 4-12% silver stained gels by Image Studio™ Lite software.

3.3.5   Protein gel electrophoresis and visualization

Purified protein was run on 6% or 4-12% Tris-Glycine SDS gels (Life Technologies, Carlsbad, CA). Gels were silver stained with the ProteoSilver™ Silver Stain Kit (Sigma-Aldrich) according to the manufacturer's protocol or Coomassie blue stained with the Quick Coomassie Stain (Cedarlane, Burlington, Ontario, Canada) for a maximum of 1 h with shaking at room temperature. Gels were also transferred to nitrocellulose paper and probed for CFTR with 1:10,000 IgG2b mAb596 antibody (University of North Carolina at Chapel Hill, Chapel Hill, NC, code: A4) at 4°C overnight with shaking and 1:5000 horseradish peroxidase-conjugated goat anti-mouse IgG secondary antibody (Pierce) at room temperature for 1 h with shaking. Immunoblots were exposed with Amersham enhanced chemiluminescent reagent (GE

Healthcare) with the Li-Cor Odyssey Fc (LI-COR Biosciences, Lincoln, NE). Immunoblot bands were analyzed with Image Studio Lite software.

3.3.6   CFTR quantification

CFTR protein was purified as previously described in amphipol to generate a standard and 100 µl of the standard was subjected to amino acid analysis conducted by Rey Interior of the SPARC BioCentre at the Hospital for Sick Children (Toronto, Ontario, Canada). The results of the amino acid analysis are shown in Figure 3.1 and Table 3.1.
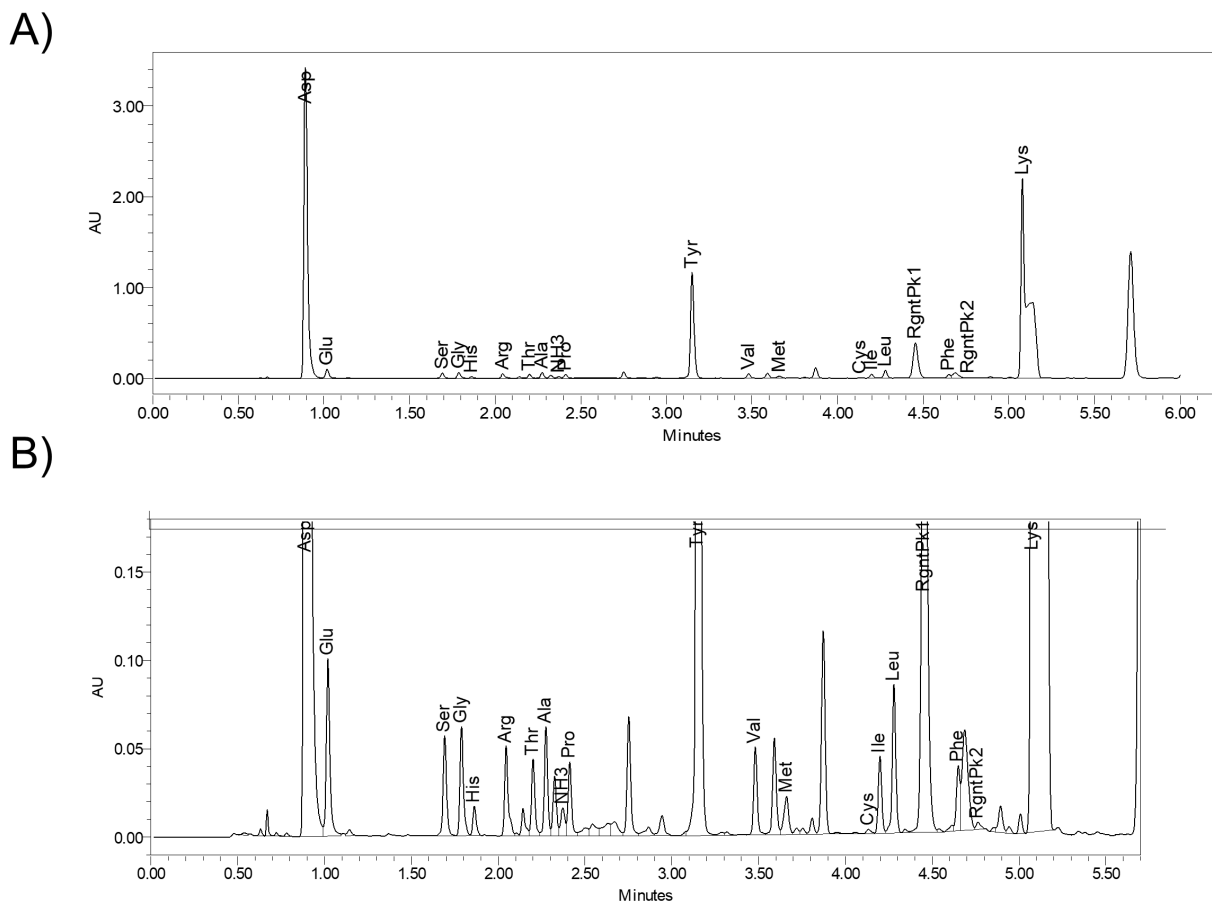
Figure 3.1: Amino acid analysis of CFTR standard.
(**A**) Chromatogram of all the amino acids present in CFTR standard. (**B**) Scaled chromatogram to show the smaller peaks.

Table 3.1: Summary table of amino acid analysis results of CFTR standard.
Table shows the amino acid (3-letter code), retention time (RT) in minutes of when the amino acid appeared, the area under the peak and the corresponding amount of the amino acid in picomoles (pmoles) in a 100 μl purified CFTR standard.

Amino acid	RT	Area	Amount (pmoles)
Asp	0.892	5099166	66398.567
Glu	1.019	147780	2021.338
Ser	1.692	79642	1035.873
Gly	1.788	86381	1139.691
His	1.862	22241	289.816
Arg	2.045	74065	947.141
Thr	2.201	59033	747.984
Ala	2.275	83745	1015.112
Pro	2.412	59190	713.162
Tyr	3.150	1680122	19755.248
Val	3.480	70278	882.894
Met	3.661	41282	496.935
Cys	4.132	4485	37.648
Ile	4.198	60431	686.995
Leu	4.279	124398	1497.008
Phe	4.650	53427	618.165
Lys	5.079	5901164	38071.770

Previous studies have found that amino acid hydrolysis with various solvents resulted in 100% recovery of alanine [230]. There are also no alanine residues present in the FLAG® peptide (Asp-

Tyr-Lys-Asp-Asp-Asp-Asp-Lys) that was used to elute the protein. Thus, we applied the amount of alanine from the amino acid analysis to determine the concentration of the CFTR standard.

The relationship between the molecular weight of the amino acid to the molecular weight of any protein is as follows:

$$\frac{weight\ amino\ acid}{weight\ protein} = \frac{number\ of\ amino\ acids*(MW\ amino\ acid)}{MW\ protein}$$

The variables required for determining the weight of the CFTR standard are summarized in Table 3.2.

Table 3.2: Variables for determining concentration of CFTR standard.

Variable	Value
MW Ala	89.0935 – 18 (for peptide bond) = 71 g/mol or pg/pmole
weight Ala	1015.12 pmoles (from chromatogram) 1015.12 pmoles x 71.0935 pg/pmole = 72065 pg
number of Ala in CFTR	83

The calculation of the concentration of the standard is as follows:

$$\frac{weight\ Ala}{weight\ CFTR} = \frac{number\ of\ Ala*(MW\ Ala)}{MW\ CFTR}$$

$$\frac{72065\ pg}{weight\ CFTR} = \frac{83*71\ pg/pmol}{170507.57\ pg/pmol}$$

Weight of CFTR = 208512269 pg or 2085.12269 ng

Volume used for amino acid analysis = 100 µl

Concentration of CFTR standard = 2085.12269 ng / 100 µl = 20.85 ng/µl

The remaining standard was aliquoted and stored at -80°C. When required, various nanogram amounts of the standard were run with purified protein samples of unknown amounts on SDS-PAGE and subjected to immunoblotting. Immunoblot bands were analyzed with Image Studio™ Lite software and densitometry of unknowns were interpolated on the standard curve on GraphPad Prism as shown in Figure 3.2.
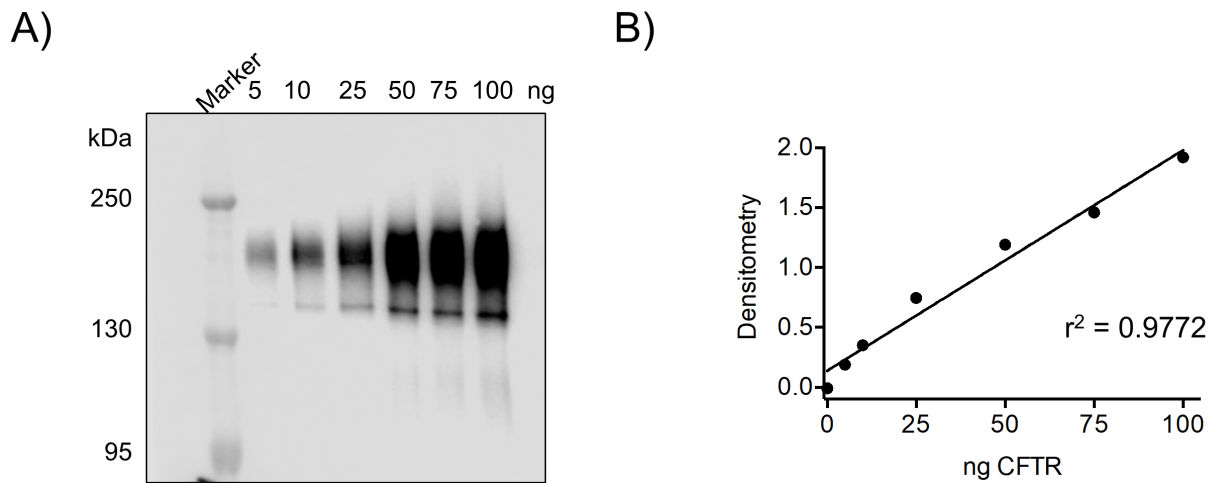
Figure 3.2: Representative immunoblot and standard curve applied for CFTR quantification.
(**A**) Immunoblot of CFTR standard at increasing amounts (nanograms). (**B**) Standard curve of (**A**) that is used for interpolation of unknown amount of purified protein.

3.3.7   Phospholipid assay

Purified protein in amphipol and LMNG and the appropriate controls were subjected to a 96 well phospholipid assay kit according to the manufacturer's protocol (Cat. no. MAK122, Sigma-Aldrich). Fluorescence was read at excitation of 530 nm and emission of 585 nm on the SpectraMax i3X plate reader (Molecular Devices).

3.3.8 Lipid TLC

Lipid containing samples were extracted as previously described [231]. The lipid containing organic phase was first dried with sodium sulfate for 1 h, filtered and concentrated under a stream of argon to a volume of 50 µl. Silica gel plates (Analtech Inc.) were first activated at 160°C for 1 h before sample application. Samples (10 µl) and polar lipid standard (2 µl, Matreya LLC) were spotted and developed using chloroform: methanol: water (65:25:4) as the solvent system. Visualization of the lipids was conducted as previously described [231].

3.3.9 ATPase assay

3.3.9.1 ATP dose-response

Purified protein (approximately 50-200 ng in 25 µl) was incubated with 50 µl of various concentrations of Na-ATP (Sigma Aldrich) solubilized in 10 mM HEPES, 100 mM NaCl, 5 mM MgCl$_2$, 1 mM DDM, pH 7.4 buffer at 37°C for 2 h. A colorimetric assay was applied as previously described [232] to detect phosphate at absorbance 800 nm on the SpectraMax i3X plate reader (Molecular Devices). Values were subtracted from controls (amphipol or LMNG buffer with various concentrations of ATP), converted to nmol phosphate by interpolation of phosphate standard curve on GraphPad Prism and then to nmol phosphate/mg protein/min after CFTR quantification as previously described. Values were fit on Michaelis-Menten curves with GraphPad Prism to determine the K$_m$ and V$_{max}$ values of ATPase activity.

3.3.9.2 ATPase studies of re-introducing lipids to CFTR in LMNG

Egg PC, porcine brain PS, or a mix of PE/brain PS/egg PC/cholesterol in a 5:2:1:1 (w/v) ratio (all lipids in chloroform and from Avanti) were dried in a glass tube under argon gas. Dried lipids were resuspended in 25 mM HEPES, 100 mM NaCl, pH 8.0 buffer with sonication to a stock concentration of 10 mg/ml. Resuspended lipid (100 µg in 10 µl) was added to purified protein (approximately 50-200 ng in 25 µl) on a 96 well plate along with controls: 1) 10 µl of 25 mM HEPES, 100 mM NaCl, pH 8.0 buffer added to 25 µl of purified protein; 2) 10 µl of resuspended lipid added to 25 µl of buffer A with 0.025% LMNG; 3) 10 µl of 25 mM HEPES, 100 mM NaCl, pH 8.0 buffer added to 25 µl buffer A with 0.025% LMNG. Protein with lipids and controls were incubated at 1 h at room temperature. Na-ATP (40 µl of 0.9375 mM stock concentration to a final concentration of 0.5 mM Na-ATP) solubilized in 10 mM HEPES, 100

mM NaCl, 5mM MgCl$_2$, 1 mM DDM, pH 7.4 buffer was added to the mix and the reaction was incubated at 37°C for 2 h. Colorimetric assay was applied as previous described above.

3.3.10   Iodide efflux

CFTR protein in amphipol was incubated with 5 mM DDM during the elution step with FLAG® peptide prior to reconstitution whereas protein in LMNG remained as is. Purified protein (approximately 0.4 µg) was reconstituted in 5 mg of POPC (Avanti) and subjected to iodide efflux as previously described [140, 192].

3.4   Results

3.4.1   CFTR: lipid complexes are purified using amphipol A8-35

Full-length human Wt-CFTR, bearing its native sequence except for two affinity tags, a FLAG tag (on the amino terminus) and a 10x histidine tag (on the carboxy terminus) was expressed in HEK-293F cells. We optimized the expression of FLAG-CFTR-His in HEK-293F cells in suspension. We have found that the optimal transfection duration was 24 h at 37°C with shaking to generate the maximal expression of CFTR in these cells (Figure 3.3A). An additional 24 h incubation of the cells with 10 mM sodium butyrate at 37°C further enhanced the expression of CFTR (Figure 3.3B). Thus, we have applied those conditions in the large-scale expression of FLAG-CFTR-His in those cells.
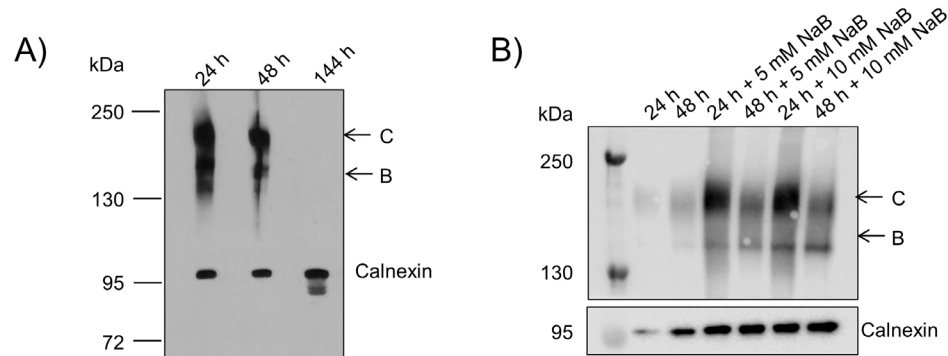
Figure 3.3: Optimization of FLAG-CFTR-His expression in HEK-293F cells.
(**A**) Immunoblot of CFTR expression in HEK-293F overtime with calnexin as loading control. CFTR expression appeared to be the highest at 24 h compared to 48 h and 144 h. (**B**) Immunoblot of CFTR expression in HEK-293F with additional treatment of sodium butyrate

(NaB) with calnexin as loading control. CFTR expression appeared to be the highest with additional 24 h treatment of 10 mM NaB.

Amphipol A8-35 at 30 mg was effective in solubilizing CFTR from 1 ml of 2 mg/ml final concentration of resuspended membranes, which corresponds to an amphipol concentration of 3% (w/v) (Figure 3.4, lane 1). Finally, CFTR was purified to near homogeneity in a single step by affinity to anti-FLAG® magnetic beads (Figure 3.4, lane 3 and 4). CFTR was detected as a major band at around 170-180 kDa on the Coomassie blue (Figure 3.4, lane 3) and silver (Figure 3.4, lane 4) stained gels. In SDS-PAGE, purified CFTR migrated as expected for the mature, complex glycosylated band *C* of the protein (170-180 kDa, Figure 3.4, lanes 3-5). The immature, core glycosylated band *B* of CFTR was also present in the eluted sample as a band at around 140-150 kDa (Figure 3.4, lanes 3-5).
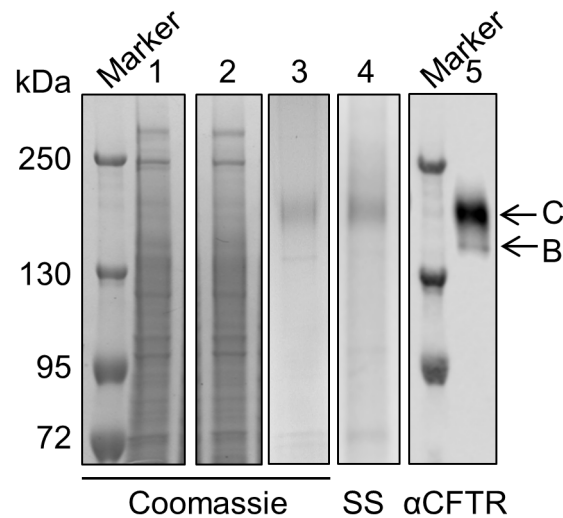
Figure 3.4: Purification of full-length CFTR in amphipol results in high degree of homogeneity of purified CFTR.
Protein gels stained by Coomassie blue of lysate solubilized by amphipol (1), unbound fraction (2) and eluate from anti-FLAG® M2 magnetic beads (3). Eluate from anti-FLAG® M2 magnetic beads was also stained by silver stain (SS) (4) and immunoblotted (5) showing that CFTR was effectively purified as a relatively pure population. CFTR appeared as two bands that include a band at approximately 170-180 kDa that represents the mature, complex glycosylated form of the protein (band *C*) and a band at approximately 140-150 kDa that represents the immature, core glycosylated form of the protein (band *B*).

Size exclusion chromatography (SEC) was used to characterize the purified CFTR protein on the basis of differences in size using 280 nm to monitor the elution of CFTR (Figure 3.5). The fractions eluting between elution volume of 9-17 ml containing both core and complex glycosylated CFTR, as confirmed by silver staining (Figure 3.5B) and immunoblotting (Figure 3.5A), co-eluted with ATPase activity (Figure 3.5A). Interestingly, the peak ATPase activity at elution volume of 14.5 ml was slightly displaced from the peak CFTR protein abundance at elution volume of 13 ml, suggesting that the population of purified CFTR molecules is heterogeneous with respect to specific enzyme activity.
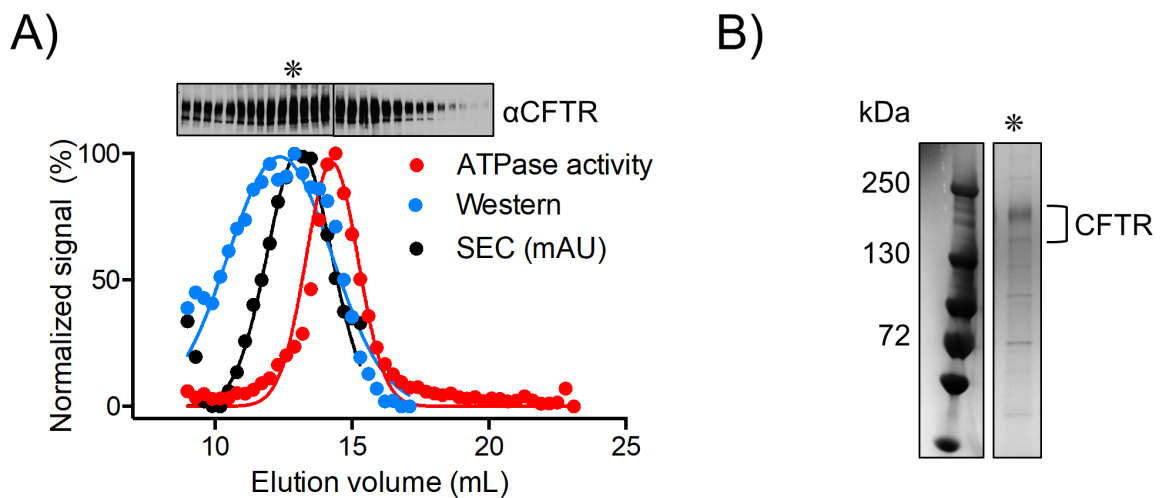
Figure 3.5: Purified CFTR in amphipol appears quite pure as shown by SEC trace with the shoulder of the SEC peak corresponding to CFTR elution exhibiting ATPase activity.
(**A**) Overlay of normalized signal of CFTR ATPase activity (red) and CFTR protein detected by immunoblot (blue) to SEC trace (black) showing that the SEC peak at (✱) corresponds to CFTR protein separation and the shoulder of that peak corresponds to functional CFTR. (**B**) Silver stain of the SEC peak (✱) shows the purified CFTR protein is relatively pure.

A previous study has found success in purifying CFTR in a detergent-free environment with another polymer known as styrene maleic acid co-polymer lipid particles (SMALPs) [233]. I also attempted to purify our CFTR protein with SMALPs. However, the protein did not appear to bind strongly to both the nickel column and anti-FLAG® magnetic beads as shown in Figure 3.6.

A)

B)
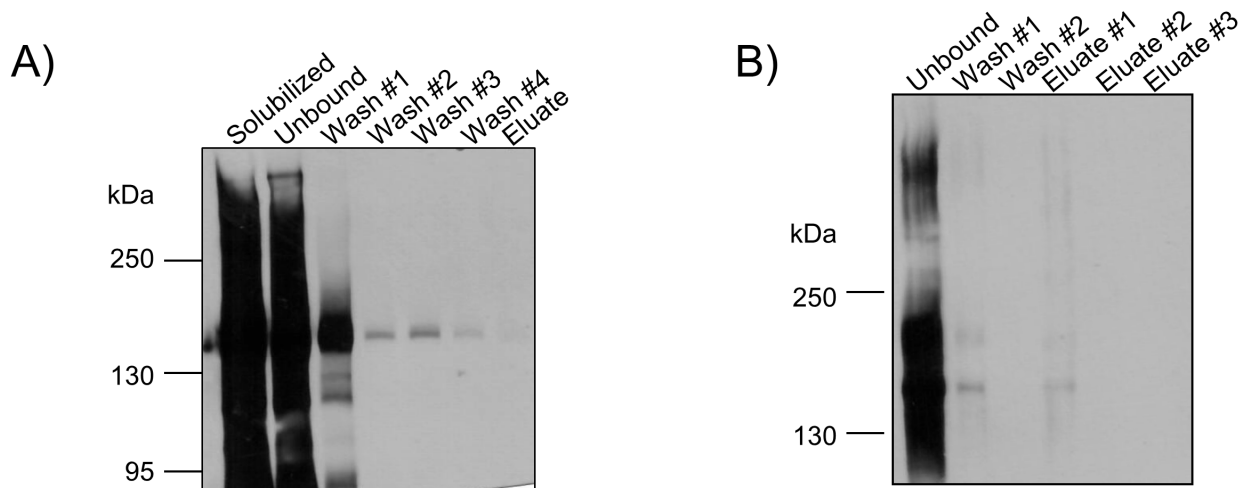
Figure 3.6: FLAG-CFTR-His could not be purified with SMALPs.
(**A**) Immunoblot of CFTR throughout nickel affinity purification steps. There appears to be a gradual decrease in amount of CFTR at each step of the purification indicating that the protein may not be binding strongly to the column and can be readily washed off. (**B**) Immunoblot of CFTR throughout FLAG affinity purification steps. There was a lot of CFTR in the unbound fraction and very little amount of CFTR that eluted from the anti-FLAG® magnetic beads with 3 different elutions: eluate 1 and 2 were conducted with the FLAG peptide and eluate 3 was conducted with SDS.

Previous studies found that amphipols do not compete with lipids, which remain associated to membrane protein: amphipol complexes [209, 210, 234]. Thus, I was interested in determining whether purified CFTR using amphipol also retained lipids. I compared the amphipol-based purification to that employed by the Chen group in their cryo-EM studies [23-25]. First, I confirmed that CFTR solubilized in Lauryl Maltose Neopentyl Glycol (LMNG) detergent micelles [23-25] could be purified using the same protocol as we developed for the amphipol preparation (Figure 3.7A and B).
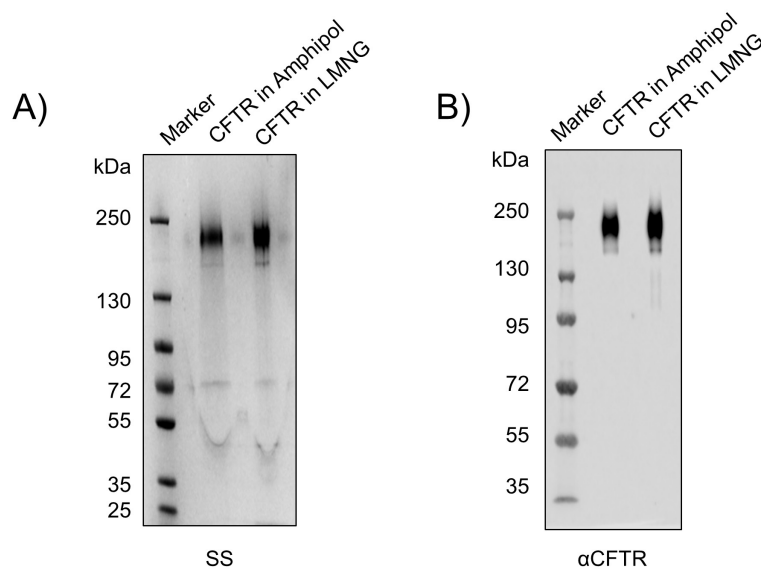
Figure 3.7: CFTR purified in LMNG exhibit similar levels of protein compared to CFTR purified in amphipol.
(**A**) Silver stain (SS) of purified protein in amphipol and LMNG showing the high purity of the samples. (**B**) Immunoblot confirming that both samples contained CFTR protein.

Then, the relative degree of phospholipid association was compared between the amphipol and detergent based purifications. Choline-containing lipids (i.e. PC, lecithin, lysolecithin and sphingomyelin) were quantified using a fluorimetric assay. This assay is a high-throughput assay for detecting choline-containing phospholipids through an enzymatic reaction that releases choline from the phospholipid which is detected by choline oxidase and a H_2O_2 specific dye (Sigma-Aldrich product information). The fluorimetric product produced is proportional to the phospholipid concentration of the sample and the linear range is between 0.6-20 µM phospholipid (Sigma-Aldrich product information). We first confirmed that the linear range of this assay is between 0.6-20 µM using a PC standard (Figure 3.8A). Applying this assay and after normalization for CFTR protein abundance (as described in the *CFTR Quantification* section of the Materials and Methods of this chapter), we detected a higher number of approximately 56 to 76 choline-containing phospholipids associated per CFTR molecule in amphipol compared to approximately 5 to 12 phospholipids associated per CFTR in LMNG detergent micelles (Figure 3.8C).
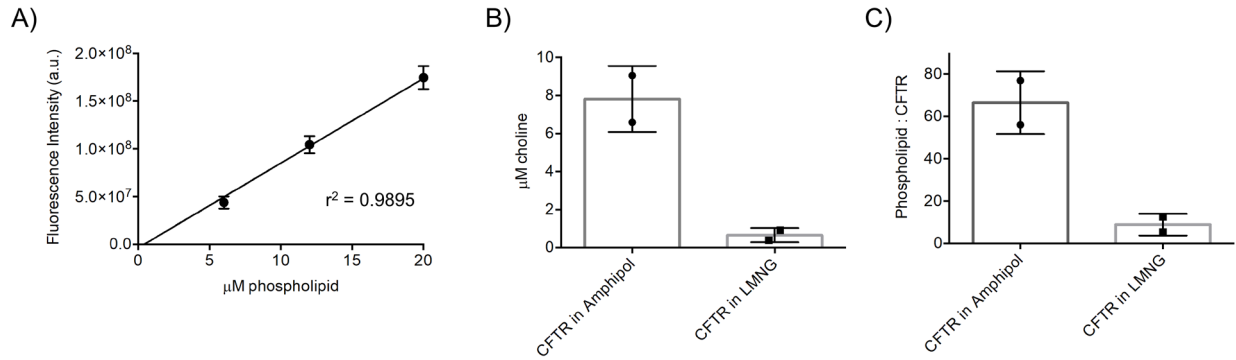
Figure 3.8: Purified CFTR in amphipol appeared to contain more choline-containing phospholipids per protein molecule than in LMNG detergent.
(**A**) Standard curve of PC standard is at a linear range between 0.6-20 µM with a r^2 value of 0.9895 which will be used for interpolation. (**B**) Concentration range of phospholipids present in purified CFTR in amphipol and in LMNG from interpolation of (**A**). (**C**) Phospholipid analysis showing that purified CFTR solubilized in amphipol contained more phospholipids (56 to 76 phospholipids per CFTR molecule) than CFTR solubilized in LMNG (5 to 12 phospholipids per CFTR molecule) after normalizing to protein amounts. The data is presented as a range of n = 2 technical replicates.

Furthermore, the phospholipids that associated with CFTR in the amphipol purification include cholesterol, PC and PE as studied by lipid thin layer chromatography (TLC) (Figure 3.9). I cannot exclude the presence of additional lipids, given the resolution of the solvent system employed for TLC. In fact, I expect that PS to be also associated given its dominant presence in the inner leaflet of biological membranes.
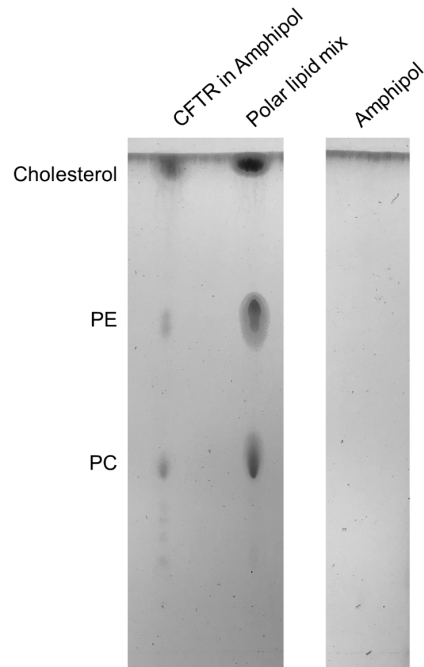
Figure 3.9: Purified CFTR in amphipol contain cholesterol, PE and PC.
Lipid TLC showing that extracted lipids from purified CFTR in amphipol include cholesterol, PE and PC as confirmed by similar migration of known lipids from polar lipid mix standard. These lipids were not present in amphipol by itself.

3.4.2 CFTR: lipid: amphipol complexes exhibit higher specific ATPase activity and higher functional reconstitution as regulated anion channels than CFTR: detergent complexes

We compared the specific ATPase activities of CFTR purified using amphipol or LMNG after PKA phosphorylation (P) to ensure that the protein in both preparations were maximally phosphorylated, a modification known to be important for CFTR function as an enzyme and channel [51, 104, 105, 109, 111]. We compared the ATPase activities of purified P-CFTR in amphipol and in LMNG by applying a high-throughput adapted colorimetric ATPase assay that has a sensitivity as low as 1 nmol phosphate [232]. The ATP dose-response curves of purified P-CFTR in amphipol and LMNG detergent were fit to Michaelis-Menten curves as shown in Figure 3.10 and the values of these curves are summarized in Table 3.3.
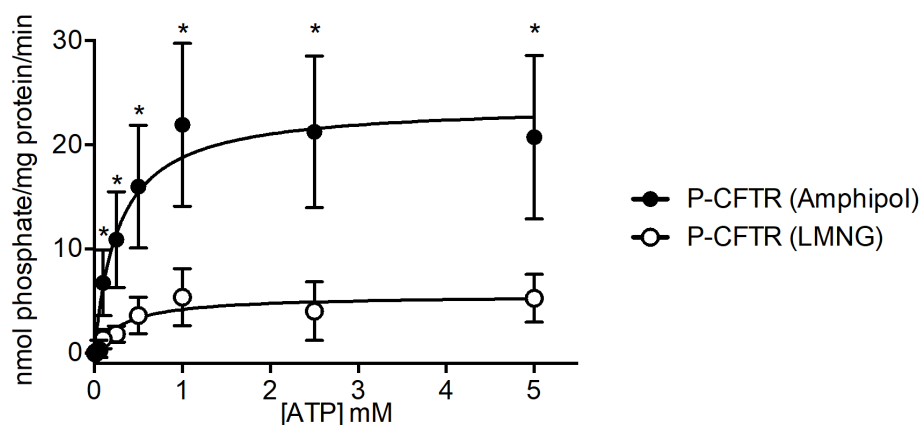
Figure 3.10: Purified P-CFTR in amphipol exhibits significantly higher ATPase activity compared to purified P-CFTR in detergent micelles.
ATPase activity of P-CFTR in amphipol and in LMNG detergent across ATP concentrations (mM) expressed as nmol phosphate/mg protein/min. Results are fitted to a Michaelis-Menten curves and are shown as mean $\pm$ SD (n = 3 biological replicates, n = 6 technical replicates, *p < 0.05, multiple t-tests).

Table 3.3: Summary of Michaelis-Menten values of purified P-CFTR in amphipol and LMNG detergent micelles.
Values include the maximum velocity (V_{max}) and the Michaelis-Menten constant or substrate concentration at half V_{max} (K_m). Values are expressed as best-fit values $\pm$ standard error (n = 3 biological replicates, n = 6 technical replicates).

	K_m	V_{max}
	(mM ATP)	(nmol phosphate/mg protein/min)
P-CFTR in amphipol	0.27 ± 0.08	23.90 ± 1.91
P-CFTR in LMNG	0.32 ± 0.14	5.54 ± 0.66

We found that the K_m values of ATP were similar for the two samples: K_m of 0.27 ± 0.08 mM ATP for the purified P-CFTR in amphipol and K_m of 0.32 ± 0.14 mM ATP for the purified P-CFTR in LMNG detergent micelles (Table 3.3). Interestingly, the maximal ATPase activities after normalization to protein amounts (as described in the *CFTR Quantification* section of the

Materials and Methods of this chapter) were significantly higher in the purified P-CFTR in amphipol: V_{max} of 23.90 ± 1.91 nmol phosphate/mg protein/min compared V_{max} of 5.54 ± 0.66 nmol phosphate/mg protein/min in purified P-CFTR in LMNG detergent micelles (Table 3.3).

I then compared our Michaelis-Menten values of the ATPase assay to previously published values and found that these values were somewhat different as summarized on Table 3.4.

Table 3.4: Previously published ATPase activity values compared to our current studies.
Erg represents ergosterol and chol represents cholesterol. The ATPase values that appear similar are highlighted in yellow. The last two rows represent the ATPase values of our current studies.

Cells	Protein environment	ATPase method	Protein quantification	K_m (mM ATP)	V_{max} (nmol/mg/min)	Citation
Sf9	PE/PS/PC/erg (5:2:1:1)	Radioactive [^{32}P]-ATP hydrolysis	Amino acid analysis	0.407	63	[235]
Sf9	*E. coli* phospholipid and octyl-ß-D-glucopyranoside	Radioactive [^{32}P]-ATP hydrolysis	Amido black 10B assay	0.150	58	[236]
Sf9	DDM	Radioactive [^{32}P]-ATP hydrolysis	ELISA	0.600	68	[140]
HEK	Digitonin	NADH/pyruvate	NanoDrop	0.220	239	[23]
HEK	Digitonin	NADH/pyruvate	NanoDrop	0.187	134	[24]
HEK	MNG10 then reconstituted into PE/brain PS/egg PC/chol (5:3:1:1)	Radioactive [^{32}P]-ATP hydrolysis	In-gel GFP fluorescence	0.500	30	[225, 237]
HEK	Amphipol	Molybdate method	Amino acid analysis and immnoblot	0.270	24	
HEK	LMNG	Molybdate method	Amino acid analysis and immnoblot	0.320	5.5	

The differences in the ATPase values may be due to differences of the protein environment as previous studies have found that purified CFTR protein in different detergents and reconstituted lipids influence its ATPase activity [225, 237]. The method applied to detect ATP hydrolysis may also lead to different ATPase values due to differences in sensitivities. Most importantly, the V_{max} values depend heavily on the protein quantity and consequently the protein quantification method. For example, the V_{max} values reported by the Chen group, that solved the higher-resolution CFTR structures with core N-glycans by cryo-EM, were significantly higher than all of the published values [23, 24]. These values may be influenced by their use of the NanoDrop for protein quantification (F. Liu, personal communication, May 23, 2018). Based on our experience and others, the NanoDrop readings are highly sensitive to contaminants that also absorb around 280 nm, are quite variable overtime and with mixing the sample, and are not very accurate for low protein concentrations [238]. In fact, we have previously applied the NanoDrop to quantify our protein concentrations. However, it resulted in negative values possibly due to the low concentration of our samples which may not be within its sensitivity range (Figure 3.11). The underestimation of the protein concentration amounts may lead to significantly higher V_{max} values from the ATPase assay.
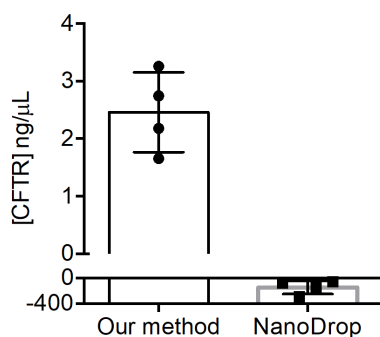
Figure 3.11: Comparison of our CFTR protein quantification with the method applied by the Chen group (NanoDrop).
Our protein quantification yielded CFTR concentrations from 1.5 – 3.5 ng/µl whereas protein quantification using NanoDrop by the Chen group resulted in negative values possibly due to its lack of sensitivity at low protein concentrations (Paired comparisons of same purified sample across methods, n = 4 biological replicates, n = 4 technical replicates for our method and n = 4 biological replicates, n = 12 technical replicates).

In contrast, our CFTR quantification method was a more direct protein quantification method that used amino acid analysis and immunoblotting to specifically detect the amount of CFTR. Interestingly, our ATPase values of P-CFTR in amphipol mostly agrees with the values of the Urbatsch group that has many similarities to our study which include: the CFTR protein was expressed in HEK-293 cells, the protein was complex glycosylated, and a direct protein quantification method was applied [225, 237, 239, 240].

I acknowledge that the Chen group that solved the cryo-EM structures conducted their ATPase assays with CFTR protein in another detergent, digitonin [23-25], but we initially observed lower ATPase activity, that was barely detectable, of the protein in digitonin compared to the protein in LMNG (Figure 3.12). Thus, I decided to apply the LMNG detergent for our functional assays in order to sufficiently detect the ATPase activity of CFTR and compare that with CFTR in amphipol.
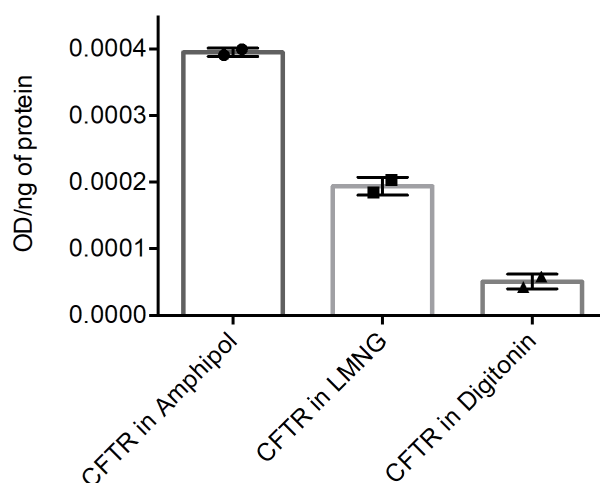
Figure 3.12: Comparison of ATPase activity at 0.5 mM ATP of purified P-CFTR in amphipol and in different detergents.
Purified P-CFTR in amphipol resulted in the highest ATPase activity normalized to CFTR protein amount at 0.5 mM ATP than purified protein in detergent which is consistent to previous results (Figure 3.10). Purified P-CFTR in LMNG detergent resulted in higher ATPase activity normalized to CFTR protein amount at 0.5 mM ATP compared to purified P-CFTR in digitonin detergent. Purified P-CFTR in digitonin detergent resulted in 25% ATPase activity of purified P-CFTR in LMNG detergent at 0.5 mM ATP. Results are shown as a range of ATPase activity relative to CFTR amounts (n = 2 technical replicates).

In order to determine the role of lipids in enhancing the ATPase activity of the amphipol preparation, we tested the effect of re-introducing PC, PS or a mix of PE:PS:PC:cholesterol (5:2:1:1 ratio by weight) in the LMNG preparation. I decided to test the effect of re-introducing the following lipids back to purified P-CFTR in LMNG detergent due to the following reasons: 1) PC as it was one of the major choline-containing phospholipid detected in purified CFTR in amphipol (Figure 3.8 and Figure 3.9), 2) porcine brain PS as it was previously shown to significantly increase the ATPase activity of CFTR [225], and 3) a mix of PE/brain PS/egg PC/cholesterol (5:2:1:1 ratio by weight) as PC, PE and cholesterol were mainly found to be associated with purified CFTR in amphipol by lipid TLC (Figure 3.9) and previous single channel studies were conducted with reconstituting purified CFTR in that lipid mix [50, 51, 141, 235]. We found that there were no significant changes in ATPase activity of purified P-CFTR in LMNG detergent micelles that were pre-treated with PC (Figure 3.13). We have found a subtle increase in ATPase activity of purified P-CFTR in LMNG that were pre-treated with brain PS (Figure 3.13). However, this increase was not statistically significant. Interestingly, we found a significant increase in ATPase activity of purified P-CFTR in LMNG detergent micelles upon pre-treatment with PE/brain PS/egg PC/cholesterol (5:2:1:1 ratio by weight) albeit only reaching half of the relative ATPase activity of purified P-CFTR in amphipol (Figure 3.13). These results suggest that the number of functional CFTR molecules is greater in the amphipol preparation than the LMNG preparation and that re-addition of lipids one day after detergent solubilization is only partially effective in restoring function.
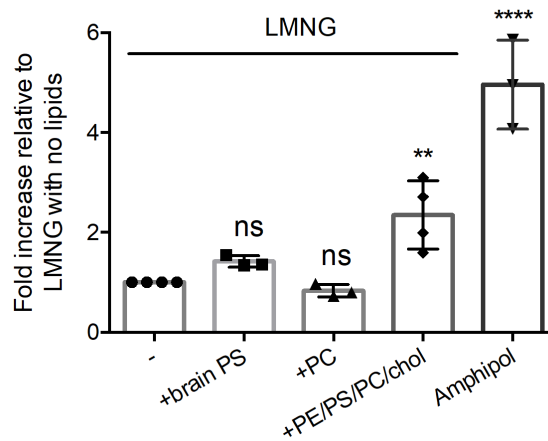
Figure 3.13: Re-introducing PE/brain PS/egg PC/cholesterol (5:2:1:1 ratio by weight) significantly increases ATPase activity of purified P-CFTR in LMNG detergent micelles.
Fold change of ATPase activity relative to protein amounts with 0.5 mM ATP of P-CFTR in LMNG detergent pre-treated with brain PS, PC or PE/brain PS/egg PC/cholesterol (PE/PS/PC/chol) mix at 5:2:1:1 weight ratio for 1 h relative to P-CFTR in LMNG detergent with P-CFTR in amphipol as a reference. Results are shown as mean ± SD (n = 3 biological replicates, n = 3 technical replicates for brain PS and amphipol conditions; n = 4 biological replicates, n = 4 technical replicates for LMNG alone and PE/PS/PC/chol, **p < 0.01, ***p < 0.001 One-way ANOVA with Dunnett's multiple comparisons test).

I was then prompted to determine if the amphipol preparation enhanced the functional reconstitution of CFTR relative to the LMNG preparation. Each preparation was separately reconstituted into pre-formed POPC liposomes. I measured anion electrodiffusion in order to determine the relative proportion of reconstituted CFTR molecules that are functional as channels [140, 192]. Briefly, in this assay, phosphorylated CFTR protein in amphipol or LMNG detergent were reconstituted into POPC proteoliposomes with equal concentrations of potassium iodide (KI) on the inside and potassium glutamate (K-Glu) on the outside to maintain the osmolarity and a concentration gradient of iodide across the liposomes [140, 192]. Addition of valinomycin (Val), an ionophore that selectively facilitates potassium ions out of the proteoliposomes, alleviates the charge build up in the proteoliposomes and allows for iodide efflux through activated CFTR as detected by an iodide-selective electrode [140, 192]. A schematic of this assay is shown in Figure 3.14A.

I observed a change in the slope of iodide efflux after valinomycin addition to the proteoliposomes with either the amphipol or LMNG preparations of P-CFTR in the presence of Mg-ATP (Figure 3.14B), conditions known to support maximal channel activity [102, 104, 140]. As expected, this flux was reduced for unphosphorylated CFTR or phosphorylated CFTR in the absence of Mg-ATP (Figure 3.14C) [140]. Similarly, the CFTR inhibitor, $CFTR_{inh}$-172, reduced flux for the phosphorylated protein as expected (Figure 3.14C) [140]. Together, these studies confirm that this proteoliposomal flux assay reports the phosphorylation- and ATP-dependent channel activity of CFTR. Importantly, I observed a significantly higher rate of iodide efflux activity from proteoliposomes containing purified P-CFTR produced using amphipol in the presence of Mg-ATP relative to the proteoliposomes containing P-CFTR extracted using LMNG plus Mg-ATP (Figure 3.14C).
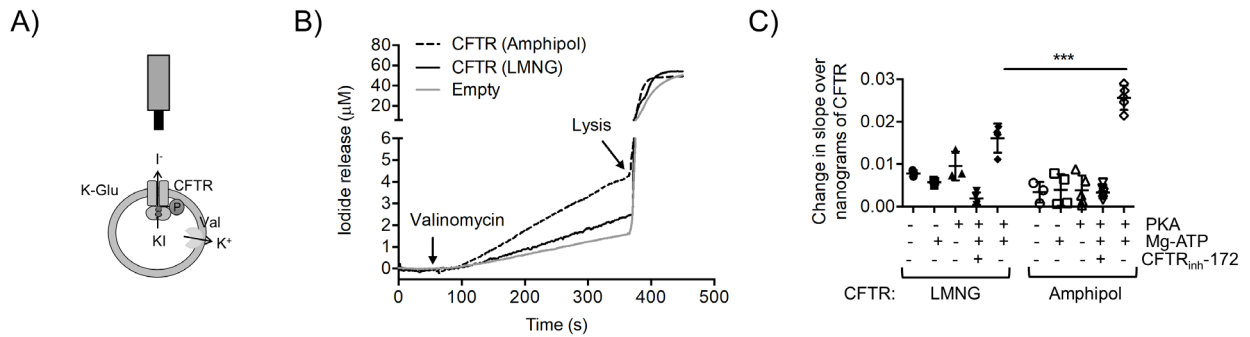
Figure 3.14: Liposomes reconstituted with purified P-CFTR in amphipol exhibit significantly higher iodide efflux activity than reconstituted purified P-CFTR in LMNG detergent.
(**A**) Cartoon showing that proteoliposomes are loaded with KI on the inside with equal concentration of K-Glu on the outside. Val moves potassium (K^+) out of the proteoliposomes creating a gradient for iodide (I^-) efflux via activated CFTR by PKA phosphorylation (P) and ATP binding. The amount of I^- efflux can be detected by an iodide-selective electrode. (**B**) Representative I^- efflux traces showing the amount of I^- release (µM) of liposomes containing P-CFTR pre-treated with Mg-ATP in amphipol and in LMNG as well as no protein (empty) treated with valinomycin and lysis of proteoliposomes with Triton. The highest amount of I^- release appeared to be in the proteoliposomes containing P-CFTR pre-treated with Mg-ATP in amphipol. (**C**) Change of slope before and after valinomycin treatment normalized to CFTR amounts in nanograms of reconstituted CFTR in LMNG detergent and amphipol with negative controls: unphosphorylated (-PKA) CFTR without (-) and with (+) Mg-ATP, phosphorylated (+PKA) CFTR without Mg-ATP and phosphorylated CFTR treated with $CFTR_{inh}$-172. Liposomes reconstituted with phosphorylated CFTR in LMNG detergent and amphipol with Mg-ATP resulted in significant increases in change of slope of iodide efflux compared to negative controls. Liposomes reconstituted with phosphorylated CFTR in amphipols with Mg-ATP resulted in a significantly higher change in slope of iodide efflux compared to reconstituted CFTR in LMNG detergent with Mg-ATP. Results are shown as mean ± SD (n = 3 biological

replicates, n > 3 technical replicates, ***$p < 0.001$, One-way ANOVA with Tukey's multiple comparisons test).

Given that these proteoliposomal efflux studies were controlled for the abundance of total CFTR reconstituted in proteoliposomes and the number of proteoliposomes (estimated by total iodide release after Triton X lysis, Figure 3.15), these findings show that the proportional functional reconstitution is greater in the amphipol preparation.
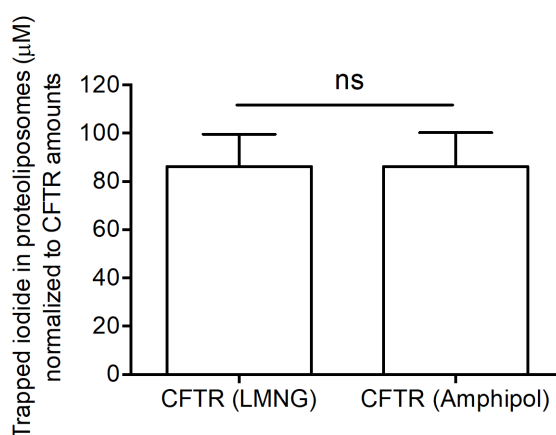
Figure 3.15: Trapped iodide is similar for the two reconstitutions, reconstitution of LMNG purified CFTR and amphipol purified CFTR.
Bars correspond to iodide measurements before valinomycin addition and after detergent lysis normalized to CFTR amounts. The data is presented as mean ± SD (n = 3 biological replicates and n = 3 technical replicates, $p > 0.05$; paired t-test).

In summary, I show that retention of interacting lipids supports the functional form of CFTR.

3.4.3 Purified CFTR in amphipol can be applied to detect direct binding of compounds on CFTR

Ivacaftor (or VX-770) potentiates the regulated channel activity of Wt-CFTR and is approved as a therapeutic intervention for a number of disease-causing mutations [140, 160, 161, 241]. To date, its binding site is unknown, although we previously showed using reconstituted CFTR

purified using the detergent, *fos*-choline 14, that VX-770 directly modulates channel opening of PKA phosphorylated CFTR [140]. Previous studies have suggested that the lipophilic compound, VX-770, interacts with the lipid bilayer and may bind at a CFTR: lipid interface [63, 161, 242]. Thus, I reasoned that CFTR extracted with its associated lipids using amphipol would exhibit a greater response to VX-770 than CFTR extracted with detergents. Now, I show in paired studies, that the fold increase in iodide electrodiffusion caused by VX-770 (1 μM) from proteoliposomes containing amphipol extracted CFTR was approximately twice that measured for proteoliposomes containing LMNG extracted protein (Figure 3.16).
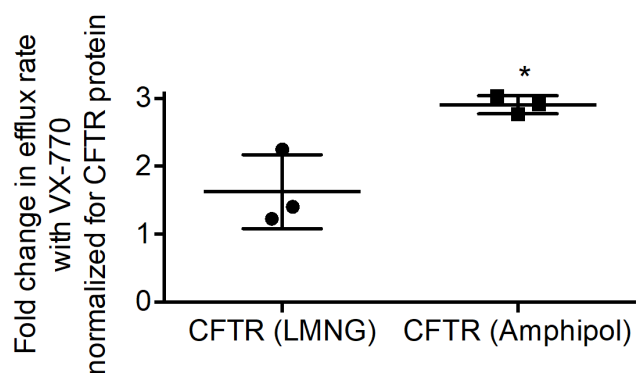
Figure 3.16: Potentiation of VX-770 was two-fold higher in proteoliposomes containing amphipol extracted CFTR than containing detergent extracted CFTR.
Fold change in iodide efflux rate normalized for CFTR protein with 1 μM VX-770 compared to vehicle shows that the potentiation effect of VX-770 was significantly higher in proteoliposomes reconstituted with P-CFTR in amphipol compared to proteoliposomes reconstituted with P-CFTR in LMNG detergent micelles. The data is presented as mean ± SD (n = 3 biological replicates, n = 3 technical replicates, *p < 0.05; paired t-test).

I was also interested in applying our purified CFTR protein in amphipol to interrogate direct binding of current and potential corrector compounds on CFTR in a more relevant lipid-containing environment. For example, I have found that potential compounds discovered as F508del-CFTR protein binders using a DNA encoded library of chemical compounds from GlaxoSmithKline (GSK) Inc. (GSK499 and GSK815) directly bind and modify intrinsic tryptophan and coumarin maleimide (CPM) fluorescence of the purified CFTR in amphipol (Figure 3.17). I have found that the GSK compounds, shifted the melting temperature (T_m) of

thermal unfolding of purified CFTR in amphipol to a greater extent than the Vertex corrector compound, VX-809, as reported by CPM fluorescence (Figure 3.17A and B). In addition, GSK499 was found to significantly increase whereas VX-809 and GSK815 were found to subtly quench intrinsic tryptophan fluorescence of purified CFTR in amphipol (Figure 3.17C and D).
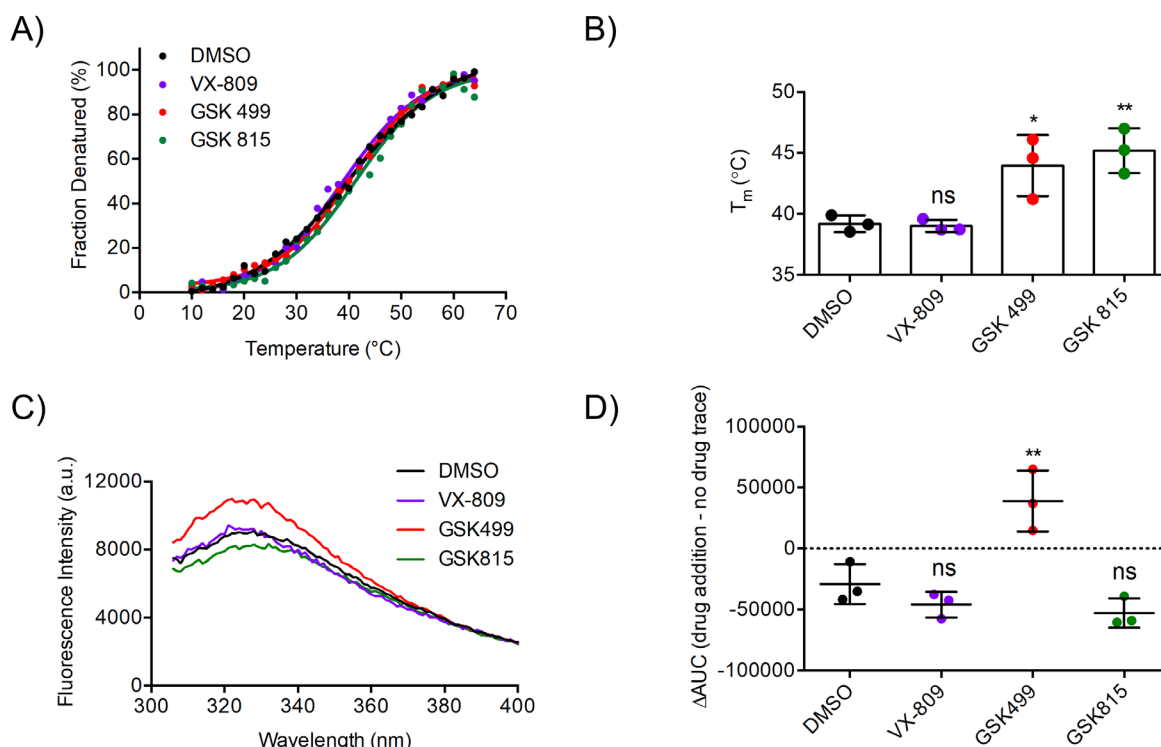
Figure 3.17: Binding effects of GSK compounds on purified CFTR in amphipol.
(**A**) Representative thermal unfolding curves of purified CFTR in amphipol treated with DMSO (black), VX-809 (purple), GSK499 (red) and GSK815 (green) using CPM fluorescence. (**B**) T_m of purified CFTR in amphipol treated with drugs from (**A**) shows increase in T_m of purified CFTR in amphipol with GSK499 and GSK815 which appears greater than with VX-809. The representative curve from (**A**) resulted in the T_m changes as indicated by the blue arrow (n = 3 biological replicates, n = 3 technical replicates, *p < 0.05, **p < 0.01, One-way ANOVA with Dunnett's test). (**C**) Representative intrinsic tryptophan fluorescence curves of purified CFTR in amphipol treated with DMSO (black), VX-809 (purple), GSK499 (red) and GSK815 (green). Traces were subtracted from the effect of buffer with the compounds. (**D**) Area under the curve (AUC) of the intrinsic tryptophan fluorescence traces shows that GSK499 significantly increased whereas GSK815 and VX-809 subtly quenched the intrinsic tryptophan fluorescence of purified CFTR in amphipol compared to vehicle (n = 3 biological replicates, n = 3 technical replicates, **p < 0.01, One-way ANOVA with Dunnett's test).

Applying the same biophysical methods, I found that the first FDA approved CF potentiator drug, VX-770, did not significantly shift the T_m throughout CFTR thermal unfolding as detected by CPM fluorescence (Figure 3.18A and B) but resulted in a significant degree of quenching of intrinsic tryptophan fluorescence of purified CFTR in amphipol at a concentration of 10 µM but not 100 nM (Figure 3.18C and D).
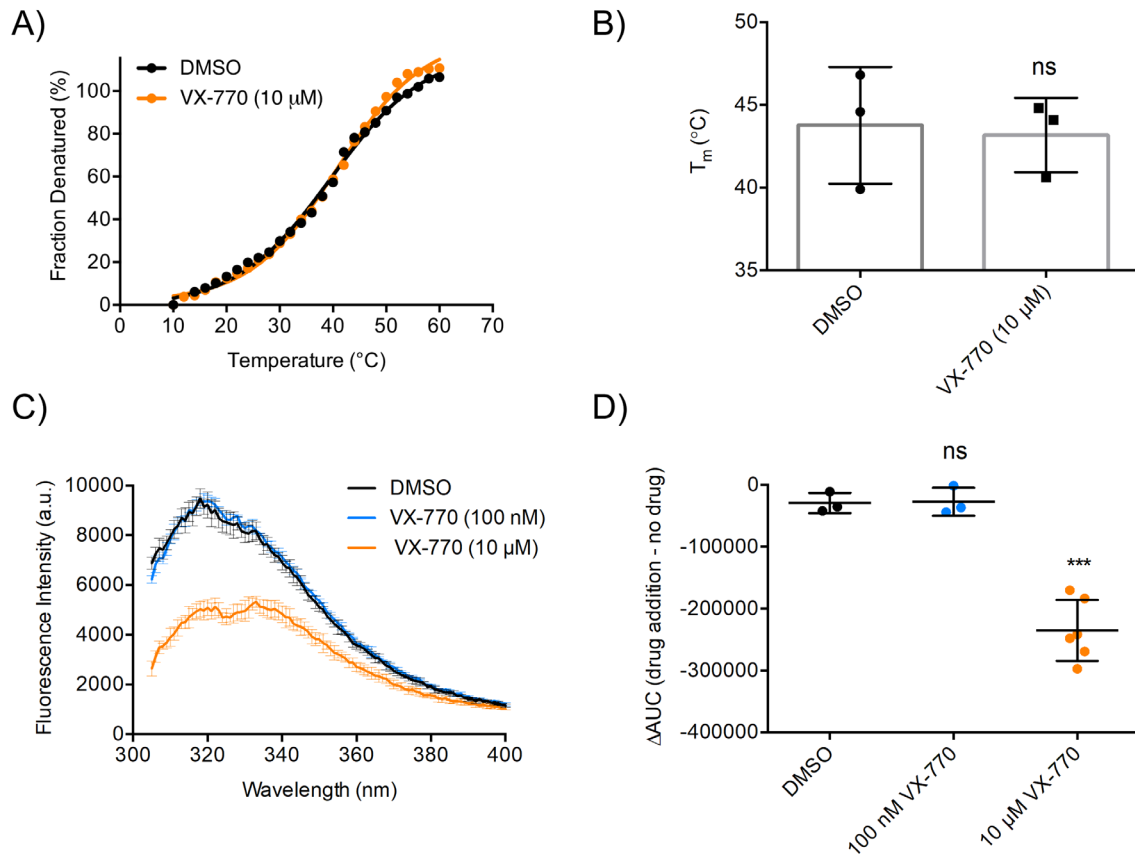
Figure 3.18: Micromolar concentration of VX-770 significantly modified the structure of purified CFTR in amphipol.
(**A**) Representative thermal unfolding curves of purified CFTR in amphipol treated with DMSO (black) and 10 µM VX-770 (orange). (**B**) T_m of purified CFTR in amphipol treated with compounds from (**A**) shows no change in thermal unfolding of purified CFTR in amphipol with 10 µM VX-770. (**C**) Representative intrinsic tryptophan fluorescence curves of purified CFTR in amphipol treated with DMSO (black), 10 µM VX-770 (orange), and 100 nM VX-770 (light blue). (**D**) Area under the curve (AUC) of the intrinsic tryptophan fluorescence traces shows that 10 µM and not 100 nM VX-770 significantly quenched the intrinsic tryptophan fluorescence of purified CFTR in amphipol compared to vehicle (n = 3 biological replicates, n = 3 technical replicates, ***p < 0.001, One-way ANOVA with Dunnett's test).

3.5   Discussion

Using a detergent-free purification method, we showed that lipid association with purified CFTR enhances its functional reconstitution as an ATPase and anion channel. We found that the proportion of functional molecules is higher following purification of CFTR: lipid complexes using amphipols than following purification in detergent. Therefore, the use of amphipols to extract and purify CFTR provides the opportunity to interrogate the role of lipid interactions in the mechanisms underlying channel gating.

Our studies suggest that purification of membrane proteins that are relatively intractable, such as CFTR, can be achieved using amphipol A8-35 with yields that are comparable to those achieved by detergents. There are several other examples of membrane proteins that have been directly extracted from membranes by amphipol A8-35 [243-245]. Further, affinity chromatography can be used to purify membrane proteins either extracted from membranes with amphipol A8-35 [243] or after exchanging detergent for amphipol A8-35 [246] since the affinity tag is accessible to solution and not embedded in the amphipol belt [247]. Once purified together with native lipids interacting in a complex with amphipols, these proteins will exhibit enhanced stability and improved suitability for biophysical studies [245].

We found that re-introducing lipids back to delipidated CFTR, initially extracted by detergent, did not completely restore its ATPase activity. It is possible that insufficient lipid was re-added relative to the detergent concentration. Alternatively, this failure suggests that a proportion of CFTR molecules were irreversibly inactivated by detergent. Based on the result that there were less functionally reconstituted CFTR molecules from the detergent LMNG compared to amphipol even with a high lipid to detergent micelle ratio, I favour the second hypothesis.

In this and previous studies, it has been shown that a non-negligible fraction of CFTR purified in detergents can be functionally reconstituted as a phosphorylated- and ATP-regulated anion channel in phospholipid liposomes [20, 50, 51, 213, 248]. In the very first purification papers, we used relatively harsh detergents to extract and purify CFTR prior to reconstitution [20, 140, 192, 248]. I estimated that the proportion of functionally reconstituted proteins after detergent purification was low, less than 20% of the total number of CFTR molecules incorporated into liposomes [20]. Unfortunately, the proportion of purified CFTR that can be functionally reconstituted as an anion channel was not routinely defined in other published purification

protocols so a systematic comparison using values in the literature is not possible. However, my proteoliposomal flux studies in the current work show that we can at least double the proportion of channel competent molecules using the amphipol A8-35 relative to the detergent LMNG.

I reason that in addition to an important role for the phospholipid interactions, the cholesterol identified in the CFTR: amphipol complexes also contributes to the enhanced function mediated by this complex. Cholesterol is present in the membranes of the endoplasmic reticulum and has been implicated in promoting stable CFTR folding during biosynthesis [249]. Cholesterol is also present at the plasma membrane and stabilizes a population of CFTR in microdomains known as lipid rafts at the cell surface [132].

The total population of CFTR containing complexes, resolved by SEC, appears micro-heterogeneous, with the maximum ATPase activity co-migrating with the shoulder of the peak eluted CFTR protein. This heterogeneity likely reflects variation in the stoichiometry of the amphipol: lipid: CFTR ratio. Analysis of the structure and function of these complexes provides the opportunity to address important questions in the field, such as the specific lipid interactions that associate with maximal catalytic and channel activity states.

I showed previously that the channel activity of detergent purified CFTR was potentiated by ivacaftor (VX-770) following its reconstitution into liposomes, supporting the claim that VX-770 acts via direct binding to CFTR [140]. Another group recently studied the interaction of VX-770 with detergent solubilized CFTR using hydrogen/deuterium exchange [250]. This method showed that there were multiple regions in CFTR that underwent changes in conformation after VX-770 interaction; however, the specific drug binding site has yet to be defined. I hypothesize that VX-770 binds at a lipid: CFTR protein interface given its lipophilicity ($\log P$ score of 5.76) [242, 251] and that VX-770 has been found to insert into the lipid bilayer [242]. In this study, I have found that the potentiation effect of VX-770 was significantly higher in liposomes reconstituted with CFTR: lipid: amphipol complexes than liposomes reconstituted with CFTR in detergent micelles (Figure 3.16). Therefore, CFTR purified together with its interacting lipids will provide a better substrate for VX-770 and enable definition of its binding site.

The dramatic effects that I observed with VX-770 on the purified CFTR protein in amphipol appears to be dose-dependent and related to its destabilizing effect on CFTR at micromolar

concentrations that have been previously reported [162, 163, 177]. According to the study described in the next chapter, this effect may be related to micromolar concentrations of VX-770 displacing the lipids of purified CFTR in amphipol due to the lipophilicity of the drug.

Chapter 4 Lipophilicity of VX-770 modifies the lipid bilayer to destabilize F508del-CFTR and other membrane proteins

Contributions:

Study was designed by Stephanie Chin and C.E.B. based on discussions with the other authors mentioned in the research article above. S.C. generated and analyzed all the data presented in this chapter with the help from all the authors. M.H. conducted and analyzed immunoblotting and FLIPR® studies on VX-770 and its derivatives. A.W. conducted and analyzed polarized total internal reflection fluorescence (pTIRF) microscopy studies. Y.-S.W. conducted and analyzed FLIPR® studies comparing potentiator activity of VX-770 and its derivative. S.A. assisted in troubleshooting and analysis of FLIPR® studies. D.Y. generated the F508del mutation on V510C/A1067C Wt cys-less variant and provided suggestions for cysteine cross-linking studies. S.E. generated SE compounds, K.T. generated KT compounds and C.M.H. assisted in generating VX-770 compounds. R.N.Y and R.D.V. assisted in communicating compound synthesis methods. C.M.Y. assisted in interpreting and communicating the pTIRF studies. Manuscript was written by S.C. and C.E.B. with input from all the authors.

4.1 Summary

F508del in CFTR is the most common CF-causing mutation. Recently, ORKAMBI®, a combination therapy that includes a corrector of the processing defect of F508del-CFTR (lumacaftor or VX-809) and a potentiator of channel activity (ivacaftor or VX-770), was approved for CF patients homozygous for this mutation. However, clinical studies revealed that the effect of ORKAMBI® on lung function is modest and it was previously proposed that this modest effect relates to a negative impact of VX-770 on the stability of F508del-CFTR. In fact, in the previous chapter, I have found that VX-770 at a supra-pharmacological concentration (10 μM) appeared to result in significant modifications of the structure of purified Wt-CFTR in amphipol using intrinsic tryptophan fluorescence as a readout. In this chapter, I show that this destabilizing effect of VX-770 at 10 μM correlated with its inhibitory effect on VX-809 mediated correction of the interface between MSD2 and NBD1 bearing F508del. Interestingly, I found that VX-770 exerted a similar destabilizing effect on the stability of other membrane localized solute carriers (SLC26A3, SLC26A9 and SLC6A14), suggesting that this destabilizing effect is not specific for F508del-CFTR. We determined that the relative destabilizing effect of a panel of VX-770 derivatives on F508del-CFTR correlated with their predicted lipophilicity. pTIRF microscopy on a supported lipid bilayer (SLB) model shows that VX-770, and not its less lipophilic derivative, increased the fluidity of and reorganized the membrane. In summary, our findings show that there is a potential for non-specific effects of VX-770 on the lipid bilayer and suggest that this effect may account for its destabilizing effect on VX-809 rescued F508del-CFTR and its previously observed structural changes of purified Wt-CFTR in amphipol as the protein contains lipids.

4.2 Introduction

CF is caused by mutations of a unique ABC anion channel, CFTR [1]. As previously mentioned, the ICL: NBD1 interface is disrupted by the major CF causing mutation, F508del, thereby compromising assembly and function of CFTR [146, 180].

The first FDA approved medicine to treat the underlying cause of CF is KALYDECO® (VX-770), a potentiator that enhances channel gating of Wt-CFTR and CFTR with certain gating mutations (i.e. G551D) at the cell surface by directly binding to the protein to prolong its open state in an ATP-independent manner [140, 160, 161]. On the other hand, patch clamp studies by

Jih and Hwang suggested that both ATP-dependent and ATP-independent CFTR channel gating are modified by VX-770 [161]. Recently, ORKAMBI®, a combination of VX-770 and a corrector compound known as VX-809, was approved for use in patients who are homozygous for the major CF mutation, F508del. The corrector compound, VX-809, acts to partially rescue the defect in protein mistrafficking and misprocessing exhibited by F508del-CFTR to the cell surface [156], by repairing the aberrant ICL: NBD1 interfaces [145, 146, 157, 158]. VX-770 acts on the VX-809 corrected F508del-CFTR to augment its activity by the mechanism that was previously described [140, 156, 160, 161].

Unfortunately, ORKAMBI® mediates modest and variable clinical responses [174] prompting further discovery efforts for more efficacious corrector compounds. In fact, a recent FDA approved medicine known as SYMDEKO™, a combination of VX-770 and another corrector compound known as tezacaftor (VX-661), has shown a better albeit modest improvement in lung function (4%) in F508del homozygous patients than ORKAMBI® (1-3%) (Vertex Pharmaceuticals Incorporated, 2018). Certain *in vitro* findings suggest that the modest *in vivo* effect of these medicines may reflect an adverse effect of VX-770 on the stability of the VX-809 or VX-661 corrected protein [162, 163, 177]. However, the mechanism of action of this destabilizing effect was not known. Thus, the aim of the current studies was to interrogate the mechanism underlying this destabilizing effect of VX-770 on VX-809 rescued F508del-CFTR by interrogating the ICL4: NBD1 interface which was shown to be important for CFTR assembly and stability [145, 146, 157, 158]. A survey of VX-770 derivatives with modifications of the left- and right-hand side of the parent VX-770 compound with various lipophilicities (Figure 4.1) were applied to further determine the mechanism of action of the destabilizing effect of VX-770 on F508del-CFTR. We also assessed the specificity of this destabilizing effect of VX-770 by studying its interaction with other membrane proteins (including SLC26A3, SLC26A9 and SLC6A14) as well as the lipid bilayer with pTIRF microscopy studies.

4.3   Materials and Methods

4.3.1   Chronic treatment of F508del-CFTR with VX-770 and its analogs

HEK-293 cells stably expressing F508del-CFTR (HEK F508del) were plated on 24 well plates (Sarstedt, Nümbrecht, Germany) and maintained in DMEM (Wisent, St-Bruno, Quebec, Canada) supplemented with 10% Fetal Bovine Serum (FBS, Wisent, St-Bruno, Quebec, Canada), 1%

non-essential amino acids (NEAA, Wisent, St-Bruno, Quebec, Canada), 0.6 mg/ml G418 sulfate (Wisent, St-Bruno, Quebec, Canada) and 5 µg/ml blasticidin (Wisent, St-Bruno, Quebec, Canada) at 37°C with 5% CO_2 overnight. For the initial chronic VX-770 studies, HEK F508del cells were pre-treated with VX-770 at a pharmacological concentration (0.1 µM) or at a supra-pharmacological concentration (10 µM) with 3 µM VX-809 (Selleck Chemicals, Houston, TX) in the previously described media at 37°C with 5% CO_2 for 48 h. For the studies with VX-770 and its derivatives, HEK F508del cells were pre-treated with VX-770 (Selleck Chemicals, Houston, TX) or its various derivatives (SE and KT compounds) synthesized in Dr. Russell Viirre's laboratory (Toronto, Ontario, Canada) (manuscript in preparation, refer to Figure 4.1 for chemical structures of VX-770 derivatives) at a pharmacological concentration (0.1 µM) or at a supra-pharmacological concentration (10 µM) in the previously described media at 27°C with 5% CO_2 for 24 h. The synthesis and characterization of the SE compounds in this paper has previously been described in detail [252]. The synthesis and characterization the KT compounds employed the same methodology as [252] for the most part but also incorporated additional reaction steps previously published by the Verkman group for modification of the left hand side of the VX-770 molecule [253].
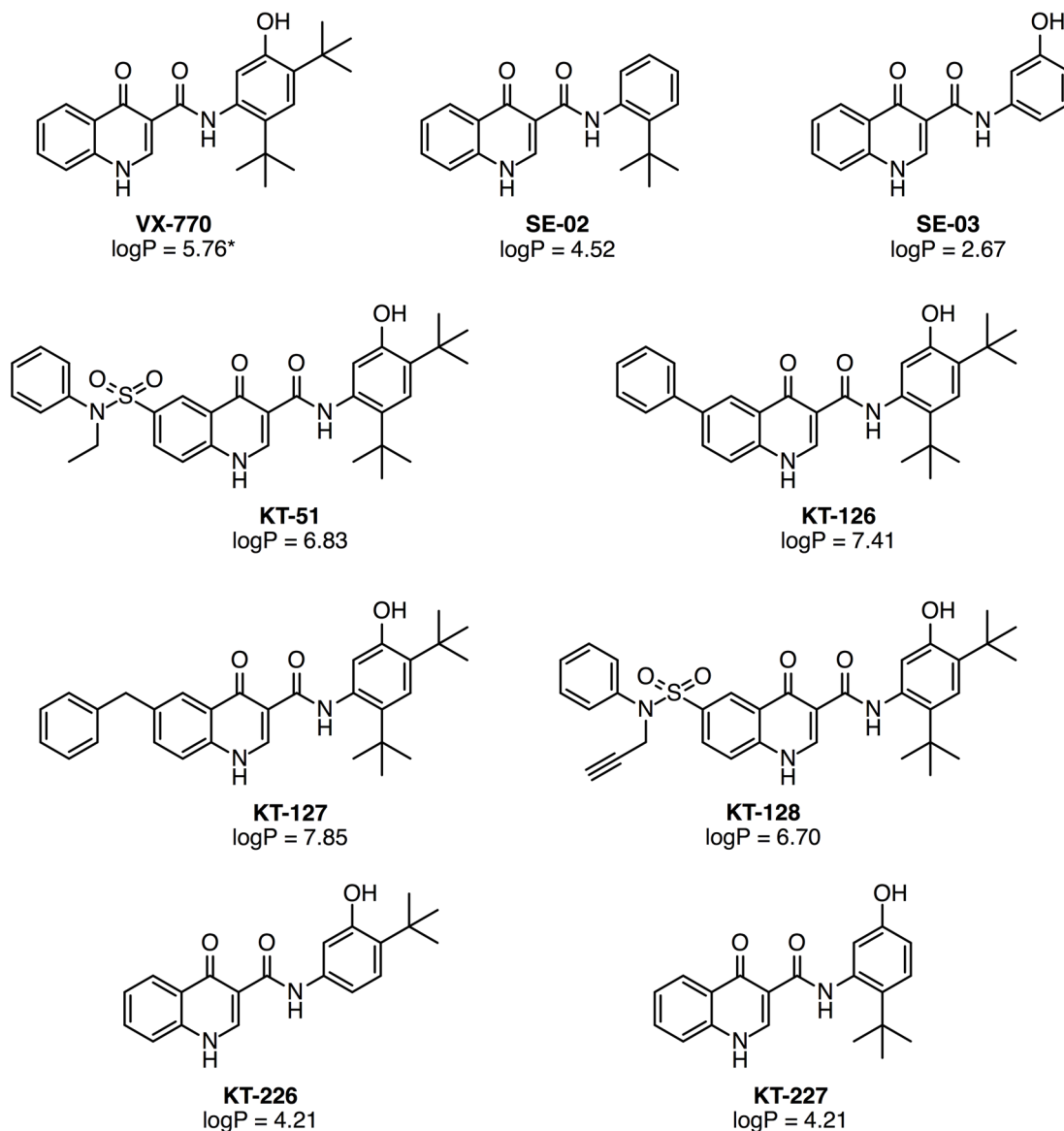
Figure 4.1: Chemical structures of VX-770 and its derivatives generated by Dr. Viirre's laboratory (manuscript in preparation) with corresponding logP values.
Derivatives with left-hand side modifications include KT-51, KT-126, KT-127 and KT-128. Derivatives with right-hand side modifications include SE-02, SE-03, KT-226 and KT-227.

4.3.2   Generation of mutants and constructs

The V510C, A1067C and V510C/A1067C cysteine-less (cys-less) variants of Wt-CFTR were kindly provided by Dr. David Clarke (Toronto, Ontario, Canada), the SLC26A3 and SLC26A9

constructs with N-terminal FLAG tags were kindly provided by Dr. Reinhart Reithmeier (Toronto, Ontario, Canada) and the SLC6A14 construct with a C-terminal FLAG tag was generated by OriGene (Rockville, MD). The F508del mutation was generated on the V510C/A1067C cys-less variant of Wt-CFTR background with primers (Forward: 5'-CATTAAAGAAAATATCATTGGTTGTTCCTATGATG-3' and Reverse: 5'-CATCATAGGAACAACCAATGATATTTTCTTTAATG-3') and the KAPA HiFi HotStart PCR Kit (KAPA Biosystems, Woburn, MA). Plasmid DNA was expanded with the QIAprep Spin Miniprep Kit (Qiagen, Hilden, Germany) and the sequence was confirmed with DNA sequencing (TCAG, Toronto, Ontario, Canada). HEK-293 GT cells, kindly provided by Dr. Daniela Rotin's laboratory (Toronto, Ontario, Canada), were maintained in DMEM (Wisent, St-Bruno, Quebec, Canada) supplemented with 10% FBS (Wisent, St-Bruno, Quebec, Canada), 1% NEAA (Wisent, St-Bruno, Quebec, Canada) and 0.6 mg/ml G418 sulfate (Wisent, St-Bruno, Quebec, Canada) at 37°C with 5% CO_2, transfected with constructs using PolyFect Transfection Reagent (Qiagen, Hilden, Germany) according to the manufacturer's protocol and temperature rescued at 27°C for 24 h while maintaining 5% CO_2.

4.3.3   Cysteine cross-linking

HEK-293 GT cells were grown on 24 well plates (Sarstedt, Nümbrecht, Germany) at 37°C with 5% CO_2 overnight and then transfected with cys-less variants of Wt- or F508del-CFTR containing double cysteines at the ICL4: NBD1 interface. Cells were treated with DMSO (0.1%), VX-809 (3 μM), VX-770 (0.1 or 10 μM), or VX-809 plus VX-770 (0.1 or 10 μM) at 27°C with 5% CO_2 for 24 h. The next day, cells were treated with 50 μM BMOE (Life Technologies, Rockford, IL) in DMEM (Wisent, St-Bruno, Quebec, Canada) supplemented with 10% FBS (Wisent, St-Bruno, Quebec, Canada), 1% NEAA (Wisent, St-Bruno, Quebec, Canada) and 0.6 mg/ml G418 sulfate (Wisent, St-Bruno, Quebec, Canada) at 27°C with 5% CO_2 for 1 h.

4.3.4   Deglycosylation studies

Cys-less variants of CFTR were lysed from HEK-293 GT cells into radioimmunoprecipitation assay (RIPA; 50 mM Tris-Base, 150 mM sodium chloride, 1 mM EDTA, 1% (v/v) Triton X-100, 0.1% (v/v) SDS, 1X protease inhibitor cocktail (AMRESCO, Cleveland, OH), pH 7.4) buffer. Protein samples were treated with Endoglycosidase H and PNGase F according to the manufacturer's protocol (New England Biolabs, Ipswich, MA).

4.3.5   Chronic treatment of SLC proteins with VX-770

HEK-293 GT cells were grown on 24 well plates (Sarstedt, Nümbrecht, Germany) at 37°C with 5% CO_2 overnight and transfected with the SLC constructs. Cells were then treated with various concentrations of VX-770 (0, 0.1, 1, 2, 10 µM) at 27°C with 5% CO_2 for 24 h.

4.3.6   Immunoblotting

HEK F508del and HEK-293 GT cells were lysed into RIPA buffer and protein samples were subjected to SDS-PAGE. CFTR protein samples were run on 6% Tris-Glycine sodium dodecyl sulfate (TG SDS) gels (Life Technologies, Carlsbad, CA) and SLC protein samples were run on 8% TG SDS gels (Life Technologies, Carlsbad, CA). Protein samples were transferred to nitrocellulose paper and probed with the following primary antibodies overnight at 4°C: IgG2b mAb596 antibody (University of North Carolina at Chapel Hill, Chapel Hill, NC, code: A4, Cystic Fibrosis Foundation Therapeutics Inc.) for CFTR protein (1:5000 for F508del-CFTR, 1:1000 for V510C/A1067C cys-less variant of Wt-CFTR, 1:500 for V510C/A1067C cys-less variant of F508del-CFTR), calnexin-specific rabbit pAb (1:10000, Sigma-Aldrich, St. Louis, MO, cat. no.: C4731) for calnexin loading control, anti-mouse FLAG antibody (Sigma-Aldrich, St. Louis, MO, 1:2500) for SLC protein, and anti-β-actin (1:10000, Abcam, Cambridge, UK, ab8229) for actin loading control. The samples were then probed with secondary antibodies (at concentrations twice as diluted as the primary antibodies used) for 1 h at room temperature shaking as follows: horseradish peroxidase-conjugated goat anti-mouse IgG secondary antibody (Pierce, Rockford, IL) for CFTR protein and actin loading control, horseradish peroxidase–conjugated goat anti-rabbit IgG secondary antibody (Pierce, Rockford, IL) for calnexin loading control, and anti-mouse HA (Covance, Princeton, NJ, MMS-101R) for SLC protein. Immunoblots were exposed using Amersham enhanced chemiluminescent reagent (GE Healthcare Life Sciences, Mississauga, Ontario, Canada) with the Li-Cor Odyssey Fc (LI-COR Biosciences, Lincoln, NE) at a linear range of exposure. Densitometry of immunoblot bands was performed with Image Studio Lite software (Version 5.2.5, LI-COR Biosciences, Lincoln, NE).

4.3.7   FLIPR® membrane potential assay

The FLIPR® membrane potential assay was conducted as previously described [199]. Briefly, HEK F508del cells were freshly split and grown overnight to 90-100% confluence on black 96

well plates with clear bottoms (Corning, Corning, NY) at 37°C with 5% CO_2. Cells were then treated with 3 μM VX-809 at 37°C with 5% CO_2 for 48 h. The next day, cells were loaded with 0.5 mg/ml FLIPR® membrane potential dye (Molecular Devices, Sunnyvale, CA) in sodium gluconate buffer as previously described [199] for 45 min with 5% CO_2 at 37°C. Fluorescence was read at excitation of 530 nm and emission of 560 nm on a SpectraMax i3X fluorescence plate reader at 37°C (Molecular Devices, Sunnyvale, CA). Baseline fluorescence was read for 5 min. CFTR was stimulated by vehicle, 1 μM forskolin (Fsk, Sigma-Aldrich, St. Louis, MO), 1 μM Fsk with VX-770 (10 μM), or 1 μM Fsk with the derivative SE-03 (10 μM) for 10 min. CFTR was then inhibited with 10 μM CFTR inhibitor-172 ($CFTR_{inh}$-172, Cystic Fibrosis Foundation Therapeutics Inc. and Rosalind Franklin University of Medicine and Science, Chicago, IL) for 12 min. Curves were normalized to last point of baseline and the maximal points of stimulation were plotted with GraphPad Prism v6.01 (GraphPad Software, San Diego, CA).

4.3.8   pTIRF microscopy

The formation of SLBs of 1:1:1 dioleoylphosphatidylcholine/egg sphingomyelin/cholesterol (DOPC/bSM/chol) and 1:1:1 DOPC/distearoylphosphatidylcholine/chol (DOPC/DSPC/chol) with $DilC_{18}$(3) (1 mol %, Life Technologies, Carlsbad, CA) in buffer (10 mM HEPES, 150 mM NaCl, pH 7.4) were prepared as previously described [254]. All images were acquired using a home-built pTIRF system incorporating four excitation laser lines built on an Olympus IX70 inverted microscope. All images were captured at 15 s intervals for 1 h with a water-cooled Evolve 512 EMCCD camera (Photometrics, Tucson, AZ) controlled by μ-Manager (http://www.micro-manager.org). Fluorescent probes were excited by substrate parallel (Fs, s-polarized) and perpendicular (Fp, p-polarized) polarized excitation at 532 nm through a half-wave liquid crystal variable retarder (LCC25 1111A, Thorlabs, Newton, NJ). Two bilayer studies were performed with multiple fields of view examined for each bilayer (3-6 fields). Order parameter <P_2> values were determined for each region of interest and calculated on a per pixel basis using an in-house macro. Refer to previous publications for more details [255, 256].

4.3.9   Statistical analyses

Results were plotted and analyzed on GraphPad Prism v6.01 (San Diego, CA). Results were presented as mean ± SD with each replicate representing one biological replicate from an individual experiment. For all statistical analyses, One-way ANOVA and Dunnett's post-hoc test were conducted on GraphPad Prism v6.01 (San Diego, CA) for multiple comparisons of conditions to the control. The p-values were automatically adjusted by GraphPad Prism v6.01 (San Diego, CA) for the multiple comparisons and $p < 0.05$ was considered significantly different from the control.

4.4   Results

4.4.1   Destabilizing effect of long-term treatment with micromolar concentrations of VX-770 on the abundance of VX-809 corrected F508del-CFTR protein

As previously reported [162, 163, 177], we observed a destabilizing effect of long-term (48 hours) treatment of VX-770 at a high concentration (10 μM) at 37°C on the relative abundance of the mature band C (Figure 4.2A and B) and immature band B (Figure 4.2A and C) forms of the VX-809 rescued F508del-CFTR protein in the HEK-293 expression system. As previously reported [162], this was not related to a significant decrease in cell viability, with comparable abundance of calnexin (CNX) expression across the treatments (Figure 4.2A).
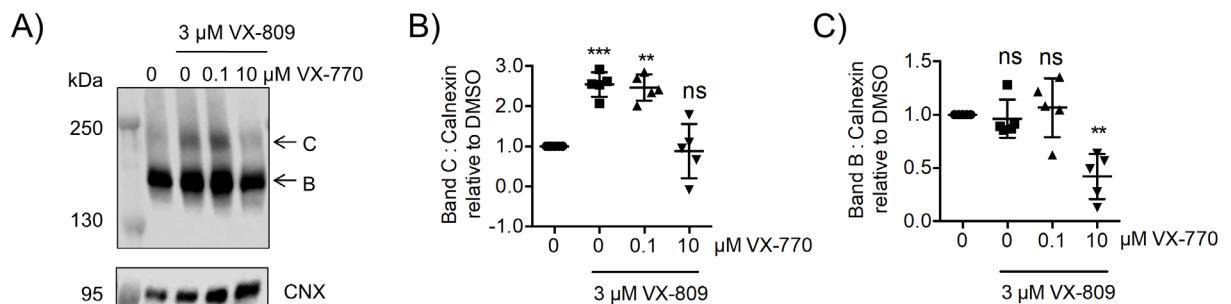
Figure 4.2: Supra-pharmacological concentration of VX-770 destabilizes protein expression of VX-809 rescued F508del-CFTR.
(**A**) Immunoblot of F508del-CFTR treated with 3 μM VX-809 and 0, 0.1 and 10 μM VX-770 at 37°C for 48 h with no VX-809 treatment as control and calnexin (CNX) as loading control. (**B**) Densitometry analysis of immunoblots of band C normalized to calnexin (CNX) and DMSO treatment shows that chronic treatment with 10 μM VX-770, and not 0.1 μM VX-770,

significantly decreased band *C* of VX-809 rescued F508del-CFTR (n = 5 for all conditions). Results are presented as mean ± SD and analyzed by One-way ANOVA and Dunnett's post-hoc test (**p < 0.01 and ***p < 0.001 compared to vehicle). (**C**) Densitometry analysis of immunoblots of band *B* abundance normalized to calnexin (CNX) loading control and DMSO treatment shows that chronic treatment with 10 µM VX-770, and not 0.1 µM VX-770, also significantly decreased band *B* abundance relative to VX-809 rescue of F508del-CFTR (n = 5 for all conditions). Results are presented as mean ± SD and analyzed by One-way ANOVA and Dunnett's post-hoc test (**p < 0.01 compared to vehicle).

4.4.2 Micromolar VX-770 reverses the effect of VX-809 in stabilizing the ICL4: NBD1 interface of cys-less variant of F508del-CFTR

I was prompted to determine if this destabilizing effect of VX-770 was due in part, to a reversal of the positive effect of VX-809 on F508del-CFTR assembly. The corrector, VX-809, is thought to act by stabilizing the aberrant interaction between F508del in NBD1 and the intracellular loop ICL4 (conferred by MSD2) [145, 146]. As in previous publications [30, 41-43, 46, 257], I assessed this interaction by studying the propensity for chemical cross-linking between cysteine residues engineered at V510 (NBD1) and A1067 (ICL4) in the context of a full-length cys-less variant of CFTR protein for both Wt and F508del. The following studies were performed at 27°C as the cys-less variant of CFTR protein is misprocessed at 37°C and requires temperature rescue at 27°C to promote its maturation [41, 45, 258, 259].

The V510C/A1067C cys-less variant of Wt-CFTR runs as two bands: the mature, complex glycosylated band *C* and the immature, core glycosylated band *B* (Figure 4.3A). As previously reported, band *C* is insensitive to Endoglycosidase (Endo) H, whereas band *B* is deglycosylated and this form is labeled as band *A*. Both band *B* and *C* are deglycosylated by PNGase F as shown on the left panels of Figure 4.3A. As previously shown in Chapter 2, I confirmed that two cysteine residues (V510C on NBD1 and A1067C on ICL4) could be cross-linked by a cell-permeable maleimide reagent, BMOE, in a V510C/A1067C cys-less variant of Wt-CFTR protein with the appearance of a cross-linked species (†) that migrates as a 250 kDa protein on a SDS-PAGE gel (Figure 4.3A) [257]. As previously shown in Chapter 2, I confirmed that this band (†) was conferred by intramolecular rather than intermolecular cross-linking as it was not produced when single cysteine containing constructs (V510C or A1067C) were expressed alone or together [257]. I showed that the band (†) is Endo H resistant and hence, complex

glycosylated. Interestingly, an N-glycanase resistant band (△) was apparent in the cross-linker treated cells but not in the absence of cross-linker (Figure 4.3A). I suggest on the basis of its glycosidase resistance, that this unique band is the cross-linked form of band *A*.

A V510C/A1067C cys-less variant of F508del-CFTR is misprocessed with no appearance of band *C* in SDS-PAGE, with just the misprocessed band *B* expressed (Figure 4.3B) [42, 43]. Treatment with the cell-permeable cross-linker (BMOE) led to the appearance of a unique band (✱). This band (✱) shifted slightly following Endo H treatment to (△), confirming that it is not the *C* band, but rather band (✱) is the cross-linked band *B*. The band (△) of this mutant protein is N-glycanase resistant, suggesting that it represents the cross-linked band *A*. This band co-migrates with the N-glycanase resistant protein detected in the cross-linked, cysteine modified version of Wt-CFTR. However, it is much less abundant in the case of F508del (Figure 4.3C). This interpretation is consistent with previous publications claiming that the major mutant exhibits a defect in assembly between NBD1 and ICL4 of MSD2 [30, 42, 43, 45, 46].
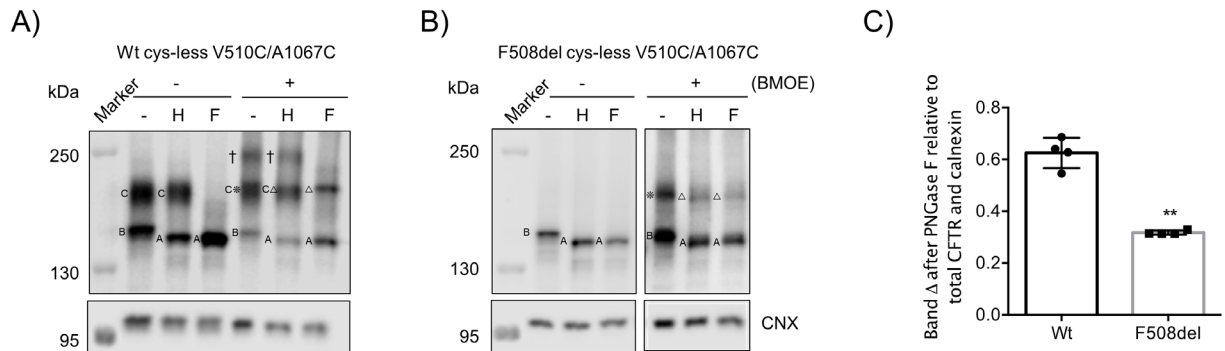
Figure 4.3: Characterization of cysteine cross-linking bands of Wt and F508del V510C/A1067C cys-less CFTR variants.
(**A**) Immunoblot of deglycosylation studies of V510C/A1067C cys-less variants of Wt-CFTR without (-) and with (+) BMOE treatment. *V510C/A1067C cys-less variant of Wt-CFTR (-) BMOE:* No glycanase (-) treatment resulted in band *C* and *B* that is normally expressed in Wt-CFTR. Endoglycosidase H (H) treatment resulted in band *C* and band *A*. PNGase F (F) treatment resulted in band *A*. *V510C/A1067C cys-less variant of Wt-CFTR (+) BMOE:* No glycanase (-) treatment resulted in cross-linked band *C* (†), population containing band *C* and cross-linked band *B* (C✱), and band *B*. Endoglycosidase H (H) treatment resulted in cross-linked band *C* (†), population of band *C* and cross-linked band *A* (C△), and band *A*. PNGase F (F) treatment resulted in cross-linked band *A* (△) and band *A*. (**B**) Immunoblot of deglycosylation studies of V510C/A1067C cys-less variants of F508del-CFTR without (-) and with (+) BMOE treatment. *V510C/A1067C cys-less variant of F508del-CFTR (-) BMOE:* No glycanase (-) treatment resulted in band *B*, Endoglycosidase H (H) treatment resulted in band *A* and PNGase F (F)

treatment resulted in band *A*. *V510C/A1067C cys-less variant of F508del-CFTR (+) BMOE:* No glycanase (-) treatment resulted in cross-linked band *B* (✳) and band *B*. Endoglycosidase H (H) treatment resulted in cross-linked band *A* (△) and band *A*. PNGase F (F) treatment resulted in cross-linked band *A* (△) and band *A*. (**C**) Quantification of the ratio of band X-linked band *A* (△) over total protein after PNGase F showed that a relatively lower N-glycosidase resistant cross-linked band of cys-less F508del V510C/A1067C compared to Wt (n = 4 biological replicates, n = 4 technical replicates). Results are presented as mean ± SD and analyzed by paired t-test (**p $<$ 0.001, paired t-test).

Long term (24 hours) treatment of V510C/A1067C cys-less variant of F508del-CFTR with VX-809 (3 μM) did not lead to its maturation and the appearance of band *C*, likely due to the number of mutations introduced to eliminate endogenous cysteines (Figure 4.4A). However, this treatment did lead to a significant increase in the cross-linking between V510C and A1067C with an increased ratio of the cross-linked band *B* (✳) relative to band *B* (Figure 4.4A and B). These findings are consistent with previous studies, showing its positive effect in improving interaction between NBD1 and ICL4 [156-158]. This positive effect of VX-809 was reversed when VX-770 (10 μM) was included in this long-term treatment (Figure 4.4A and B). This abolition of NBD1: ICL4 assembly following the combination treatment could explain the effect observed on processing as documented in Figure 4.2. As in the case of the protein processing studies shown in Figure 4.2, the destabilizing effect of VX-770 on domain: domain assembly is dose-dependent and no destabilizing effect on cross-linking was observed following co-treatment with VX-770 at 0.1 μM (Figure 4.4A and B).
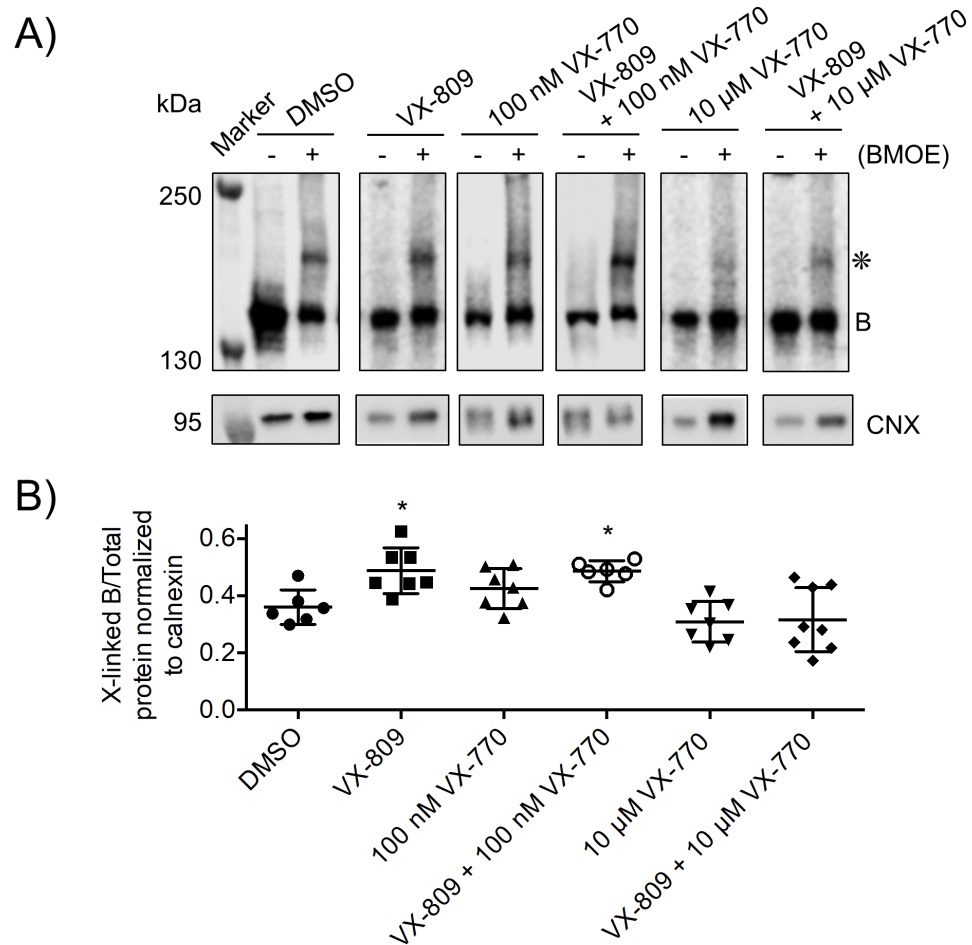
Figure 4.4: Supra-pharmacological concentration of VX-770 abolishes VX-809 rescue effect at the ICL4: NBD1 interface of cys-less variant of F508del-CFTR.
(**A**) Immunoblot of V510C/A1067C cys-less variant of F508del-CFTR pre-treated with vehicle (DMSO, 0.1%), VX-809 (3 μM), VX-770 (100 nM or 10 μM), or combination of VX-809 and (+) VX-770 (100 nM VX-770 or 10 μM) at 27°C for 24 h. (**B**) Densitometry results of normalized cross (X)-linked band *B* (✱) to band *B* show that VX-809 significantly increased the abundance of relative X-linked band *B* (✱) and this effect was abolished upon additional treatment with 10 μM VX-770 but not with 100 nM VX-770 (n = 6 for DMSO and VX-809 + 100 nM VX-770 conditions; n = 7 for VX-809, 100 nM VX-770 and 10 μM VX-770 conditions; and n = 8 for VX-809 + 10 μM VX-770 condition). Results are presented as mean ± SD and analyzed by One-way ANOVA and Dunnett's post-hoc test (*p < 0.05 compared to vehicle).

4.4.3 Micromolar concentrations of VX-770 also exert a destabilizing impact on other membrane proteins

I was interested to determine if the destabilizing effect of 10 μM VX-770 was specific to F508del-CFTR. In order to maintain similar conditions to my cysteine cross-linking studies, I

tested its specificity by applying this concentration of VX-770 at 27°C on HEK-293 cells expressing other membrane proteins, including SLCs: SLC26A3, SLC26A9 and SLC6A14. These membrane proteins are particularly important as they have been shown to interact with and/or modify CFTR channel activity in various epithelial tissues [134, 135, 260-265]. Further, these SLC genes have been shown to modify CF disease phenotypes [164-167]. Thus, I reason that it would be disadvantageous for CFTR modulatory drugs to also affect the expression of these membrane proteins.

Firstly, analysis of the SLC proteins by SDS-PAGE revealed multiple glycosylation states as previously reported [266]. Interestingly, the steady state abundance of all the SLCs in this study was significantly decreased with chronic treatment with micromolar concentrations of VX-770 at 27°C (Figure 4.5). SLC26A3 appeared to be the most susceptible to VX-770 as its protein expression significantly decreased at concentrations of VX-770 as low as 0.1 µM (Figure 4.5A). On the other hand, the abundance of SLC26A9 and SLC6A14 was significantly decreased starting at higher concentrations of 2 µM and 10 µM VX-770 respectively (Figure 4.5B and C). Therefore, the destabilizing effect of supra-pharmacological concentrations of VX-770 is not specific to F508del-CFTR.
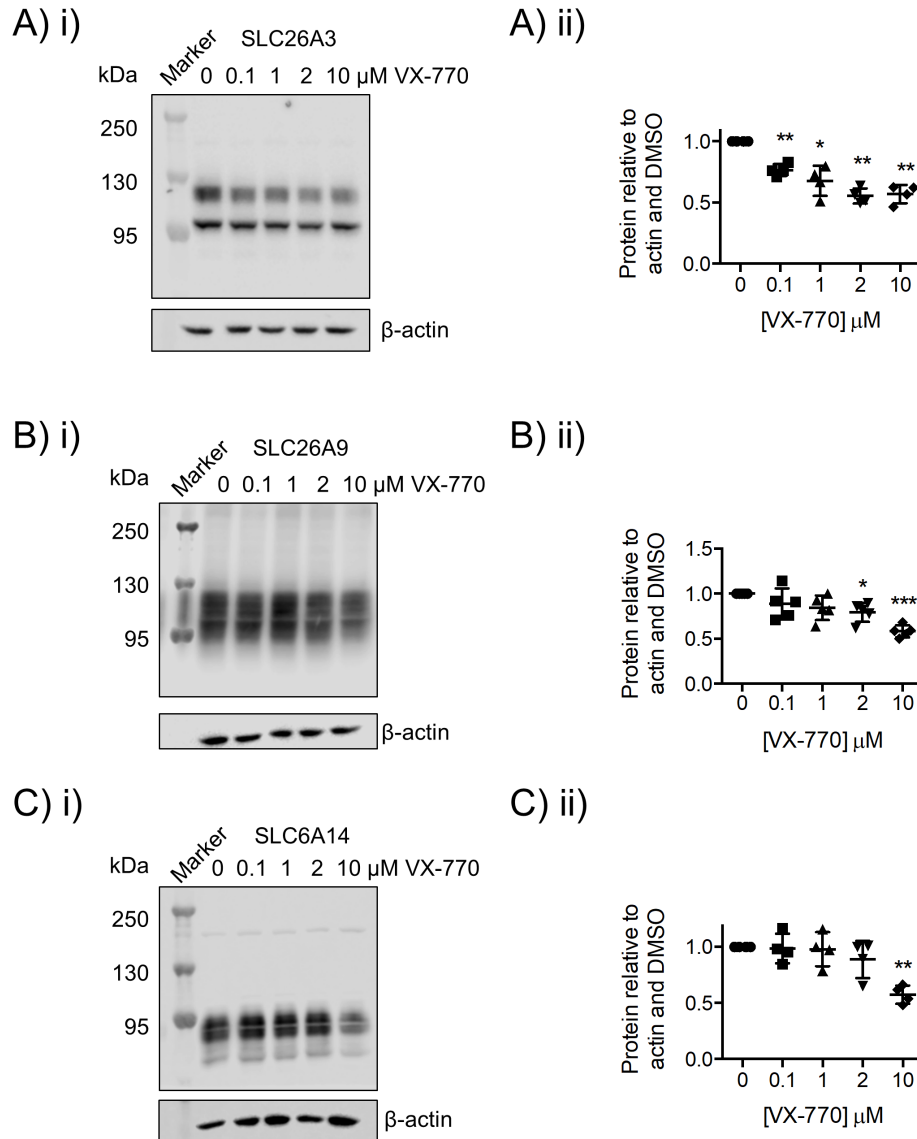
Figure 4.5: VX-770 exerts destabilizing effect on membrane proteins of the solute carrier (SLC) family.
(**i**) Representative immunoblots of (**A**) SLC26A3, (**B**) SLC26A9, and (**C**) SLC6A14 show different glycosylation forms of the proteins as previously reported [266]. SLC proteins were treated with 0, 0.1, 1, 2 and 10 µM of VX-770 at 27°C for 24 h with actin as loading control. (**ii**) Densitometry analyses of total protein relative to DMSO treatment and actin loading control of (**A**) SLC26A3 (n = 4 for all conditions), (**B**) SLC26A9 (n = 5 for all conditions), and (**C**) SLC6A14 (n = 4 for all conditions). SLC26A3 expression significantly decreased after 0.1 µM VX-770, SLC26A9 expression significantly decreased after 2 µM VX-770, and SLC6A14 expression significantly decreased after 10 µM VX-770. Results are presented as mean ± SD and analyzed by One-way ANOVA and Dunnett's post-hoc test (*p < 0.05, **p < 0.01, and ***p < 0.001 compared to vehicle).

4.4.4 Lipophilicity of VX-770 appears to be correlated with the destabilizing effect on F508del-CFTR

I propose that the non-specific, destabilizing effects of supra-pharmacological concentrations of VX-770 may be related to the known effects of this compound on the lipid bilayer [242]. To test this idea, VX-770 derivatives (Figure 4.1) with varying degrees of lipophilicity, as assessed by their partition coefficient (log$P$) values that were determined by a consensus method in MarvinSketch, were incubated with HEK-293 cells expressing temperature–rescued F508del-CFTR and their effects on the processing (band $C/C+B$) of F508del-CFTR determined.

In this study, the HEK-293 cells expressing F508del-CFTR were treated with VX-770 or a derivative for 24 hours at 0.1 or 10 µM at 27ºC. We observed a negative correlation between the lipophilicity or log$P$ values and the relative band $C/C+B$ ratio (Figure 4.6). Derivatives with low log$P$ scores (i.e. SE-02, SE-03, KT-226 and KT-227) were associated with a higher band $C/C+B$ ratio than the derivatives with high log$P$ scores (i.e. KT-51, KT-126, KT-127 and KT-128) (Figure 4.6A and B).
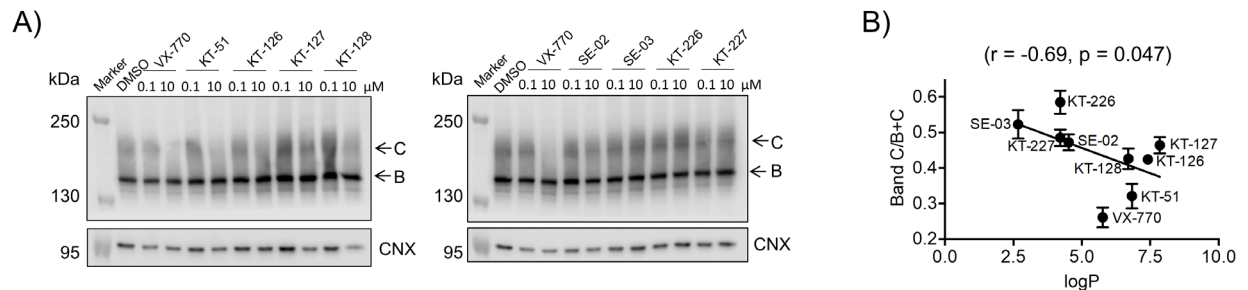
Figure 4.6: Lipophilicity of VX-770 appears to be correlated with the destabilizing effect of F508del-CFTR.
(**A**) Immunoblots of F508del-CFTR from HEK-293 overexpressing F508del-CFTR cells chronically treated with VX-770 and its derivatives at 0.1 µM or 10 µM at 27°C for 24 h compared to DMSO as a negative control. Calnexin (CNX) was used as a loading control. (**B**) Correlation plot of the lipophilicity measure also known as log$P$ and the abundance of cell surface band C relative to band C and band B ($C+B$) of F508del-CFTR treated with 10 µM of VX-770 and its derivatives at 27°C for 24 h. There was a significant correlation suggesting that the higher the lipophilicity of the drug derivative may correlate to less cell surface expression of F508del-CFTR (n = 4 for all derivatives). Results were analyzed by linear regression and Spearman's correlation (r = -0.69 and *p < 0.05).

4.4.5 A VX-770 derivative with a low lipophilicity did not exhibit destabilizing effects on F508del-CFTR and SLC26A3

The VX-770 derivative SE-03, while exhibiting potentiator activity (Figure 4.7C and D), did not reduce steady state protein abundance at 10 μM (Figure 4.7A and B).
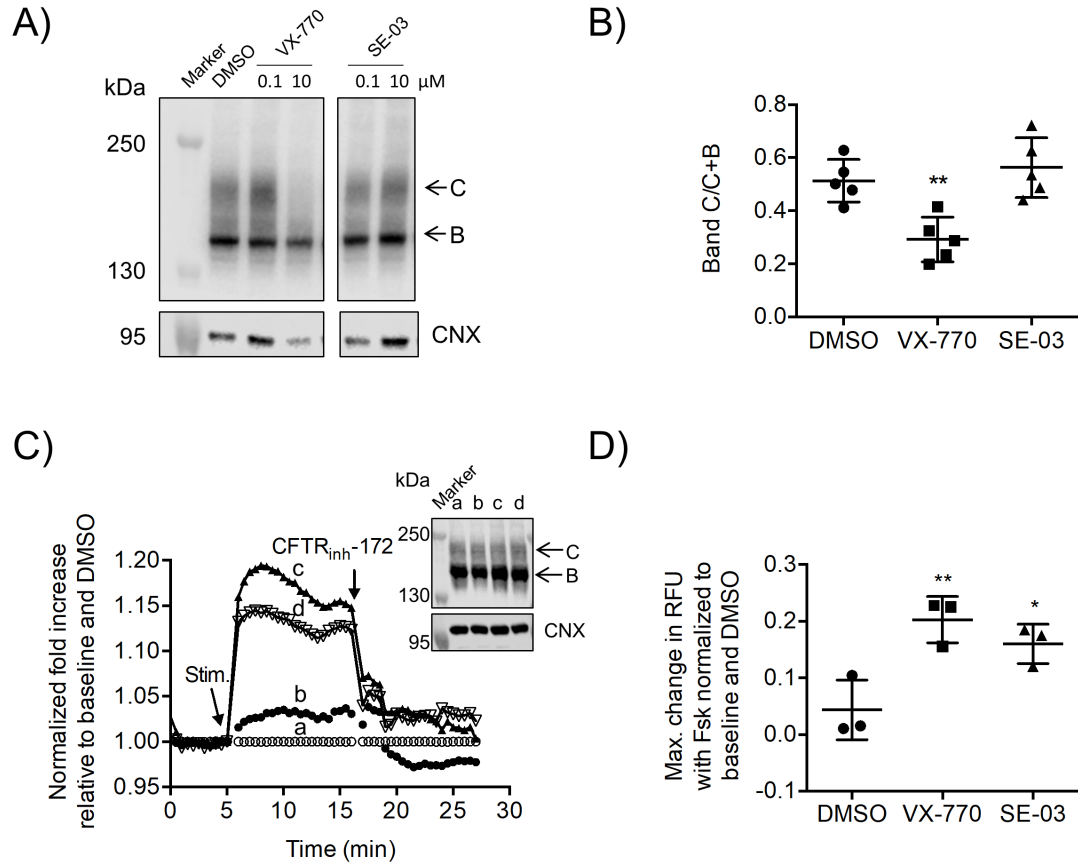
Figure 4.7: The VX-770 derivative, SE-03, did not reduce steady state protein abundance at 10 μM while exhibiting potentiator activity.
(**A**) Representative immunoblot of F508del-CFTR from HEK-293 overexpressing F508del-CFTR cells chronically treated with VX-770 and its derivative, SE-03, at 0.1 μM or 10 μM at 27°C for 24 h compared to DMSO as a negative control. Calnexin (CNX) was used as a loading control. (**B**) Comparisons of band *C* relative to band *C* and band *B* (*C+B*) of F508del-CFTR chronically treated with DMSO, 10 μM VX-770 and 10 μM SE-03 at 27°C for 24 h. Densitometry analyses show that treatment with 10 μM VX-770 significantly decreased band *C* relative to band *C+B* of F508del-CFTR whereas treatment with 10 μM SE-03 did not compared to DMSO (n = 5 for all conditions). Results are presented as mean ± SD and analyzed by One-way ANOVA and Dunnett's post-hoc test (**p < 0.01 compared to vehicle). (**C**) FLIPR® channel function studies of VX-809 rescued F508del-CFTR stimulated (Stim.) with vehicle (labeled as "a"), 1 μM cAMP agonist, forskolin (Fsk) (labeled as "b"), 1 μM Fsk and 10 μM VX-770 (labeled as "c"), or 1 μM Fsk and 10 μM SE-03 (labeled as "d"), and then inhibited with CFTR$_{inh}$-172. *Inset*: Immunoblot of F508del-CFTR after the FLiPR® assay shows that the level

of band *C* in each condition were relatively similar compared to calnexin (CNX) as a loading control. (**D**) Quantification of the maximum peak of Fsk stimulation in the FLIPR® assay relative to baseline and DMSO show that acute treatment with 10 µM VX-770 and 10 µM SE-03 with 1 µM Fsk significantly potentiated CFTR chloride flux compared to 1 µM Fsk alone (DMSO, n = 3 for all conditions, average of 8 wells per replicate). Results are presented as mean ± SD and analyzed by One-way ANOVA and Dunnett's post-hoc test (*p < 0.05 and **p < 0.01 compared to 1 µM Fsk).

I also observed that SE-03 did not destabilize the most sensitive SLC protein from my studies, SLC26A3, at both low (100 nM) and high (10 µM) concentrations (Figure 4.8).
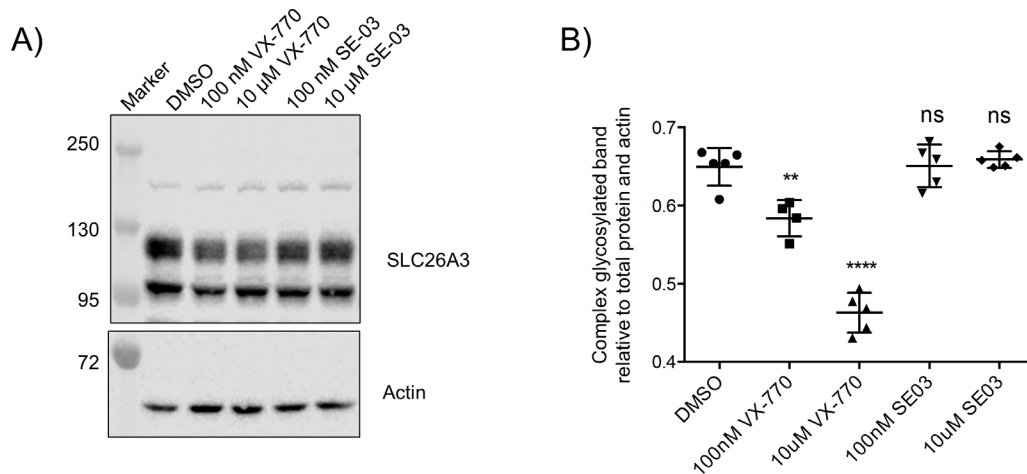
Figure 4.8: SE-03 does not cause destabilization of SLC26A3 compared to VX-770.
(**A**) Immunoblot of SLC26A3 chronically treated with 0.1 or 10 µM VX-770, SE-03 or vehicle. (**B**) VX-770 at both 0.1 and 10 µM caused a significant decrease in the cell surface expression of SLC26A3 whereas SE-03 did not have this destabilizing effect (n = 5 biological replicates, n = 5 technical replicates). Results are presented as mean ± SD and analyzed by One-way ANOVA and Dunnett's post-hoc test (**p < 0.01, ****p < 0.0001 compared to DMSO).

4.4.6 Micromolar concentrations of VX-770 increase the membrane fluidity in a lipid raft model

Given the potential role for lipophilicity in VX-770 dependent effects on membrane protein stability, I was prompted to determine if the non-specific destabilizing effects of micromolar concentrations of VX-770 were mediated by disrupting lipid rafts. We tested this hypothesis using a synthetic lipid raft model and tested the effect of micromolar VX-770 on membrane fluidity and bilayer integrity. pTIRF microscopy was employed to study the effect of 10 µM VX-

770 on a SLB that contained DOPC/cholesterol/DSPC and DOPC/cholesterol/ bSM bathed in a HEPES buffer [175, 176]. Two distinct bilayers were tested for the effect of VX-770 with 3-6 fields of view analyzed per bilayer (Figure 4.9A and B). Order parameter $<P_2>$ measurements and the histogram movies demonstrated that 10 μM VX-770 immediately increased the bilayer fluidity as well as reorganized subdomains within the DOPC/bSM/cholesterol SLB. The histograms were determined from the selected field of view and that same field of view was used to track the dynamic changes in the bilayer upon VX-770 addition. As such, our interpretations as to the effect of these agents on membrane stability and structure are drawn from relative changes in the individual histogram characteristics for the chosen field of view. From that perspective, we can clearly see that there is a clear shift to a higher mean $<P_2>$ value and a tighter distribution upon VX-770, which is strongly suggestive of increased membrane fluidity. This interpretation is certainly bolstered by the before- and after-VX-770 addition, which shows significant changes in the bilayer domain structures. Conversely, the relative decrease and broadening of the distribution of $<P_2>$ values (i.e. emergence of a second lower $<P_2>$ peak) upon SE-03 addition can only be interpreted at this point as evidence of a greater extent of membrane reorganization. Intriguingly, the extent of sub-domain restructuring due to SE-03 addition appears to be significantly less than in the VX-770 case, as is evidenced by the relatively minor changes in bilayer morphology (Figure 4.9C and D), supporting the claim the VX-770 effects are mediated at least in part by its relative lipophilicity.
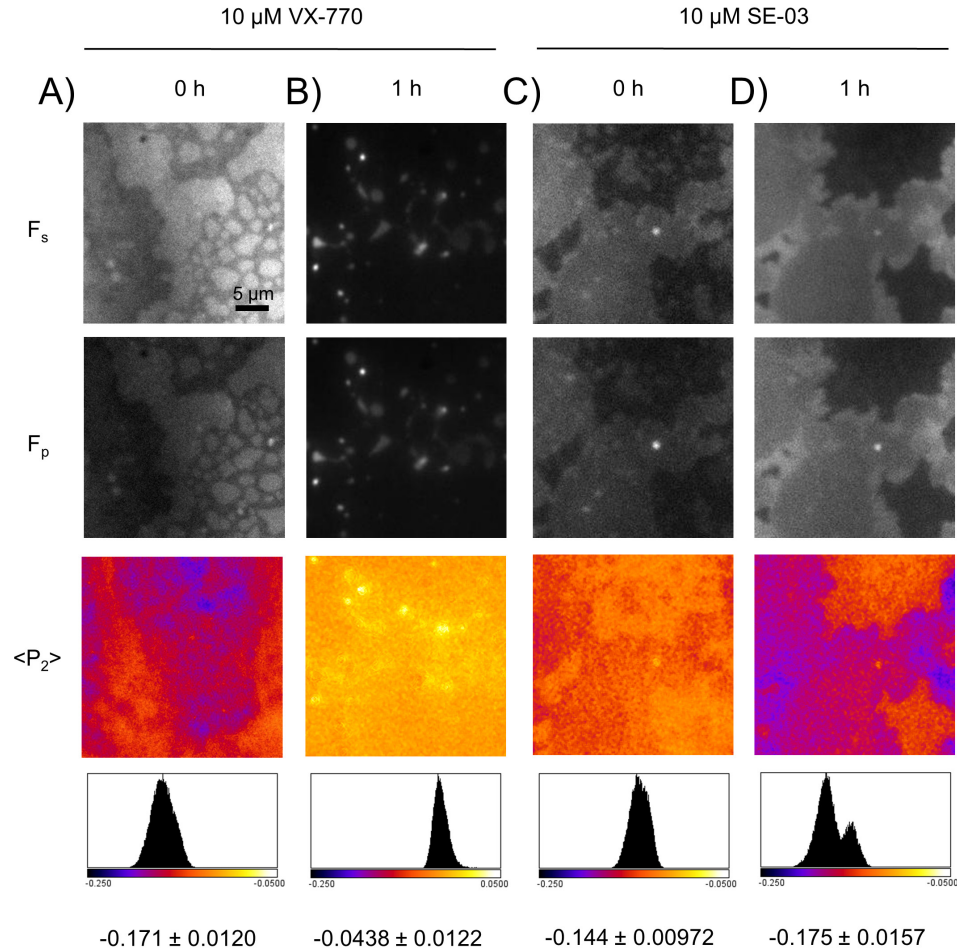
Figure 4.9: Supra-pharmacological concentration of VX-770 appears to increase membrane fluidity and reorganize the bilayer.
Representative pTIRF images of a 30 x 30 µm section of a DOPC/bSM/cholesterol lipid raft-like model prior to addition of (**A**) 10 µM VX-770 and (**C**) 10 µM SE-03. pTIRF images at 1 h incubation with (**B**) 10 µM VX-770 and (**D**) 10 µM SE-03. First row represents the pTIRF images obtained by substrate parallel excitation (F_s) and the second row represents the pTIRF images obtained by perpendicular excitation (F_p) of the DiI-C$_{18}$ fluorescent dye. Third row represents the same images coloured by the order parameter <P$_2$>. The last row represents the histogram summarizing the range of <P$_2$> with the mean value and margin of error indicated at the bottom. Two bilayers were studied per condition with 3-6 fields analyzed per bilayer.

4.5 Discussion

The current studies provide a potential explanation for the concentration-dependent, destabilizing effects of chronic exposure to VX-770 on VX-809 rescued F508del-CFTR protein [162, 163, 177]. At the concentrations of VX-770 that reduce F508del-CFTR protein stability, I also

observed reduction of the abundance of other membrane proteins (SLC26A3, SLC26A9 and SLC6A14) pointing to its lack of specificity. From our studies of model lipid rafts, I deduce that this negative effect of high concentrations of VX-770 is related to its lipophilicity and disruption of these membrane structures. In addition, the fluorescence-based modifications reflecting the structural changes of purified Wt-CFTR in amphipol with 10 µM and not 100 nM VX-770 shown in the previous chapter may be due to the potentiator displacing the lipids associated with the purified protein at that concentration.

My cysteine cross-linking studies showed that the concentration of VX-770 (10 µM) that reduced VX-809-mediated augmentation in F508del-CFTR processing also reversed VX-809 mediated enhancement of the ICL4: NBD1 interface that was also presented in Chapter 2. As in previous studies [30, 41-43, 46, 257], I probed the interaction at this interface in the context of a cys-less variant of F508del-CFTR protein harbouring cysteine residues engineered in ICL4 (A1067C) and NBD1 (V510C). In my experimental system, I could not detect VX-809 induced maturation and processing of the V510C/A1067C cys-less variant of F508del-CFTR protein in immunoblots. However, VX-809 induced interface assembly in the immature, core-glycosylated band *B* of the protein was detectable as a unique cross-linked band (✳) and the relative abundance of this band was reduced in the presence of 10 µM VX-770 but not in the presence of 100 nM VX-770. Hence, I interpret the destabilizing effects of VX-770 at this concentration to be due to inhibition of the positive effects of VX-809 at this interface. However, as discussed in the subsequent paragraphs, this effect is likely not specific to this interface or even- the mutant CFTR protein.

The same concentration of VX-770 that induced destabilizing effects on F508del-CFTR assembly also reduced the steady state abundance of the three SLC proteins tested. I chose these proteins because they are known to be localized in the same tissues and membranes as CFTR and modify epithelial transport function [135, 164, 267]. Hence, any non-specific effect of VX-770 on these membrane proteins may have a potential to modify disease and/or therapeutic response to ORKAMBI®. Of these proteins, SLC26A3 was the most sensitive to the destabilizing effect of VX-770, with a significant decrease in protein abundance apparent (at least in the HEK-293 expression system) at 1 µM, the serum concentration (1-2 µM) reported by Vertex Pharmaceuticals (Vertex Pharmaceuticals Incorporated, 2017). Previous studies have shown that

loss of function mutations of SLC26A3 caused a rare disease known as congenital chloride-losing diarrhea via impaired chloride absorption and fluid/bicarbonate secretion [268]. Intestinal inflammation, which is common in diarrhea, has been found to further reduce SLC26A3 expression through direct binding to NF-kB [269]. Hence, it is possible that the destabilizing effect of VX-770 that I observed on SLC26A3 may modify the ORKAMBI® response in the intestinal tissues.

SLC26A9 confers an apical anion channel and this function augments the cAMP-regulated channel activity of CFTR in the non-CF airway epithelium and in the epithelium of patients bearing gating mutations such as G551D [261, 270]. Strug et al. showed that polymorphisms in the *SLC26A9* gene associate with the response of patients bearing G551D to VX-770 and interpreted these results to suggest that functional expression of SLC26A9 enhances the therapeutic efficacy of VX-770 in this cohort of patients [167]. Therefore, VX-770 in patient tissues is not impairing the positive affect of SLC26A9 on the potentiation of the G551D channel. On the other hand, the misfolded F508del-CFTR protein interacts with and prevents SLC26A9 trafficking to the apical surface [261, 270]. Correction of F508del-CFTR by VX-809, is thought to promote SLC26A9 trafficking to the cell surface indirectly [261, 270]. *In vitro* studies of bronchial explant tissue from F508del homozygotes suggest that the magnitude of pharmacological correction by VX-809 is also augmented by SLC26A9 expression [167]. Hence, the results of the current study suggest that the possible deleterious effect of chronic VX-770 on SLC26A9 protein stability should be further studied given its importance in modifying the pharmacological rescue conferred by this therapy.

SLC6A14 is an apical amino acid transporter and we have shown that it functions to remove nutrient amino acids from the surface of respiratory epithelial cells [271]. This function is associated with reduced adherence of *P. aeruginosa* to the surface of respiratory epithelial cells [271]. I speculate that reduced surface stability of SLC6A14 induced by high concentrations of VX-770 would potentially enhance *P. aeruginosa* attachment and biofilm formation and we are testing this hypothesis.

I propose that the destabilizing effect of VX-770 is related to its lipophilic property. Interestingly, treatment of F508del-CFTR with a panel of VX-770 derivatives showed that the

degree of VX-770 lipophilicity is correlated to its destabilizing effect. SE-03 lacks two tert-butyl groups on the phenol ring (Figure 4.1) and is less lipophilic than VX-770 (the log$P$ value of SE-03 is 2.67 whereas it is 5.76 for VX-770), yet it retains activity as a potentiator. Interestingly, SE-03 does not reduce F508del-CFTR protein stability even at the high concentration of 10 μM. Biophysical studies of a lipid raft model showed that unlike VX-770, SE-03 addition did not disperse lipid rafts comprised of cholesterol and sphingomyelin. Together, these findings support the hypothesis that the non-specific effects of VX-770 on membrane protein stability are mediated through VX-770 interaction with and disruption of lipid rafts, a membrane organizing structure known to facilitate protein interactions and signaling [132, 272-274].

The non-specific effect of chronic VX-770 on the steady state abundance of F508del-CFTR, other membrane proteins and lipid rafts was observed at the supra-pharmacological concentration of 10 μM VX-770. According to Matthes et al., a peak free plasma concentration of VX-770 is 1.5-8.5 nM, considerably lower than other estimates and the concentration at which we observed the non-specific effects of VX-770 [177, 275]. According to the drug data sheet provided by Vertex, after a single recommended dose of 150 mg administered after a meal, the peak plasma concentration reaches 768 ng/ml or 1-2 μM (Vertex Pharmaceuticals Incorporated, 2017). This value is an order of magnitude less than the concentration (10 μM) that caused significant loss of CFTR and other membrane proteins (including SLC26A9) in the *in vitro* studies of this paper. However, according to a previous study [276], there was a large range in serum concentrations of VX-770 in different patients, ranging from 400-3000 ng/ml, with the upper limit approaching 10 μM. Importantly, the concentration of VX-770 in the tissues of CF patients treated with VX-770 is uncertain. According to the European Medicine Agency (EMA/473279/2012), VX-770 accumulates in lung and tracheal epithelial tissues relative to plasma in rat studies (European Medicine Agency, 2012). Hence, it remains unknown if tissue concentrations could approach the higher concentration of 10 μM shown to exert non-specific, destabilizing effects.

It is important to acknowledge that VX-770 exerts a beneficial effect overall when given as a monotherapy to individuals bearing gating mutations in CFTR. However, our studies suggest that future clinical studies are required to monitor off-target effects in this population taking this monotherapy continuously over their lifetime. Finally, it remains possible that the variable

clinical efficacy of ORKAMBI® in the F508del patient population is partially associated with variation in its tissue accumulation amongst patients and/or off-target effects of VX-770 on other membrane proteins variably expressed in different patients. This calls for a more personalized approach to screen for these off-target effects of VX-770 in different patients.

Chapter 5 Summary, Discussion and Future Directions

5.1   Consequences of CFTR modulations at the cell surface

CF is caused by various mutations of an ABC anion channel known as CFTR that functions to maintain hydration on the epithelia where it is expressed. At the cell surface, CFTR channel activity is modulated by PKA phosphorylation and ATP binding, lipids, other membrane proteins, and potentiator drug compounds like VX-770. However, the molecular mechanisms of these modulations were unclear. The studies highlighted in the chapters of this thesis provided more insights on the effects of these modulations on CFTR structure and function that are summarized in this chapter.

5.1.1   PKA phosphorylation modifies transmission interface interactions of CFTR

CFTR channel gating at the cell surface is regulated by PKA phosphorylation and ATP binding. The transmission interface that involves the CHs of the ICLs extending from the MSDs and the NBDs is essential for the channel gating of CFTR [277]. However, not much was known about the conformational changes of PKA phosphorylation on the transmission interface of full-length CFTR. Towards this, I have developed the first reported biophysical assays on purified full-length CFTR to study its structure and show that our purified protein is properly folded which is very important for our assays. Our biophysical studies suggest that PKA phosphorylation may be enhancing the alpha-helical content and protecting the transmission interface of purified full-length CFTR from urea unfolding and iodide quenching. I have specifically probed the transmission interface with cysteine cross-linking studies and have found that the interactions induced by PKA phosphorylation may be too dynamic or subtle for cysteine cross-linking studies to detect. Functional studies of disease-causing mutations at the CHs (R170G on CH1 and A1067T on CH4) of the transmission interface were able to show that interactions at the transmission interface are necessary for phosphorylation-dependent activation of CFTR.

The recent cryo-EM structures of zCFTR have shown that PKA phosphorylation results in the following conformational changes of CFTR: the R domain is removed from the gap of the two NBDs of the CFTR molecule, the NBDs are closer together, and the TMs exhibit subtle conformational changes [25]. However, the conformational changes at the transmission interface from these structures remain unclear. In fact, the zCFTR structure with PKA phosphorylation and ATP binding does not appear to be an "open" channel [25] which may explain the absence

of changes at the transmission interface. Thus, our studies provided more insight on the conformational changes of PKA phosphorylation on the transmission interface that was not clear given the information provided by the cryo-EM structures. The overall effect of PKA phosphorylation and ATP binding on the structure of CFTR at the cell surface is summarized on Figure 5.1.
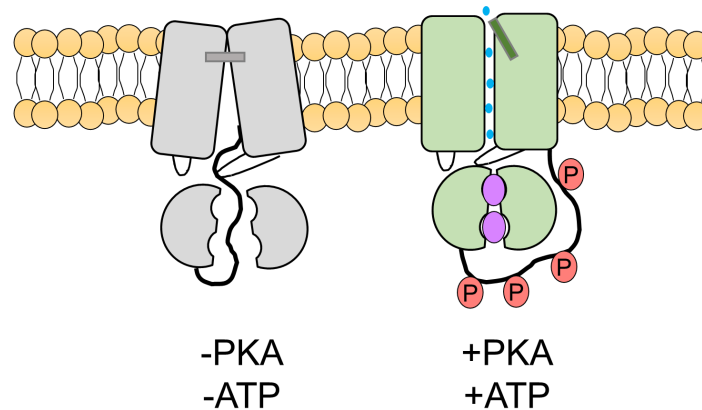
Figure 5.1: Conformational changes of CFTR upon PKA phosphorylation and ATP binding.
Left: CFTR in the dephosphorylated (-PKA) and non-ATP bound (-ATP) state (in gray). The R domain (thick black line) is located at the centre of the two halves of the CFTR molecule and prevents NBD1: NBD2 and transmission interface (CH1 and CH4, shown as black loops, with NBD1) interactions. As a result, the channel gate is closed at the extracellular side. Right: CFTR in the phosphorylated (+PKA in red circles) and ATP bound (+ATP, in purple circles) state (in green). The R domain moves out of the gap between the two NBDs of the CFTR molecule which allows for enhanced interactions at the NBD1: NBD2 and the transmission interface. As a result, the channel gate is open at the extracellular side to allow for anion flux.

5.1.1.1 Future directions

This study mainly focused on the effects of PKA phosphorylation on the transmission interface of NBD1 of CFTR. In order to obtain a complete picture of the transmission interface, future studies are needed to investigate the effect of PKA phosphorylation on the CH: NBD2 interfaces (CH2: NBD2 and CH3: NBD2) in the context of the full-length CFTR. It would also be interesting to compare the effect of PKA phosphorylation on CH: NBD1 and on CH: NBD2 interfaces to determine whether PKA phosphorylation has a greater effect on the different sides of the transmission interface as I expect there will be some asymmetry at the transmission

interface based on the structural asymmetry between ICL: NBD1 and ICL: NBD2 observed on the higher resolution CFTR structures solved by cryo-EM [23-25, 63].

In addition, other interactions that modify CFTR channel gating at the cell surface may also have effects on the transmission interface. For example, other types of phosphorylation like PKC phosphorylation and potentiators like VX-770 regulate or enhance CFTR channel gating but not much is known of their effects on the interactions of the transmission interface. Future channel function studies applying FLIPR® on the disease-causing mutations (R170G and A1067T) at the transmission interface will aim to determine these effects on the transmission interface of CFTR.

5.1.2   Lipid interactions are essential for CFTR channel opening

As previously mentioned, the cryo-EM structure of zCFTR in detergent micelles does not appear to be "open" upon PKA phosphorylation and ATP binding [25]. This may be due to the effect of the detergent micelles that may affect the conformation of the protein especially at the hydrophobic regions of the TMs that tend to interact with the detergent. There have been numerous structural and functional studies have found that the structure and function of various membrane proteins are highly dependent on their lipid interactions at the membrane. Some of these membrane proteins include scaffolding proteins like NHERF1 that has been previously shown to be essential for the stability of CFTR at the cell surface [278], receptors like GPCRs [279-281], ion channels [231, 282-284], and ABC transporters that are similar to CFTR [285-287]. A previous review has claimed that lipids appear essential for the structure and function of CFTR [288]. However, the specific effects of these lipids on CFTR channel function remain unknown [288]. Towards this, we developed a novel purification method that can purify CFTR using amphipol in a detergent-free environment. A previous study has shown that CFTR can be purified in a detergent-free environment using SMALPs [233]. However, not much is known of the structural or functional properties of that purified protein [233]. We have found that our purified CFTR in amphipol contains significantly more lipids than purified CFTR in detergent micelles. These lipids include cholesterol, PC and PE. In addition, our purified CFTR in amphipol resulted in significantly higher ATPase and iodide efflux activity than purified CFTR in detergent micelles. This higher level of CFTR function may be due to the effect of the lipids present in the purified protein that stabilizes and preserves the channel-competent state of CFTR that is necessary for its channel gating. The importance of lipids was further highlighted by the

enhancement of ATPase activity of purified CFTR in detergent micelles after re-introducing the lipids (PE/PS/PC/cholesterol) that are present in the lipid bilayer back to the purified protein. However, the asymmetry of the lipid bilayer and the specific interaction of TM regions of CFTR to different lipids appears to be important as simply re-introducing back the lipids present in the lipid bilayer did not reach the ATPase activity of purified CFTR in amphipol that had those specific lipid interactions preserved since the beginning of the purification. The significance of lipid interactions with CFTR that could be captured by amphipol are highlighted in Figure 5.2.
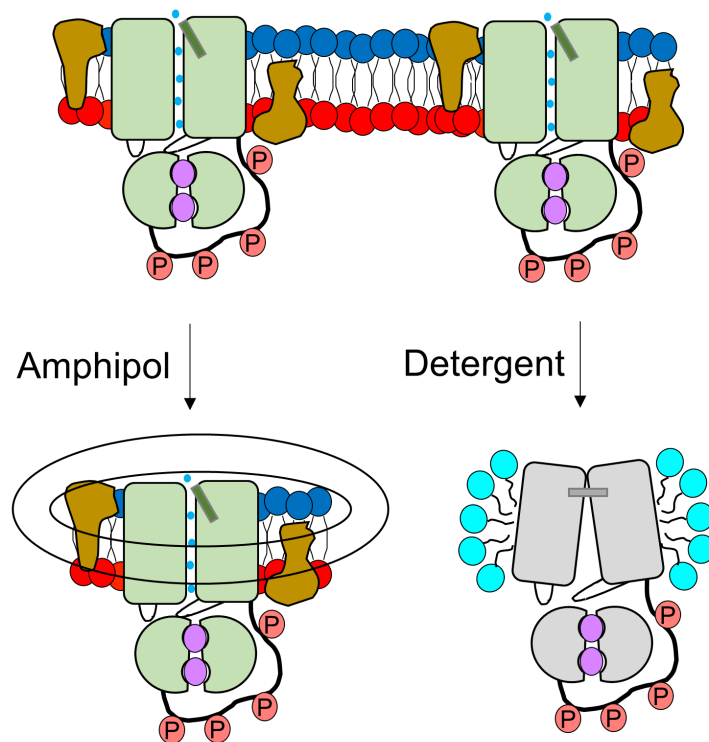
Figure 5.2: Lipid interactions of CFTR are essential for its channel function.
Left: Extraction and purification of CFTR in amphipol (black outlined ring) results in preservation of lipid interactions with CFTR. Specific TM regions interact with outer leaflet lipids (in blue, mainly PC) whereas other specific TM regions interact with inner leaflet lipids (in red, mainly PS and PE). CFTR also has specific interactions with cholesterol (brown) at either the outer or inner leaflet of the membrane. These interactions lead to preservation of channel gating as assessed by ATPase and iodide efflux assays. Right: Extraction and purification of CFTR in detergent (light blue) results in loss of lipid interactions with CFTR. This results in capturing the CFTR protein in an artificial state that may be observed in the cryo-EM studies in which the R domain moves out of the gap between the two NBDs of the CFTR molecule, the NBDs move closer but the gate remains closed. In addition, the ATPase and channel flux activities are significantly lower than protein in amphipol. *Note:* This is a simplified schematic of the CFTR structure in detergent captured by cryo-EM. The subtle changes in the TMs of the protein in detergent upon PKA phosphorylation and ATP binding are not shown in this diagram.

The protein in detergent may not be closed the entire time but may exhibit some opening not shown in this diagram.

5.1.2.1 Future directions

The observation that our purified CFTR in amphipol contains lipids is of great interest due to its improvement from other purification methods of CFTR [20, 108, 140, 240, 248, 289-292]. The specific lipid interactions with CFTR are of particular interest and future studies would require a more intensive approach like molecular dynamics or lipid mass spectrometry, that has previously shown to be feasible to define specific protein-lipid interactions [287, 293], to uncover the regions of the protein that interact with each individual lipid.

I have applied iodide efflux assay to study CFTR channel function as it has been developed and well-established by my laboratory [140, 192]. However, this is not the native anion of the channel and future studies may be needed to develop, optimize and apply a chloride efflux assay to better compare the channel function of purified CFTR in amphipol and in detergent. Since we observed that re-introducing different lipids back to purified CFTR in detergent micelles resulted in varying improvements in ATPase activity of CFTR, it would be interesting to determine whether iodide or chloride efflux is also affected by reconstitution of the protein in different lipids like PC, PS or PE/PS/PC/cholesterol (5:2:1:1 ratio by weight).

There have been a few studies on the binding of drugs like VX-770 and VX-809 on purified CFTR protein in detergent micelles [250, 289]. Since it appears that the structure and function of CFTR is dependent on its lipid environment, future studies will investigate whether the binding of corrector and potentiator compounds to CFTR is different in the presence of its lipids in amphipol compared to a detergent micelle environment using the biophysical methods mentioned above.

5.1.3 Micromolar concentrations of VX-770 destabilizes membrane proteins by modulating the lipid bilayer

The potentiator, VX-770, enhances the channel gating of CFTR protein that reaches the cell surface [160]. However, VX-770 was found to have a destabilizing effect of VX-809 rescued F508del-CFTR at high micromolar (10 µM) concentrations [162, 163, 177] but its mechanism is

not known. My studies have found that VX-770 inhibits the VX-809 corrective effect at the CH4: NBD1 transmission interface of F508del-CFTR. I have further found that the destabilizing effect of VX-770 was not specific but also had a destabilizing effect on other membrane proteins like the SLCs. This destabilizing effect was found to be related to the lipophilic property of VX-770 that increased the fluidity and reorganized the lipid bilayer. This, in turn, has a destabilizing effect on the membrane proteins localized at the cell membrane. This study further supports the importance of lipid interactions on stabilizing CFTR and other membrane proteins at the cell surface. The dose-dependent effect of VX-770 on the lipid bilayer and membrane proteins is shown in Figure 5.3.
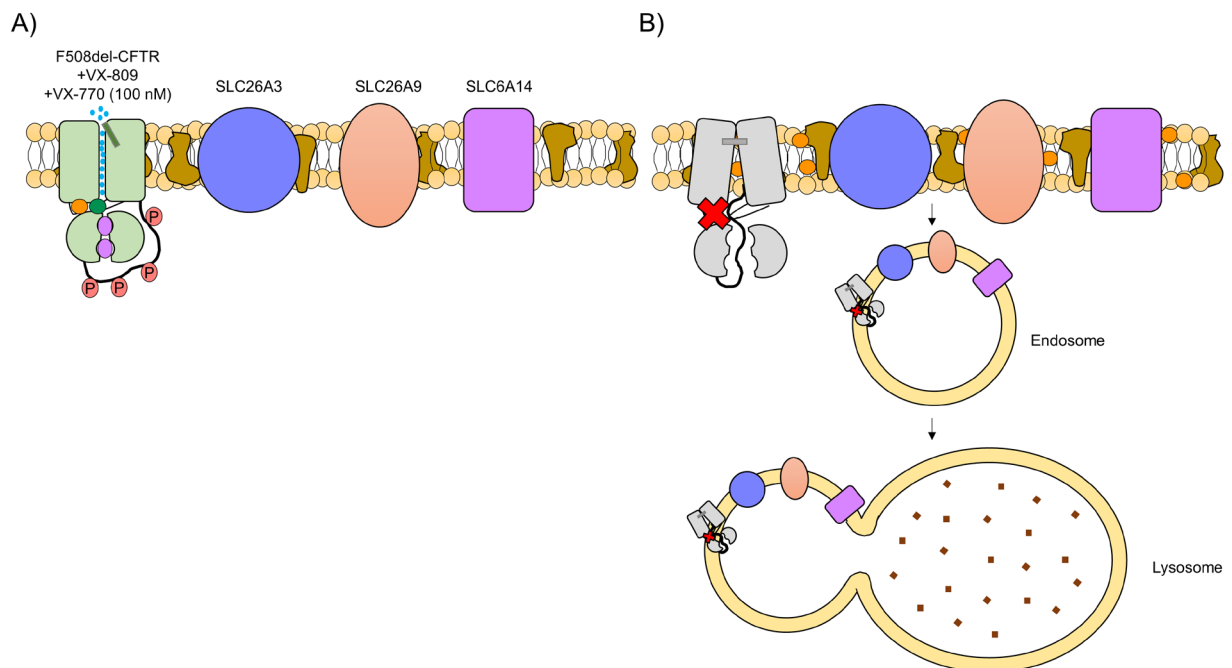
Figure 5.3: The effect of VX-770 on the lipid bilayer and membrane proteins.
(**A**) Low concentrations of VX-770 (i.e. 100 nM) does not have the destabilizing effect on the lipid bilayer and membrane proteins. Instead, VX-770 at this concentration enhances channel function of CFTR that reaches the cell surface (i.e. VX-809 rescued F508del-CFTR). (**B**) High concentrations of VX-770 (i.e. 10 µM) goes into the lipid bilayer to increase its fluidity and reorganize the membrane. This leads to destabilization of the F508del-CFTR via the lack of ICL4: NBD1 interaction which was previously shown to be necessary for phosphorylation-dependent gating. This also leads to destabilization of other membrane proteins like the SLCs. These unstable proteins are recognized and removed from the membrane by peripheral quality control via endosomes and sent for lysosomal degradation. *Note:* These are simplified schematics to show the membrane proteins affected by high concentration of VX-770 and does not reflect that they are all expressed at the same level or in the same tissue.

The peak plasma concentration of VX-770 in patients after a single recommended dose of 150 mg administered after a meal was reported to be 1-2 µM (Vertex Pharmaceuticals Incorporated, 2017) which is lower than the concentration (10 µM) that resulted in the non-specific destabilization effects observed in this study. In fact, VX-770 has an overall beneficial effect on CF patients bearing CFTR gating mutations (Vertex Pharmaceuticals Incorporated, 2017). However, the peak plasma concentration of VX-770 may be variable across patients and it remains unknown whether it can reach a concentration of 10 µM. In addition, a previous study has found that the multi-drug exporter, P-glycoprotein, can transport VX-770 out of cells and consequently reduce the bioavailability of the drug [294]. Thus, the expression and level of activity of P-glycoprotein in each patient may vary and this may affect the concentration of VX-770 that is taken up in cells.

However, if the peak plasma concentration of VX-770 in patients does reach 10 µM, this may result in the previously described destabilizing effect of VX-770 on F508del-CFTR and the SLCs at the cell surface which may consequently affect the efficacy of the FDA approved medicines that contain VX-770, ORKAMBI® and SYMDEKO™, at different epithelial tissues of F508del homozygous patients. At airway epithelia, SLC26A9 has a positive effect on CFTR channel activity and appears to augment F508del-CFTR correction by VX-809 [167, 261, 270] and SLC6A14 removes *P. aeruginosa* adherence by removing its amino acid nutrient source [271]. At intestinal epithelia, SLC26A3 has an important role in chloride absorption and fluid/bicarbonate secretion [268]. Thus, these important roles of the SLCs may be compromised by high concentrations of VX-770 which may modify ORKAMBI® or SYMDEKO™ response at those tissues. In addition, the peak plasma concentration of VX-770 is quite variable across patients which may account for the variability in tissue-specific responses to ORKAMBI® or SYMDEKO™.

5.1.3.1 Future directions

In this study, I have investigated the effect of high concentrations of VX-770 on the SLCs that interact with CFTR. CFTR also interacts with other membrane proteins that modulate its function at the cell surface. As previously mentioned, the ABC transporter, MRP4, regulates

intracellular cAMP concentrations which in turn, regulates CFTR function at the cell surface [170-173]. TMEM16A, a calcium-activated chloride channel, is also essential for CFTR function and membrane expression [295]. Thus, it will be interesting to determine whether VX-770 at micromolar concentrations also destabilizes those membrane proteins in future studies.

Since the peak plasma concentration of VX-770 appears quite variable across patients, it would be interesting to analyze the peak plasma concentrations of VX-770 for each CF patient after taking KALYDECO®, ORKAMBI® or SYMDEKO™ overtime and correlating those values with their clinical outcomes like FEV_1. I am particularly interested in monitoring patients with the A1067T mutation that were approved for KALDECO® or SYMDEKO™ as we have previously studied the consequence of this mutation, which is located at the CH4: NBD1 interface, on phosphorylation-dependent channel activation. These patients were approved for these medicines based on *in vitro* results [241] but their clinical outcomes after taking these drugs remain unknown (Vertex Pharmaceuticals, 2018).

5.2 Key insights from novel assays developed to study CFTR structure

5.2.1 Summary

The chapters of this thesis have described the development of several novel assays that provided important insights on the consequences CFTR structure and function of modifications at the cell surface. Notably, I have learned some important lessons and precautions from the cysteine cross-linking studies and the development of the novel purification and functional reconstitution protocols of CFTR in amphipol.

5.2.2 Precautions for cysteine cross-linking studies

Cysteine cross-linking studies have been traditionally applied to study interactions at interfaces of interest. Multiple cysteine cross-linking studies have claimed that the presence of a cross-linked band, a high molecular weight band at around 250 kDa, on an immunoblot to indicate an interaction of the interface of interest [30, 41-45]. My cysteine cross-linking studies showed that both band *B* and *C* of the cys-less variant of CFTR can be cross-linked. There are also shifts in the molecular weights of both band *B* and *C* that are caused by the cross-linker interacting with any cysteine present on the cys-less variant of CFTR and thus, cannot be interpreted as a

consequence of intramolecular interactions. It is also important to keep in mind that it is difficult to capture dynamic or subtle interactions (i.e. with phosphorylation) with cysteine cross-linking as the readout is on an immunoblot that shows the steady-state abundance of the cross-linked band. Perhaps applying a different assay like intramolecular Fluorescence Resonance Energy Transfer (FRET) [296] may be a better approach for detecting dynamic or subtle intramolecular interactions of CFTR.

5.2.3   Lessons from the development of the novel purification and functional reconstitution protocols of CFTR

During the development and optimization of the novel purification of CFTR in amphipol, I realized that CFTR is indeed a tricky membrane protein to purify. We have found that more steps in the purification usually led to less CFTR protein. We previously included nickel purification, FLAG purification and SEC to purify CFTR which have resulted in low amounts of CFTR. We have found that these multiple steps tend to enhance problems during the purification (i.e. problems with nickel binding, problems with FLAG binding or problems with both) and this led to constant troubleshooting. We have also found that the binding of CFTR protein to the affinity beads cannot be rushed as speeding up the purification resulted in very low CFTR amounts. Thus, we decided to only apply a FLAG purification with an overnight FLAG binding step as it gave us the cleanest sample compared to a nickel purification and it consistently yielded an appropriate amount of protein for our functional studies.

We have also found that the purified CFTR protein cannot be easily concentrated. Previously, we would pool SEC fractions that contained CFTR and concentrate the protein but that usually led to loss of protein possibly to aggregation. To combat this issue, we had to use more membranes and modify the volume of FLAG® peptide to elute the protein for achieving the appropriate protein concentration without the need of concentrating the protein.

Another important consideration is to apply the appropriate protein quantification methods for accurately quantifying the amount of purified CFTR protein. It is imperative to accurately normalize the functional response to protein amounts in order to accurately compare the channel function across conditions (i.e. CFTR in amphipol compared to CFTR in LMNG). For example, we have found that the NanoDrop method, that the Chen group have used for their protein

quantification, is not accurate for low protein concentrations and may result in different V_{max} values in the ATPase assay.

Lastly, there have only been a few studies that have successfully conducted functional reconstitution of membrane proteins in amphipol [297]. From my studies, it took a substantial amount of work to optimize the reconstitution of purified CFTR in amphipol for the iodide efflux assays. From these optimizations, I have found that incubation of the purified CFTR protein in amphipol with a mild detergent (DDM) prior to its addition to the empty liposomes was required to coax the protein into the proteoliposomes. I have also found that the detergent removal step was extremely important to form tight proteoliposomes otherwise the proteoliposomes become leaky, which results in un-regulated flux of iodide out of the proteoliposomes prior to valinomycin addition, and this becomes quite problematic as it would be difficult to differentiate the CFTR-specific iodide efflux from the background leak. In addition, the purified protein to lipid ratio must be optimized in order to obtain sufficient signals in the iodide efflux assay. Towards this, I have varied the amount of purified protein while keeping the amount of lipid consistent and this eventually led to my established approximate amount of protein to lipid ratio for this assay.

5.3 Path towards determining the native structure and conformational changes of CFTR at the cell membrane

Our purified CFTR protein has certain properties that are different from the purified CFTR protein applied in the cryo-EM structures by the Chen group [23-25]. These properties include lipid association, complex glycosylation and higher functional activity that resembles the CFTR channel at the cell surfaces. Thus, the determination of the structure of our purified CFTR in amphipol is of great interest. As previously mentioned, studies have shown that the structure of purified membrane proteins in amphipol can be solved by cryo-EM [210, 298-303]. Thus, this method may be feasible for purified full-length CFTR in amphipol. However, future studies are needed to optimize the conditions of purified full-length CFTR in amphipol for negative stain EM and then cryo-EM studies.

If EM studies are feasible for purified CFTR in amphipol, I would like to apply this method to study the specific effects of lipid-CFTR interactions, particularly at the pore of CFTR, through comparing potential structures of CFTR in amphipol with CFTR in detergent micelles. In

addition, I would like to apply this method to study the structure of the major mutant, F508del-CFTR, in amphipol and it would be interesting to determine whether this structure is modified in the absence or presence of lipids. Previous studies have also shown that cryo-EM can be applied for studying drug binding on proteins [304, 305]. Thus, if feasible, I would also like to apply cryo-EM to determine the binding sites of potential drugs on CFTR that are currently not known. These compounds include the GSK compounds (GSK499 and GSK815) that were previously shown to directly bind to and stabilize the purified full-length CFTR protein and the FDA approved drug, VX-770.

I am also interested to study the conformational changes of purified full-length CFTR in amphipol upon PKA phosphorylation and ATP binding. I am particularly interested to observe the conformational changes at the transmission interface that was found to be essential for phosphorylation-dependent gating. Future studies that can study conformational changes of membrane proteins like electron paramagnetic resonance spectroscopy [306] or fluorescence based methods may be applied for this purpose.

References

1.   Cutting, G.R., *Cystic fibrosis genetics: from molecular understanding to clinical application.* Nat Rev Genet, 2015. **16**(1): p. 45-56.

2.   Konstan, M.W., et al., *Bronchoalveolar lavage findings in cystic fibrosis patients with stable, clinically mild lung disease suggest ongoing infection and inflammation.* Am J Respir Crit Care Med, 1994. **150**(2): p. 448-54.

3.   Heijerman, H., *Infection and inflammation in cystic fibrosis: a short review.* J Cyst Fibros, 2005. **4 Suppl 2**: p. 3-5.

4.   Hjelm, M., P. Brown, and A. Briddon, *Sweat sodium related to amount of sweat after sweat test in children with and without cystic fibrosis.* Acta Paediatr Scand, 1986. **75**(4): p. 652-6.

5.   Gibson, L.E. and R.E. Cooke, *A test for concentration of electrolytes in sweat in cystic fibrosis of the pancreas utilizing pilocarpine by iontophoresis.* Pediatrics, 1959. **23**(3): p. 545-9.

6.   Kobelska-Dubiel, N., B. Klincewicz, and W. Cichy, *Liver disease in cystic fibrosis.* Prz Gastroenterol, 2014. **9**(3): p. 136-41.

7.   Freeman, A.J. and C.Y. Ooi, *Pancreatitis and pancreatic cystosis in Cystic Fibrosis.* J Cyst Fibros, 2017. **16 Suppl 2**: p. S79-s86.

8.   Singh, V.K. and S.J. Schwarzenberg, *Pancreatic insufficiency in Cystic Fibrosis.* J Cyst Fibros, 2017. **16 Suppl 2**: p. S70-s78.

9.   Yung, B., et al., *Diagnosis of cystic fibrosis related diabetes: a selective approach in performing the oral glucose tolerance test based on a combination of clinical and biochemical criteria.* Thorax, 1999. **54**(1): p. 40-3.

10.   Sathe, M. and R. Houwen, *Meconium ileus in Cystic Fibrosis.* J Cyst Fibros, 2017. **16 Suppl 2**: p. S32-s39.

11.   Canny, J.D., A. Brookes, and D.B. Bowley, *Distal intestinal obstruction syndrome and colonic pathologies in cystic fibrosis.* Br J Hosp Med (Lond), 2017. **78**(1): p. 38-43.

12.   Ong, T., et al., *Cystic Fibrosis and Congenital Absence of the Vas Deferens*, in *GeneReviews((R))*, M.P. Adam, et al., Editors. 1993, University of Washington, Seattle

University of Washington, Seattle. GeneReviews is a registered trademark of the University of Washington, Seattle. All rights reserved.: Seattle (WA).

13.   Kerem, E., et al., *Factors associated with FEV1 decline in cystic fibrosis: analysis of the ECFS patient registry.* Eur Respir J, 2014. **43**(1): p. 125-33.

14.   Corey, M., et al., *Longitudinal analysis of pulmonary function decline in patients with cystic fibrosis.* J Pediatr, 1997. **131**(6): p. 809-14.

15.   Schluchter, M.D., M.W. Konstan, and P.B. Davis, *Jointly modelling the relationship between survival and pulmonary function in cystic fibrosis patients.* Stat Med, 2002. **21**(9): p. 1271-87.

16.   Rommens, J.M., et al., *Identification of the cystic fibrosis gene: chromosome walking and jumping.* Science, 1989. **245**(4922): p. 1059-65.

17.   Kerem, B., et al., *Identification of the cystic fibrosis gene: genetic analysis.* Science, 1989. **245**(4922): p. 1073-80.

18.   Tsui, L.C., et al., *Cystic fibrosis locus defined by a genetically linked polymorphic DNA marker.* Science, 1985. **230**(4729): p. 1054-7.

19.   Riordan, J.R., et al., *Identification of the cystic fibrosis gene: cloning and characterization of complementary DNA.* Science, 1989. **245**(4922): p. 1066-73.

20.   Bear, C.E., et al., *Purification and functional reconstitution of the cystic fibrosis transmembrane conductance regulator (CFTR).* Cell, 1992. **68**(4): p. 809-18.

21.   McCarthy, V.A. and A. Harris, *The CFTR gene and regulation of its expression.* Pediatr Pulmonol, 2005. **40**(1): p. 1-8.

22.   Kim, S.J. and W.R. Skach, *Mechanisms of CFTR Folding at the Endoplasmic Reticulum.* Front Pharmacol, 2012. **3**: p. 201.

23.   Zhang, Z. and J. Chen, *Atomic Structure of the Cystic Fibrosis Transmembrane Conductance Regulator.* Cell, 2016. **167**(6): p. 1586-1597.e9.

24.   Liu, F., et al., *Molecular Structure of the Human CFTR Ion Channel.* Cell, 2017. **169**(1): p. 85-95.e8.

25.   Zhang, Z., F. Liu, and J. Chen, *Conformational Changes of CFTR upon Phosphorylation and ATP Binding.* Cell, 2017. **170**(3): p. 483-491.e8.

26.   Rost, B., *Twilight zone of protein sequence alignments.* Protein Eng, 1999. **12**(2): p. 85-94.

27.   Kinjo, A.R. and K. Nishikawa, *Eigenvalue analysis of amino acid substitution matrices reveals a sharp transition of the mode of sequence conservation in proteins.* Bioinformatics, 2004. **20**(16): p. 2504-8.

28.   Bagnat, M., et al., *Cse1l is a negative regulator of CFTR-dependent fluid secretion.* Curr Biol, 2010. **20**(20): p. 1840-5.

29.   Navis, A. and M. Bagnat, *Loss of cftr function leads to pancreatic destruction in larval zebrafish.* Dev Biol, 2015. **399**(2): p. 237-48.

30.   Serohijos, A.W., et al., *Phenylalanine-508 mediates a cytoplasmic-membrane domain contact in the CFTR 3D structure crucial to assembly and channel function.* Proc Natl Acad Sci U S A, 2008. **105**(9): p. 3256-61.

31.   Dalton, J., et al., *New model of cystic fibrosis transmembrane conductance regulator proposes active channel-like conformation.* J Chem Inf Model, 2012. **52**(7): p. 1842-53.

32.   Mornon, J.P., P. Lehn, and I. Callebaut, *Molecular models of the open and closed states of the whole human CFTR protein.* Cell Mol Life Sci, 2009. **66**(21): p. 3469-86.

33.   Fay, J.F., et al., *Cryo-EM visualization of an active high open probability CFTR ion channel.* bioRxiv, 2018.

34.   Ford, B., *CFTR structure: lassoing cystic fibrosis.* Nat Struct Mol Biol, 2017. **24**(1): p. 13-14.

35.   Gee, H.Y., et al., *Syntaxin 16 binds to cystic fibrosis transmembrane conductance regulator and regulates its membrane trafficking in epithelial cells.* J Biol Chem, 2010. **285**(46): p. 35519-27.

36.   Linsdell, P., *Architecture and functional properties of the CFTR channel pore.* Cell Mol Life Sci, 2017. **74**(1): p. 67-83.

37.   Liu, X., et al., *CFTR: a cysteine at position 338 in TM6 senses a positive electrostatic potential in the pore.* Biophys J, 2004. **87**(6): p. 3826-41.

38.   Aubin, C.N. and P. Linsdell, *Positive charges at the intracellular mouth of the pore regulate anion conduction in the CFTR chloride channel.* J Gen Physiol, 2006. **128**(5): p. 535-45.

39.   Hwang, T.C. and K.L. Kirk, *The CFTR ion channel: gating, regulation, and anion permeation.* Cold Spring Harb Perspect Med, 2013. **3**(1): p. a009498.

40.   Corradi, V., P. Vergani, and D.P. Tieleman, *Cystic Fibrosis Transmembrane Conductance Regulator (CFTR): CLOSED AND OPEN STATE CHANNEL MODELS.* J Biol Chem, 2015. **290**(38): p. 22891-906.

41.   He, L., et al., *Multiple membrane-cytoplasmic domain contacts in the cystic fibrosis transmembrane conductance regulator (CFTR) mediate regulation of channel gating.* J Biol Chem, 2008. **283**(39): p. 26383-90.

42.   Loo, T.W., M.C. Bartlett, and D.M. Clarke, *Processing mutations disrupt interactions between the nucleotide binding and transmembrane domains of P-glycoprotein and the cystic fibrosis transmembrane conductance regulator (CFTR).* J Biol Chem, 2008. **283**(42): p. 28190-7.

43.   Loo, T.W. and D.M. Clarke, *Repair of CFTR folding defects with correctors that function as pharmacological chaperones.* Methods Mol Biol, 2011. **741**: p. 23-37.

44. Loo, T.W. and D.M. Clarke, *The Transmission Interfaces Contribute Asymmetrically to the Assembly and Activity of Human P-glycoprotein.* J Biol Chem, 2015. **290**(27): p. 16954-63.

45. He, L., et al., *Correctors of DeltaF508 CFTR restore global conformational maturation without thermally stabilizing the mutant protein.* Faseb j, 2013. **27**(2): p. 536-45.

46. Aleksandrov, A.A., et al., *Regulatory insertion removal restores maturation, stability and function of DeltaF508 CFTR.* J Mol Biol, 2010. **401**(2): p. 194-210.

47. Davidson, A.L., et al., *Structure, function, and evolution of bacterial ATP-binding cassette systems.* Microbiol Mol Biol Rev, 2008. **72**(2): p. 317-64, table of contents.

48. Hwang, T.C. and D.N. Sheppard, *Gating of the CFTR Cl- channel by ATP-driven nucleotide-binding domain dimerisation.* J Physiol, 2009. **587**(Pt 10): p. 2151-61.

49. Mense, M., et al., *In vivo phosphorylation of CFTR promotes formation of a nucleotide-binding domain heterodimer.* Embo j, 2006. **25**(20): p. 4728-39.

50. Ramjeesingh, M., et al., *The intact CFTR protein mediates ATPase rather than adenylate kinase activity.* Biochem J, 2008. **412**(2): p. 315-21.

51. Li, C., et al., *ATPase activity of the cystic fibrosis transmembrane conductance regulator.* J Biol Chem, 1996. **271**(45): p. 28463-8.

52. Stratford, F.L., et al., *The Walker B motif of the second nucleotide-binding domain (NBD2) of CFTR plays a key role in ATPase activity by the NBD1-NBD2 heterodimer.* Biochem J, 2007. **401**(2): p. 581-6.

53. Lewis, H.A., et al., *Structure of nucleotide-binding domain 1 of the cystic fibrosis transmembrane conductance regulator.* Embo j, 2004. **23**(2): p. 282-93.

54. Ostedgaard, L.S., O. Baldursson, and M.J. Welsh, *Regulation of the cystic fibrosis transmembrane conductance regulator Cl- channel by its R domain.* J Biol Chem, 2001. **276**(11): p. 7689-92.

55. Rich, D.P., et al., *Effect of deleting the R domain on CFTR-generated chloride channels.* Science, 1991. **253**(5016): p. 205-7.

56. Baker, J.M., et al., *CFTR regulatory region interacts with NBD1 predominantly via multiple transient helices.* Nat Struct Mol Biol, 2007. **14**(8): p. 738-45.

57. Kanelis, V., et al., *NMR evidence for differential phosphorylation-dependent interactions in WT and DeltaF508 CFTR.* Embo j, 2010. **29**(1): p. 263-77.

58. Hudson, R.P., et al., *Conformational changes relevant to channel activity and folding within the first nucleotide binding domain of the cystic fibrosis transmembrane conductance regulator.* J Biol Chem, 2012. **287**(34): p. 28480-94.

59.   Dawson, J.E., P.J. Farber, and J.D. Forman-Kay, *Allosteric coupling between the intracellular coupling helix 4 and regulatory sites of the first nucleotide-binding domain of CFTR.* PLoS One, 2013. **8**(9): p. e74347.

60.   Gadsby, D.C., *Ion channels versus ion pumps: the principal difference, in principle.* Nat Rev Mol Cell Biol, 2009. **10**(5): p. 344-52.

61.   Liu, X., S.S. Smith, and D.C. Dawson, *CFTR: what's it like inside the pore?* J Exp Zool A Comp Exp Biol, 2003. **300**(1): p. 69-75.

62.   Linsdell, P., *Mechanism of chloride permeation in the cystic fibrosis transmembrane conductance regulator chloride channel.* Exp Physiol, 2006. **91**(1): p. 123-9.

63.   Hwang, T.C., et al., *Structural mechanisms of CFTR function and dysfunction.* J Gen Physiol, 2018. **150**(4): p. 539-570.

64.   Lin, W.Y., Y. Sohma, and T.C. Hwang, *Synergistic Potentiation of Cystic Fibrosis Transmembrane Conductance Regulator Gating by Two Chemically Distinct Potentiators, Ivacaftor (VX-770) and 5-Nitro-2-(3-Phenylpropylamino) Benzoate.* Mol Pharmacol, 2016. **90**(3): p. 275-85.

65.   Kunzelmann, K. and A. Mehta, *CFTR: a hub for kinases and crosstalk of cAMP and Ca2+.* Febs j, 2013. **280**(18): p. 4417-29.

66.   Billet, A., et al., *Potential sites of CFTR activation by tyrosine kinases.* Channels (Austin), 2016. **10**(3): p. 247-51.

67.   Billet, A., et al., *Regulation of the cystic fibrosis transmembrane conductance regulator anion channel by tyrosine phosphorylation.* Faseb j, 2015. **29**(9): p. 3945-53.

68.   Billet, A. and J.W. Hanrahan, *The secret life of CFTR as a calcium-activated chloride channel.* J Physiol, 2013. **591**(21): p. 5273-8.

69.   Chappe, V., et al., *Phosphorylation of protein kinase C sites in NBD1 and the R domain control CFTR channel activation by PKA.* J Physiol, 2003. **548**(Pt 1): p. 39-52.

70.   Chappe, V., et al., *Stimulatory and inhibitory protein kinase C consensus sequences regulate the cystic fibrosis transmembrane conductance regulator.* Proc Natl Acad Sci U S A, 2004. **101**(1): p. 390-5.

71.   Farinha, C.M., et al., *Regulatory Crosstalk by Protein Kinases on CFTR Trafficking and Activity.* Front Chem, 2016. **4**: p. 1.

72.   Fischer, H. and T.E. Machen, *The tyrosine kinase p60c-src regulates the fast gate of the cystic fibrosis transmembrane conductance regulator chloride channel.* Biophys J, 1996. **71**(6): p. 3073-82.

73.   Liang, L., et al., *A novel role of protein tyrosine kinase2 in mediating chloride secretion in human airway epithelial cells.* PLoS One, 2011. **6**(7): p. e21991.

74.   Billet, A., et al., *Role of tyrosine phosphorylation in the muscarinic activation of the cystic fibrosis transmembrane conductance regulator (CFTR).* J Biol Chem, 2013. **288**(30): p. 21815-23.

75.   Chen, J., B.L. Martin, and D.L. Brautigan, *Regulation of protein serine-threonine phosphatase type-2A by tyrosine phosphorylation.* Science, 1992. **257**(5074): p. 1261-4.

76.   Treharne, K.J., et al., *Inhibition of protein kinase CK2 closes the CFTR Cl channel, but has no effect on the cystic fibrosis mutant deltaF508-CFTR.* Cell Physiol Biochem, 2009. **24**(5-6): p. 347-60.

77.   Pagano, M.A., et al., *Modulation of protein kinase CK2 activity by fragments of CFTR encompassing F508 may reflect functional links with cystic fibrosis pathogenesis.* Biochemistry, 2008. **47**(30): p. 7925-36.

78.   Venerando, A., et al., *Detection of phospho-sites generated by protein kinase CK2 in CFTR: mechanistic aspects of Thr1471 phosphorylation.* PLoS One, 2013. **8**(9): p. e74232.

79.   Luz, S., et al., *Contribution of casein kinase 2 and spleen tyrosine kinase to CFTR trafficking and protein kinase A-induced activity.* Mol Cell Biol, 2011. **31**(22): p. 4392-404.

80.   Cesaro, L., et al., *Phosphorylation of cystic fibrosis transmembrane conductance regulator (CFTR) serine-511 by the combined action of tyrosine kinases and CK2: the implication of tyrosine-512 and phenylalanine-508.* Amino Acids, 2013. **45**(6): p. 1423-9.

81.   Campbell, J.C., et al., *Structural Basis of Cyclic Nucleotide Selectivity in cGMP-dependent Protein Kinase II.* J Biol Chem, 2016. **291**(11): p. 5623-33.

82.   Tien, X.Y., et al., *Activation of the cystic fibrosis transmembrane conductance regulator by cGMP in the human colonic cancer cell line, Caco-2.* J Biol Chem, 1994. **269**(1): p. 51-4.

83.   Lin, M., A.C. Nairn, and S.E. Guggino, *cGMP-dependent protein kinase regulation of a chloride channel in T84 cells.* Am J Physiol, 1992. **262**(5 Pt 1): p. C1304-12.

84.   Sullivan, S.K., L.B. Agellon, and R. Schick, *Identification and partial characterization of a domain in CFTR that may bind cyclic nucleotides directly.* Curr Biol, 1995. **5**(10): p. 1159-67.

85.   Picciotto, M.R., et al., *Phosphorylation of the cystic fibrosis transmembrane conductance regulator.* J Biol Chem, 1992. **267**(18): p. 12742-52.

86.   Hallows, K.R., et al., *Inhibition of cystic fibrosis transmembrane conductance regulator by novel interaction with the metabolic sensor AMP-activated protein kinase.* J Clin Invest, 2000. **105**(12): p. 1711-21.

87.   Hallows, K.R., et al., *Regulation of channel gating by AMP-activated protein kinase modulates cystic fibrosis transmembrane conductance regulator activity in lung submucosal cells.* J Biol Chem, 2003. **278**(2): p. 998-1004.

88.   Hallows, K.R., et al., *Physiological modulation of CFTR activity by AMP-activated protein kinase in polarized T84 cells.* Am J Physiol Cell Physiol, 2003. **284**(5): p. C1297-308.

89.   Walker, J., et al., *Activation of AMP-activated protein kinase reduces cAMP-mediated epithelial chloride secretion.* Am J Physiol Gastrointest Liver Physiol, 2003. **285**(5): p. G850-60.

90.   Kongsuphol, P., et al., *Mechanistic insight into control of CFTR by AMPK.* J Biol Chem, 2009. **284**(9): p. 5645-53.

91.   Wilkinson, D.J., et al., *CFTR activation: additive effects of stimulatory and inhibitory phosphorylation sites in the R domain.* Am J Physiol, 1997. **273**(1 Pt 1): p. L127-33.

92.   Csanady, L., et al., *Preferential phosphorylation of R-domain Serine 768 dampens activation of CFTR channels by PKA.* J Gen Physiol, 2005. **125**(2): p. 171-86.

93.   Boissan, M., et al., *The mammalian Nm23/NDPK family: from metastasis control to cilia movement.* Mol Cell Biochem, 2009. **329**(1-2): p. 51-62.

94.   King, J.D., Jr., et al., *Role of binding and nucleoside diphosphate kinase A in the regulation of the cystic fibrosis transmembrane conductance regulator by AMP-activated protein kinase.* J Biol Chem, 2012. **287**(40): p. 33389-400.

95.   Borthwick, L.A., et al., *Role of Interaction and Nucleoside Diphosphate Kinase B in Regulation of the Cystic Fibrosis Transmembrane Conductance Regulator Function by cAMP-Dependent Protein Kinase A.* PLoS One, 2016. **11**(3): p. e0149097.

96.   Anderson, M.P., et al., *Generation of cAMP-activated chloride currents by expression of CFTR.* Science, 1991. **251**(4994): p. 679-82.

97.   Bear, C.E., et al., *Cl- channel activity in Xenopus oocytes expressing the cystic fibrosis gene.* J Biol Chem, 1991. **266**(29): p. 19142-5.

98.   Kartner, N., et al., *Expression of the cystic fibrosis gene in non-epithelial invertebrate cells produces a regulated anion conductance.* Cell, 1991. **64**(4): p. 681-91.

99.   Tabcharani, J.A., et al., *Phosphorylation-regulated Cl- channel in CHO cells stably expressing the cystic fibrosis gene.* Nature, 1991. **352**(6336): p. 628-31.

100.   Berger, H.A., et al., *Identification and regulation of the cystic fibrosis transmembrane conductance regulator-generated chloride channel.* J Clin Invest, 1991. **88**(4): p. 1422-31.

101.   Pasyk, S., et al., *The major cystic fibrosis causing mutation exhibits defective propensity for phosphorylation.* Proteomics, 2015. **15**(2-3): p. 447-61.

102.   Gadsby, D.C. and A.C. Nairn, *Regulation of CFTR Cl- ion channels by phosphorylation and dephosphorylation.* Adv Second Messenger Phosphoprotein Res, 1999. **33**: p. 79-106.

103.   Cheng, S.H., et al., *Phosphorylation of the R domain by cAMP-dependent protein kinase regulates the CFTR chloride channel.* Cell, 1991. **66**(5): p. 1027-36.

104.   Chang, X.B., et al., *Protein kinase A (PKA) still activates CFTR chloride channel after mutagenesis of all 10 PKA consensus phosphorylation sites.* J Biol Chem, 1993. **268**(15): p. 11304-11.

105.   Seibert, F.S., et al., *Influence of phosphorylation by protein kinase A on CFTR at the cell surface and endoplasmic reticulum.* Biochim Biophys Acta, 1999. **1461**(2): p. 275-83.

106.   Neville, D.C., et al., *Evidence for phosphorylation of serine 753 in CFTR using a novel metal-ion affinity resin and matrix-assisted laser desorption mass spectrometry.* Protein Sci, 1997. **6**(11): p. 2436-45.

107.   Hegedus, T., et al., *Role of individual R domain phosphorylation sites in CFTR regulation by protein kinase A.* Biochim Biophys Acta, 2009. **1788**(6): p. 1341-9.

108.   McClure, M., et al., *Purification of CFTR for mass spectrometry analysis: identification of palmitoylation and other post-translational modifications.* Protein Eng Des Sel, 2012. **25**(1): p. 7-14.

109.   Winter, M.C. and M.J. Welsh, *Stimulation of CFTR activity by its phosphorylated R domain.* Nature, 1997. **389**(6648): p. 294-6.

110.   Mihalyi, C., B. Torocsik, and L. Csanady, *Obligate coupling of CFTR pore opening to tight nucleotide-binding domain dimerization.* Elife, 2016. **5**.

111.   Szellas, T. and G. Nagel, *Apparent affinity of CFTR for ATP is increased by continuous kinase activity.* FEBS Lett, 2003. **535**(1-3): p. 141-6.

112.   Wang, W., et al., *ATP-independent CFTR channel gating and allosteric modulation by phosphorylation.* Proc Natl Acad Sci U S A, 2010. **107**(8): p. 3888-93.

113.   Zhang, L., et al., *Architecture of the cystic fibrosis transmembrane conductance regulator protein and structural changes associated with phosphorylation and nucleotide binding.* J Struct Biol, 2009. **167**(3): p. 242-51.

114.   Naren, A.P., et al., *CFTR chloride channel regulation by an interdomain interaction.* Science, 1999. **286**(5439): p. 544-8.

115. Fu, J. and K.L. Kirk, *Cysteine substitutions reveal dual functions of the amino-terminal tail in cystic fibrosis transmembrane conductance regulator channel gating.* J Biol Chem, 2001. **276**(38): p. 35660-8.

116. Ehrhardt, A., et al., *Channel Gating Regulation by the Cystic Fibrosis Transmembrane Conductance Regulator (CFTR) First Cytosolic Loop.* J Biol Chem, 2016. **291**(4): p. 1854-65.

117. Chin, S., M. Hung, and C.E. Bear, *Current insights into the role of PKA phosphorylation in CFTR channel activity and the pharmacological rescue of cystic fibrosis disease-causing mutants.* Cell Mol Life Sci, 2017. **74**(1): p. 57-66.

118. Glozman, R., et al., *N-glycans are direct determinants of CFTR folding and stability in secretory and endocytic membrane traffic*, in *J Cell Biol*. 2009. p. 847-62.

119. McDonald, R.A., et al., *Basal expression of the cystic fibrosis transmembrane conductance regulator gene is dependent on protein kinase A activity.* Proc Natl Acad Sci U S A, 1995. **92**(16): p. 7560-4.

120. Matthews, R.P. and G.S. McKnight, *Characterization of the cAMP response element of the cystic fibrosis transmembrane conductance regulator gene promoter.* J Biol Chem, 1996. **271**(50): p. 31869-77.

121. Liang, X., et al., *Phosphorylation-dependent 14-3-3 protein interactions regulate CFTR biogenesis.* Mol Biol Cell, 2012. **23**(6): p. 996-1009.

122. Rennolds, J., et al., *Cystic fibrosis transmembrane conductance regulator trafficking is mediated by the COPI coat in epithelial cells.* J Biol Chem, 2008. **283**(2): p. 833-9.

123. Stevers, L.M., et al., *Characterization and small-molecule stabilization of the multisite tandem binding between 14-3-3 and the R domain of CFTR.* Proc Natl Acad Sci U S A, 2016. **113**(9): p. E1152-61.

124. Cantiello, H.F., *Role of the actin cytoskeleton in the regulation of the cystic fibrosis transmembrane conductance regulator.* Exp Physiol, 1996. **81**(3): p. 505-14.

125. Louvet-Vallee, S., *ERM proteins: from cellular architecture to cell signaling.* Biol Cell, 2000. **92**(5): p. 305-16.

126. Naren, A.P., et al., *A macromolecular complex of beta 2 adrenergic receptor, CFTR, and ezrin/radixin/moesin-binding phosphoprotein 50 is regulated by PKA.* Proc Natl Acad Sci U S A, 2003. **100**(1): p. 342-6.

127. Li, C., et al., *Molecular assembly of cystic fibrosis transmembrane conductance regulator in plasma membrane.* J Biol Chem, 2004. **279**(23): p. 24673-84.

128. Monterisi, S., et al., *CFTR regulation in human airway epithelial cells requires integrity of the actin cytoskeleton and compartmentalized cAMP and PKA activity.* J Cell Sci, 2012. **125**(Pt 5): p. 1106-17.

129.   Sun, F., et al., *E3KARP mediates the association of ezrin and protein kinase A with the cystic fibrosis transmembrane conductance regulator in airway cells.* J Biol Chem, 2000. **275**(38): p. 29539-46.

130.   Short, D.B., et al., *An apical PDZ protein anchors the cystic fibrosis transmembrane conductance regulator to the cytoskeleton.* J Biol Chem, 1998. **273**(31): p. 19797-801.

131.   Holleran, J.P., et al., *Regulated recycling of mutant CFTR is partially restored by pharmacological treatment.* J Cell Sci, 2013. **126**(Pt 12): p. 2692-703.

132.   Abu-Arish, A., et al., *Cholesterol modulates CFTR confinement in the plasma membrane of primary epithelial cells.* Biophys J, 2015. **109**(1): p. 85-94.

133.   Bozoky, Z., et al., *Regulatory R region of the CFTR chloride channel is a dynamic integrator of phospho-dependent intra- and intermolecular interactions.* Proc Natl Acad Sci U S A, 2013. **110**(47): p. E4427-36.

134.   Chang, M.H., et al., *Slc26a9 is inhibited by the R-region of the cystic fibrosis transmembrane conductance regulator via the STAS domain.* J Biol Chem, 2009. **284**(41): p. 28306-18.

135.   Ko, S.B., et al., *Gating of CFTR by the STAS domain of SLC26 transporters.* Nat Cell Biol, 2004. **6**(4): p. 343-50.

136.   Favia, M., et al., *Na+/H+ exchanger regulatory factor 1 overexpression-dependent increase of cytoskeleton organization is fundamental in the rescue of F508del cystic fibrosis transmembrane conductance regulator in human airway CFBE41o- cells.* Mol Biol Cell, 2010. **21**(1): p. 73-86.

137.   Veit, G., et al., *From CFTR biology toward combinatorial pharmacotherapy: expanded classification of cystic fibrosis mutations.* Mol Biol Cell, 2016. **27**(3): p. 424-33.

138.   Bompadre, S.G., et al., *G551D and G1349D, two CF-associated mutations in the signature sequences of CFTR, exhibit distinct gating defects.* J Gen Physiol, 2007. **129**(4): p. 285-98.

139.   Gregory, R.J., et al., *Maturation and function of cystic fibrosis transmembrane conductance regulator variants bearing mutations in putative nucleotide-binding domains 1 and 2.* Mol Cell Biol, 1991. **11**(8): p. 3886-93.

140.   Eckford, P.D., et al., *Cystic fibrosis transmembrane conductance regulator (CFTR) potentiator VX-770 (ivacaftor) opens the defective channel gate of mutant CFTR in a phosphorylation-dependent but ATP-independent manner.* J Biol Chem, 2012. **287**(44): p. 36639-49.

141.   Pasyk, S., et al., *Direct interaction of a small-molecule modulator with G551D-CFTR, a cystic fibrosis-causing mutation associated with severe disease.* Biochem J, 2009. **418**(1): p. 185-90.

142. Ren, X.Q., et al., *Function of the ABC signature sequences in the human multidrug resistance protein 1.* Mol Pharmacol, 2004. **65**(6): p. 1536-42.

143. Wang, C., et al., *Integrated biophysical studies implicate partial unfolding of NBD1 of CFTR in the molecular pathogenesis of F508del cystic fibrosis.* Protein Sci, 2010. **19**(10): p. 1932-47.

144. Protasevich, I., et al., *Thermal unfolding studies show the disease causing F508del mutation in CFTR thermodynamically destabilizes nucleotide-binding domain 1.* Protein Sci, 2010. **19**(10): p. 1917-31.

145. Okiyoneda, T., et al., *Mechanism-based corrector combination restores DeltaF508-CFTR folding and function.* Nat Chem Biol, 2013. **9**(7): p. 444-54.

146. Rabeh, W.M., et al., *Correction of both NBD1 energetics and domain interface is required to restore DeltaF508 CFTR folding and function.* Cell, 2012. **148**(1-2): p. 150-63.

147. Riordan, J.R., *Assembly of functional CFTR chloride channels.* Annu Rev Physiol, 2005. **67**: p. 701-18.

148. Younger, J.M., et al., *A foldable CFTR{Delta}F508 biogenic intermediate accumulates upon inhibition of the Hsc70-CHIP E3 ubiquitin ligase.* J Cell Biol, 2004. **167**(6): p. 1075-85.

149. Younger, J.M., et al., *Sequential quality-control checkpoints triage misfolded cystic fibrosis transmembrane conductance regulator.* Cell, 2006. **126**(3): p. 571-82.

150. Farinha, C.M. and M.D. Amaral, *Most F508del-CFTR is targeted to degradation at an early folding checkpoint and independently of calnexin.* Mol Cell Biol, 2005. **25**(12): p. 5242-52.

151. Hegedus, T., et al., *F508del CFTR with two altered RXR motifs escapes from ER quality control but its channel activity is thermally sensitive.* Biochim Biophys Acta, 2006. **1758**(5): p. 565-72.

152. Kim Chiaw, P., et al., *Functional rescue of DeltaF508-CFTR by peptides designed to mimic sorting motifs.* Chem Biol, 2009. **16**(5): p. 520-30.

153. Okiyoneda, T., et al., *Peripheral protein quality control removes unfolded CFTR from the plasma membrane.* Science, 2010. **329**(5993): p. 805-10.

154. Gentzsch, M., et al., *Endocytic trafficking routes of wild type and DeltaF508 cystic fibrosis transmembrane conductance regulator.* Mol Biol Cell, 2004. **15**(6): p. 2684-96.

155. Denning, G.M., et al., *Processing of mutant cystic fibrosis transmembrane conductance regulator is temperature-sensitive.* Nature, 1992. **358**(6389): p. 761-4.

156. Van Goor, F., et al., *Correction of the F508del-CFTR protein processing defect in vitro by the investigational drug VX-809.* Proc Natl Acad Sci U S A, 2011. **108**(46): p. 18843-8.

157. Ren, H.Y., et al., *VX-809 corrects folding defects in cystic fibrosis transmembrane conductance regulator protein through action on membrane-spanning domain 1.* Mol Biol Cell, 2013. **24**(19): p. 3016-24.

158. Loo, T.W., M.C. Bartlett, and D.M. Clarke, *Corrector VX-809 stabilizes the first transmembrane domain of CFTR.* Biochem Pharmacol, 2013. **86**(5): p. 612-9.

159. Abbattiscianni, A.C., et al., *Correctors of mutant CFTR enhance subcortical cAMP-PKA signaling through modulating ezrin phosphorylation and cytoskeleton organization.* J Cell Sci, 2016. **129**(6): p. 1128-40.

160. Van Goor, F., et al., *Rescue of CF airway epithelial cell function in vitro by a CFTR potentiator, VX-770.* Proc Natl Acad Sci U S A, 2009. **106**(44): p. 18825-30.

161. Jih, K.Y. and T.C. Hwang, *Vx-770 potentiates CFTR function by promoting decoupling between the gating cycle and ATP hydrolysis cycle.* Proc Natl Acad Sci U S A, 2013. **110**(11): p. 4404-9.

162. Cholon, D.M., et al., *Potentiator ivacaftor abrogates pharmacological correction of DeltaF508 CFTR in cystic fibrosis.* Sci Transl Med, 2014. **6**(246): p. 246ra96.

163. Veit, G., et al., *Some gating potentiators, including VX-770, diminish DeltaF508-CFTR functional expression.* Sci Transl Med, 2014. **6**(246): p. 246ra97.

164. Sun, L., et al., *Multiple apical plasma membrane constituents are associated with susceptibility to meconium ileus in individuals with cystic fibrosis.* Nat Genet, 2012. **44**(5): p. 562-9.

165. Li, W., et al., *Unraveling the complex genetic model for cystic fibrosis: pleiotropic effects of modifier genes on early cystic fibrosis-related morbidities.* Hum Genet, 2014. **133**(2): p. 151-61.

166. Corvol, H., et al., *Genome-wide association meta-analysis identifies five modifier loci of lung disease severity in cystic fibrosis.* Nat Commun, 2015. **6**: p. 8382.

167. Strug, L.J., et al., *Cystic fibrosis gene modifier SLC26A9 modulates airway response to CFTR-directed therapeutics.* Hum Mol Genet, 2016. **25**(20): p. 4590-4600.

168. Loureiro, C.A., et al., *A molecular switch in the scaffold NHERF1 enables misfolded CFTR to evade the peripheral quality control checkpoint.* Sci Signal, 2015. **8**(377): p. ra48.

169. Turner, M.J., et al., *The dual phosphodiesterase 3 and 4 inhibitor RPL554 stimulates CFTR and ciliary beating in primary cultures of bronchial epithelia.* Am J Physiol Lung Cell Mol Physiol, 2016. **310**(1): p. L59-70.

170. Li, C. and A.P. Naren, *Analysis of CFTR interactome in the macromolecular complexes.* Methods Mol Biol, 2011. **741**: p. 255-70.

171. Li, C. and A.P. Naren, *CFTR chloride channel in the apical compartments: spatiotemporal coupling to its interacting partners.* Integr Biol (Camb), 2010. **2**(4): p. 161-77.

172. Li, C., et al., *Spatiotemporal coupling of cAMP transporter to CFTR chloride channel function in the gut epithelia.* Cell, 2007. **131**(5): p. 940-51.

173. Moon, C., et al., *Compartmentalized accumulation of cAMP near complexes of multidrug resistance protein 4 (MRP4) and cystic fibrosis transmembrane conductance regulator (CFTR) contributes to drug-induced diarrhea.* J Biol Chem, 2015. **290**(18): p. 11246-57.

174. Boyle, M.P., et al., *A CFTR corrector (lumacaftor) and a CFTR potentiator (ivacaftor) for treatment of patients with cystic fibrosis who have a phe508del CFTR mutation: a phase 2 randomised controlled trial.* Lancet Respir Med, 2014. **2**(7): p. 527-38.

175. Simons, K. and D. Toomre, *Lipid rafts and signal transduction.* Nat Rev Mol Cell Biol, 2000. **1**(1): p. 31-9.

176. Calder, P.C. and P. Yaqoob, *Lipid rafts--composition, characterization, and controversies.* J Nutr, 2007. **137**(3): p. 545-7.

177. Matthes, E., et al., *Low free drug concentration prevents inhibition of F508del CFTR functional expression by the potentiator VX-770 (ivacaftor).* Br J Pharmacol, 2016. **173**(3): p. 459-70.

178. Dawson, R.J. and K.P. Locher, *Structure of a bacterial multidrug ABC transporter.* Nature, 2006. **443**(7108): p. 180-5.

179. Ward, A., et al., *Flexibility in the ABC transporter MsbA: Alternating access with a twist.* Proc Natl Acad Sci U S A, 2007. **104**(48): p. 19005-10.

180. Mendoza, J.L., et al., *Requirements for efficient correction of DeltaF508 CFTR revealed by analyses of evolved sequences.* Cell, 2012. **148**(1-2): p. 164-74.

181. Chappe, V., et al., *Phosphorylation of CFTR by PKA promotes binding of the regulatory domain.* Embo j, 2005. **24**(15): p. 2730-40.

182. Miles, A.J., et al., *Calibration and Standardisation of Synchrotron Radiation Circular Dichroism and Conventional Circular Dichroism Spectrophotometers.* Spectroscopy, 2003. **17**(4).

183. Miles, A.J., L. Whitmore, and B.A. Wallace, *Spectral magnitude effects on the analyses of secondary structure from circular dichroism spectroscopic data.* Protein Sci, 2005. **14**(2): p. 368-74.

184. Lees, J.G., et al., *CDtool-an integrated software package for circular dichroism spectroscopic data processing, analysis, and archiving.* Anal Biochem, 2004. **332**(2): p. 285-9.

185. Schlamadinger, D.E. and J.E. Kim, *Thermodynamics of membrane protein folding measured by fluorescence spectroscopy.* J Vis Exp, 2011(50).

186. Chang, X.B., et al., *Role of N-linked oligosaccharides in the biosynthetic processing of the cystic fibrosis membrane conductance regulator.* J Cell Sci, 2008. **121**(Pt 17): p. 2814-23.

187. Schneider, C.A., W.S. Rasband, and K.W. Eliceiri, *NIH Image to ImageJ: 25 years of image analysis.* Nat Methods, 2012. **9**(7): p. 671-5.

188. Roy, A., A. Kucukural, and Y. Zhang, *I-TASSER: a unified platform for automated protein structure and function prediction.* Nat Protoc, 2010. **5**(4): p. 725-38.

189. Yang, J., et al., *The I-TASSER Suite: protein structure and function prediction.* Nat Methods, 2015. **12**(1): p. 7-8.

190. Yang, J. and Y. Zhang, *I-TASSER server: new development for protein structure and function predictions.* Nucleic Acids Res, 2015. **43**(W1): p. W174-81.

191. Zhang, Y., *I-TASSER server for protein 3D structure prediction.* BMC Bioinformatics, 2008. **9**: p. 40.

192. Eckford, P.D., C. Li, and C.E. Bear, *Functional reconstitution and channel activity measurements of purified wildtype and mutant CFTR protein.* J Vis Exp, 2015(97).

193. Charalambous, K., et al., *Thermal and chemical unfolding and refolding of a eukaryotic sodium channel.* Biochim Biophys Acta, 2009. **1788**(6): p. 1279-86.

194. Dulhanty, A.M. and J.R. Riordan, *Phosphorylation by cAMP-dependent protein kinase causes a conformational change in the R domain of the cystic fibrosis transmembrane conductance regulator.* Biochemistry, 1994. **33**(13): p. 4072-9.

195. Di Bartolo, N.D., et al., *In vitro folding and assembly of the Escherichia coli ATP-binding cassette transporter, BtuCD.* J Biol Chem, 2011. **286**(21): p. 18807-15.

196. DiBartolo, N. and P.J. Booth, *Unravelling the folding and stability of an ABC (ATP-binding cassette) transporter.* Biochem Soc Trans, 2011. **39**(3): p. 751-60.

197. Eckford, P.D. and F.J. Sharom, *Functional characterization of Escherichia coli MsbA: interaction with nucleotides and substrates.* J Biol Chem, 2008. **283**(19): p. 12840-50.

198. Kanelis, V., et al., *NMR evidence for differential phosphorylation-dependent interactions in WT and DeltaF508 CFTR.* Embo J. **29**(1): p. 263-77.

199.   Molinski, S.V., et al., *Facilitating Structure-Function Studies of CFTR Modulator Sites with Efficiencies in Mutagenesis and Functional Screening.* J Biomol Screen, 2015. **20**(10): p. 1204-17.

200.   Seibert, F.S., et al., *Disease-associated mutations in the fourth cytoplasmic loop of cystic fibrosis transmembrane conductance regulator compromise biosynthetic processing and chloride channel activity.* J Biol Chem, 1996. **271**(25): p. 15139-45.

201.   Yang, J., Y. Wang, and Y. Zhang, *ResQ: An Approach to Unified Estimation of B-Factor and Residue-Specific Error in Protein Structure Prediction.* J Mol Biol, 2016. **428**(4): p. 693-701.

202.   Linsdell, P., *Structural Changes Fundamental to Gating of the Cystic Fibrosis Transmembrane Conductance Regulator Anion Channel Pore.* Adv Exp Med Biol, 2016.

203.   Sorum, B., D. Czege, and L. Csanady, *Timing of CFTR pore opening and structure of its transition state.* Cell, 2015. **163**(3): p. 724-33.

204.   Gao, X. and T.C. Hwang, *Localizing a gate in CFTR.* Proc Natl Acad Sci U S A, 2015. **112**(8): p. 2461-6.

205.   Golin, J. and S.V. Ambudkar, *The multidrug transporter Pdr5 on the 25th anniversary of its discovery: an important model for the study of asymmetric ABC transporters.* Biochem J, 2015. **467**(3): p. 353-63.

206.   Eggensperger, S., et al., *An annular lipid belt is essential for allosteric coupling and viral inhibition of the antigen translocation complex TAP (transporter associated with antigen processing).* J Biol Chem, 2014. **289**(48): p. 33098-108.

207.   Wang, F., et al., *Deletion of phenylalanine 508 causes attenuated phosphorylation-dependent activation of CFTR chloride channels.* J Physiol, 2000. **524 Pt 3**: p. 637-48.

208.   Drumm, M.L., et al., *Chloride conductance expressed by delta F508 and other mutant CFTRs in Xenopus oocytes.* Science, 1991. **254**(5039): p. 1797-9.

209.   Bechara, C., et al., *MALDI-TOF mass spectrometry analysis of amphipol-trapped membrane proteins.* Anal Chem, 2012. **84**(14): p. 6128-35.

210.   Gohon, Y., et al., *Bacteriorhodopsin/amphipol complexes: structural and functional properties.* Biophys J, 2008. **94**(9): p. 3523-37.

211.   Vergani, P., et al., *CFTR channel opening by ATP-driven tight dimerization of its nucleotide-binding domains.* Nature, 2005. **433**(7028): p. 876-80.

212.   Aleksandrov, A.A., L.A. Aleksandrov, and J.R. Riordan, *CFTR (ABCC7) is a hydrolyzable-ligand-gated channel.* Pflugers Arch, 2007. **453**(5): p. 693-702.

213.   Kogan, I., et al., *Studies of the molecular basis for cystic fibrosis using purified reconstituted CFTR protein.* Methods Mol Med, 2002. **70**: p. 143-57.

214. Kogan, I., et al., *Perturbation of the pore of the cystic fibrosis transmembrane conductance regulator (CFTR) inhibits its atpase activity.* J Biol Chem, 2001. **276**(15): p. 11575-81.

215. Kidd, J.F., et al., *A heteromeric complex of the two nucleotide binding domains of cystic fibrosis transmembrane conductance regulator (CFTR) mediates ATPase activity.* J Biol Chem, 2004. **279**(40): p. 41664-9.

216. Jackson, S.M., et al., *Structural basis of small-molecule inhibition of human multidrug transporter ABCG2.* Nat Struct Mol Biol, 2018. **25**(4): p. 333-340.

217. Taylor, N.M.I., et al., *Structure of the human multidrug transporter ABCG2.* Nature, 2017. **546**(7659): p. 504-509.

218. Josts, I., et al., *Conformational States of ABC Transporter MsbA in a Lipid Environment Investigated by Small-Angle Scattering Using Stealth Carrier Nanodiscs.* Structure, 2018.

219. Ambudkar, S.V., et al., *Purification and reconstitution of human P-glycoprotein.* Methods Enzymol, 1998. **292**: p. 492-504.

220. Ritchie, T.K., et al., *Chapter 11 - Reconstitution of membrane proteins in phospholipid bilayer nanodiscs.* Methods Enzymol, 2009. **464**: p. 211-31.

221. Hirayama, H., et al., *ATPase activity of human ABCG1 is stimulated by cholesterol and sphingomyelin.* J Lipid Res, 2013. **54**(2): p. 496-502.

222. Infed, N., et al., *Influence of detergents on the activity of the ABC transporter LmrA.* Biochim Biophys Acta, 2011. **1808**(9): p. 2313-21.

223. Kawai, T., et al., *Catalytic activity of MsbA reconstituted in nanodisc particles is modulated by remote interactions with the bilayer.* FEBS Lett, 2011. **585**(22): p. 3533-7.

224. Doerrler, W.T. and C.R. Raetz, *ATPase activity of the MsbA lipid flippase of Escherichia coli.* J Biol Chem, 2002. **277**(39): p. 36697-705.

225. Hildebrandt, E., et al., *Specific stabilization of CFTR by phosphatidylserine.* Biochim Biophys Acta, 2017. **1859**(2): p. 289-293.

226. Yang, Z., et al., *Membrane protein stability can be compromised by detergent interactions with the extramembranous soluble domains.* Protein Sci, 2014. **23**(6): p. 769-89.

227. Ereno-Orbea, J., et al., *Molecular basis of human CD22 function and therapeutic targeting.* Nat Commun, 2017. **8**(1): p. 764.

228. Ereno-Orbea, J., et al., *Characterization of Glycoproteins with the Immunoglobulin Fold by X-Ray Crystallography and Biophysical Techniques.* J Vis Exp, 2018(137).

229. Bradford, M.M., *A rapid and sensitive method for the quantitation of microgram quantities of protein utilizing the principle of protein-dye binding.* Anal Biochem, 1976. **72**: p. 248-54.

230. Adebiyi, A.P., et al., *Acid hydrolysis of protein in a microcapillary tube for the recovery of tryptophan.* Biosci Biotechnol Biochem, 2005. **69**(1): p. 255-7.

231. Dorr, J.M., et al., *Detergent-free isolation, characterization, and functional reconstitution of a tetrameric K+ channel: the power of native nanodiscs.* Proc Natl Acad Sci U S A, 2014. **111**(52): p. 18607-12.

232. Chifflet, S., et al., *A method for the determination of inorganic phosphate in the presence of labile organic phosphate and high concentrations of protein: application to lens ATPases.* Anal Biochem, 1988. **168**(1): p. 1-4.

233. Gulati, S., et al., *Detergent-free purification of ABC (ATP-binding-cassette) transporters.* Biochem J, 2014. **461**(2): p. 269-78.

234. Martinez, K.L., et al., *Allosteric transitions of Torpedo acetylcholine receptor in lipids, detergent and amphipols: molecular interactions vs. physical constraints.* FEBS Lett, 2002. **528**(1-3): p. 251-6.

235. Ramjeesingh, M., et al., *Walker mutations reveal loose relationship between catalytic and channel-gating activities of purified CFTR (cystic fibrosis transmembrane conductance regulator).* Biochemistry, 1999. **38**(5): p. 1463-8.

236. Ketchum, C.J., G.V. Rajendrakumar, and P.C. Maloney, *Characterization of the adenosinetriphosphatase and transport activities of purified cystic fibrosis transmembrane conductance regulator.* Biochemistry, 2004. **43**(4): p. 1045-53.

237. Hildebrandt, E., et al., *A survey of detergents for the purification of stable, active human cystic fibrosis transmembrane conductance regulator (CFTR).* Biochim Biophys Acta, 2014. **1838**(11): p. 2825-37.

238. Desjardins, P., J.B. Hansen, and M. Allen, *Microvolume protein concentration determination using the NanoDrop 2000c spectrophotometer.* J Vis Exp, 2009(33).

239. Drew, D., et al., *Optimization of membrane protein overexpression and purification using GFP fusions.* Nat Methods, 2006. **3**(4): p. 303-13.

240. Hildebrandt, E., et al., *A stable human-cell system overexpressing cystic fibrosis transmembrane conductance regulator recombinant protein at the cell surface.* Mol Biotechnol, 2015. **57**(5): p. 391-405.

241. Van Goor, F., et al., *Effect of ivacaftor on CFTR forms with missense mutations associated with defects in protein processing or function.* J Cyst Fibros, 2014. **13**(1): p. 29-36.

242. Baroni, D., et al., *Direct interaction of a CFTR potentiator and a CFTR corrector with phospholipid bilayers.* Eur Biophys J, 2014. **43**(6-7): p. 341-6.

243. Popot, J.L., *Membrane Proteins in Aqueous Solutions*. 1 ed. 2018: Springer International Publishing. 708.

244. Popot, J.L., et al., *Amphipols: polymeric surfactants for membrane biology research.* Cell Mol Life Sci, 2003. **60**(8): p. 1559-74.

245. Marconnet, A., Pozza, A., Ilioaia, O., Giusti, F. & Zoonens, M. , *Efficiency of amphipathic polymers in solubilizing and stabilizing membrane proteins: a comparative study (in preparation).* 2019.

246. Giusti, F., et al., *Synthesis of a Polyhistidine-bearing Amphipol and its Use for Immobilizing Membrane Proteins.* Biomacromolecules, 2015. **16**(12): p. 3751-61.

247. Etzkorn, M., et al., *How amphipols embed membrane proteins: global solvent accessibility and interaction with a flexible protein terminus.* J Membr Biol, 2014. **247**(9-10): p. 965-70.

248. Ramjeesingh, M., et al., *A novel procedure for the efficient purification of the cystic fibrosis transmembrane conductance regulator (CFTR).* Biochem J, 1997. **327 (Pt 1)**: p. 17-21.

249. Gentzsch, M., et al., *Misassembled mutant DeltaF508 CFTR in the distal secretory pathway alters cellular lipid trafficking.* J Cell Sci, 2007. **120**(Pt 3): p. 447-55.

250. Byrnes, L.J., et al., *Sites associated with Kalydeco binding on human Cystic Fibrosis Transmembrane Conductance Regulator revealed by Hydrogen/Deuterium Exchange.* Sci Rep, 2018. **8**(1): p. 4664.

251. Chin, S., et al., *Lipophilicity of the Cystic Fibrosis Drug, Ivacaftor (VX-770), and Its Destabilizing Effect on the Major CF-causing Mutation: F508del.* Mol Pharmacol, 2018. **94**(2): p. 917-925.

252. Elmallah, *Progress toward the synthesis of labeled derivatives of the Cystic Fibrosis drug, ivacaftor.* 2012.

253. Pedemonte, N., et al., *Phenylglycine and sulfonamide correctors of defective delta F508 and G551D cystic fibrosis transmembrane conductance regulator chloride-channel gating.* Mol Pharmacol, 2005. **67**(5): p. 1797-807.

254. Walsh, P., et al., *The mechanism of membrane disruption by cytotoxic amyloid oligomers formed by prion protein(106-126) is dependent on bilayer composition.* J Biol Chem, 2014. **289**(15): p. 10419-30.

255. Oreopoulos, J., et al., *Peptide-induced domain formation in supported lipid bilayers: direct evidence by combined atomic force and polarized total internal reflection fluorescence microscopy.* Biophys J, 2010. **98**(5): p. 815-23.

256. Oreopoulos, J. and C.M. Yip, *Probing membrane order and topography in supported lipid bilayers by combined polarized total internal reflection fluorescence-atomic force microscopy.* Biophys J, 2009. **96**(5): p. 1970-84.

257. Chin, S., et al., *Attenuation of Phosphorylation-dependent Activation of Cystic Fibrosis Transmembrane Conductance Regulator (CFTR) by Disease-causing Mutations at the Transmission Interface.* J Biol Chem, 2017. **292**(5): p. 1988-1999.

258. Wang, Y., et al., *Correctors promote maturation of cystic fibrosis transmembrane conductance regulator (CFTR)-processing mutants by binding to the protein.* J Biol Chem, 2007. **282**(46): p. 33247-51.

259. Loo, T.W. and D.M. Clarke, *Using a cysteine-less mutant to provide insight into the structure and mechanism of CFTR.* J Physiol, 2006. **572**(Pt 2): p. 312.

260. Karunakaran, S., et al., *SLC6A14 (ATB0,+) protein, a highly concentrative and broad specific amino acid transporter, is a novel and effective drug target for treatment of estrogen receptor-positive breast cancer.* J Biol Chem, 2011. **286**(36): p. 31830-8.

261. Bertrand, C.A., et al., *SLC26A9 is a constitutively active, CFTR-regulated anion conductance in human bronchial epithelia.* J Gen Physiol, 2009. **133**(4): p. 421-38.

262. Xu, J., et al., *SLC26A9 is expressed in gastric surface epithelial cells, mediates Cl-/HCO3- exchange, and is inhibited by NH4+.* Am J Physiol Cell Physiol, 2005. **289**(2): p. C493-505.

263. Avella, M., et al., *SLC26A9 stimulates CFTR expression and function in human bronchial cell lines.* J Cell Physiol, 2011. **226**(1): p. 212-23.

264. Anagnostopoulou, P., et al., *SLC26A9-mediated chloride secretion prevents mucus obstruction in airway inflammation.* J Clin Invest, 2012. **122**(10): p. 3629-34.

265. Gupta, N., et al., *Up-regulation of the amino acid transporter ATB(0,+) (SLC6A14) in carcinoma of the cervix.* Gynecol Oncol, 2006. **100**(1): p. 8-13.

266. Li, J., F. Xia, and R.A. Reithmeier, *N-glycosylation and topology of the human SLC26 family of anion transport membrane proteins.* Am J Physiol Cell Physiol, 2014. **306**(10): p. C943-60.

267. Mount, D.B. and M.F. Romero, *The SLC26 gene family of multifunctional anion exchangers.* Pflugers Arch, 2004. **447**(5): p. 710-21.

268. Hoglund, P., et al., *Mutations of the Down-regulated in adenoma (DRA) gene cause congenital chloride diarrhoea.* Nat Genet, 1996. **14**(3): p. 316-9.

269. Kumar, A., et al., *Activation of Nuclear Factor-kappaB by Tumor Necrosis Factor in Intestinal Epithelial Cells and Mouse Intestinal Epithelia Reduces Expression of the Chloride Transporter SLC26A3.* Gastroenterology, 2017. **153**(5): p. 1338-1350.e3.

270. Bertrand, C.A., et al., *The CFTR trafficking mutation F508del inhibits the constitutive activity of SLC26A9.* Am J Physiol Lung Cell Mol Physiol, 2017. **312**(6): p. L912-l925.

271. Di Paola, M., et al., *SLC6A14 Is a Genetic Modifier of Cystic Fibrosis That Regulates Pseudomonas aeruginosa Attachment to Human Bronchial Epithelial Cells.* MBio, 2017. **8**(6).

272. Patel, H.H., F. Murray, and P.A. Insel, *G-protein-coupled receptor-signaling components in membrane raft and caveolae microdomains.* Handb Exp Pharmacol, 2008(186): p. 167-84.

273. Bi, K., et al., *Antigen-induced translocation of PKC-theta to membrane rafts is required for T cell activation.* Nat Immunol, 2001. **2**(6): p. 556-63.

274. Steinberg, S.F., *Structural basis of protein kinase C isoform function.* Physiol Rev, 2008. **88**(4): p. 1341-78.

275. Hanrahan, J.W., et al., *Corrector combination therapies for F508del-CFTR.* Curr Opin Pharmacol, 2017. **34**: p. 105-111.

276. Trittler, R. and M. Hug, *PKP-017 Monitoring of ivacaftor serum levels.* European Journal of Hospital Pharmacy: Science and Practice, 2014. **21**(Suppl 1): p. A143-A144.

277. Corradi, V., et al., *Structure of Transmembrane Helix 8 and Possible Membrane Defects in CFTR.* Biophys J, 2018. **114**(8): p. 1751-1754.

278. Sheng, R., et al., *Cholesterol modulates cell signaling and protein networking by specifically interacting with PDZ domain-containing scaffold proteins.* Nat Commun, 2012. **3**: p. 1249.

279. Dawaliby, R., et al., *Allosteric regulation of G protein-coupled receptor activity by phospholipids.* Nat Chem Biol, 2016. **12**(1): p. 35-9.

280. Rasmussen, S.G., et al., *Crystal structure of the human beta2 adrenergic G-protein-coupled receptor.* Nature, 2007. **450**(7168): p. 383-7.

281. Jastrzebska, B., et al., *Phospholipids are needed for the proper formation, stability, and function of the photoactivated rhodopsin-transducin complex.* Biochemistry, 2009. **48**(23): p. 5159-70.

282. Poveda, J.A., et al., *Lipid modulation of ion channels through specific binding sites.* Biochim Biophys Acta, 2014. **1838**(6): p. 1560-7.

283. Jiang, Q.X. and T. Gonen, *The influence of lipids on voltage-gated ion channels.* Curr Opin Struct Biol, 2012. **22**(4): p. 529-36.

284. Weingarth, M., et al., *Structural determinants of specific lipid binding to potassium channels.* J Am Chem Soc, 2013. **135**(10): p. 3983-8.

285. Domicevica, L., H. Koldso, and P.C. Biggin, *Multiscale molecular dynamics simulations of lipid interactions with P-glycoprotein in a complex membrane.* J Mol Graph Model, 2018. **80**: p. 147-156.

286. Mi, W., et al., *Structural basis of MsbA-mediated lipopolysaccharide transport.* Nature, 2017. **549**(7671): p. 233-237.

287. Barrera, N.P., M. Zhou, and C.V. Robinson, *The role of lipids in defining membrane protein interactions: insights from mass spectrometry.* Trends Cell Biol, 2013. **23**(1): p. 1-8.

288. Farinha, C.M., E. Miller, and N. McCarty, *Protein and lipid interactions - Modulating CFTR trafficking and rescue.* J Cyst Fibros, 2018. **17**(2s): p. S9-s13.

289. Meng, X., et al., *Two Small Molecules Restore Stability to a Subpopulation of the Cystic Fibrosis Transmembrane Conductance Regulator with the Predominant Disease-causing Mutation.* J Biol Chem, 2017. **292**(9): p. 3706-3719.

290. Aleksandrov, L.A., et al., *Thermal stability of purified and reconstituted CFTR in a locked open channel conformation.* Protein Expr Purif, 2015. **116**: p. 159-66.

291. Li, C., M. Ramjeesingh, and C.E. Bear, *Purified cystic fibrosis transmembrane conductance regulator (CFTR) does not function as an ATP channel.* J Biol Chem, 1996. **271**(20): p. 11623-6.

292. Pollock, N., et al., *Purification of the cystic fibrosis transmembrane conductance regulator protein expressed in Saccharomyces cerevisiae.* J Vis Exp, 2014(87).

293. Liu, Y., et al., *Characterization of Membrane Protein-Lipid Interactions by Mass Spectrometry Ion Mobility Mass Spectrometry.* J Am Soc Mass Spectrom, 2017. **28**(4): p. 579-586.

294. Lingam, S., N. Thonghin, and R.C. Ford, *Investigation of the effects of the CFTR potentiator ivacaftor on human P-glycoprotein (ABCB1).* Sci Rep, 2017. **7**(1): p. 17481.

295. Benedetto, R., et al., *Epithelial Chloride Transport by CFTR Requires TMEM16A.* Sci Rep, 2017. **7**(1): p. 12397.

296. Xu, T.R., et al., *Intramolecular fluorescence resonance energy transfer (FRET) sensors of the orexin OX1 and OX2 receptors identify slow kinetics of agonist activation.* J Biol Chem, 2012. **287**(18): p. 14937-49.

297. Nagy, J.K., et al., *Use of amphipathic polymers to deliver a membrane protein to lipid bilayers.* FEBS Lett, 2001. **501**(2-3): p. 115-20.

298. Althoff, T., et al., *Arrangement of electron transport chain components in bovine mitochondrial supercomplex I1III2IV1.* Embo j, 2011. **30**(22): p. 4652-64.

299. Cvetkov, T.L., et al., *Molecular architecture and subunit organization of TRPA1 ion channel revealed by electron microscopy.* J Biol Chem, 2011. **286**(44): p. 38168-76.

300. Liao, M., et al., *Structure of the TRPV1 ion channel determined by electron cryo-microscopy.* Nature, 2013. **504**(7478): p. 107-12.

301. Cao, E., et al., *TRPV1 structures in distinct conformations reveal activation mechanisms.* Nature, 2013. **504**(7478): p. 113-8.

302. Flotenmeyer, M., et al., *The use of amphipathic polymers for cryo electron microscopy of NADH:ubiquinone oxidoreductase (complex I).* J Microsc, 2007. **227**(Pt 3): p. 229-35.

303. Arunmanee, W., J.R. Harris, and J.H. Lakey, *Outer membrane protein F stabilised with minimal amphipol forms linear arrays and LPS-dependent 2D crystals.* J Membr Biol, 2014. **247**(9-10): p. 949-56.

304. Merk, A., et al., *Breaking Cryo-EM Resolution Barriers to Facilitate Drug Discovery.* Cell, 2016. **165**(7): p. 1698-1707.

305. Renaud, J.P., et al., *Cryo-EM in drug discovery: achievements, limitations and prospects.* Nat Rev Drug Discov, 2018.

306. Van Eps, N., et al., *Characterizing rhodopsin signaling by EPR spectroscopy: from structure to dynamics.* Photochem Photobiol Sci, 2015. **14**(9): p. 1586-97.
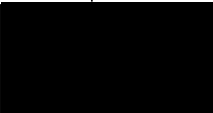
SPRINGER NATURE LICENSE
TERMS AND CONDITIONS

Nov 03, 2018

This Agreement between Stephanie Chin ("You") and Springer Nature ("Springer Nature") consists of your license details and the terms and conditions provided by Springer Nature and Copyright Clearance Center.

License Number	4461610392789
License date	Nov 03, 2018
Licensed Content Publisher	Springer Nature
Licensed Content Publication	Cellular and Molecular Life Sciences
Licensed Content Title	Current insights into the role of PKA phosphorylation in CFTR channel activity and the pharmacological rescue of cystic fibrosis disease-causing mutants
Licensed Content Author	Stephanie Chin, Maurita Hung, Christine E. Bear
Licensed Content Date	Jan 1, 2016
Licensed Content Volume	74
Licensed Content Issue	1
Type of Use	Thesis/Dissertation
Requestor type	academic/university or research institute
Format	print and electronic
Portion	full article/chapter
Will you be translating?	no
Circulation/distribution	<501
Author of this Springer Nature content	yes
Title	Regulation of CFTR function and stability by phosphorylation and its membrane environment
Institution name	University of Toronto
Expected presentation date	Mar 2020
Requestor Location	Stephanie Chin
	Attn: Miss. Stephanie Chin
Billing Type	Invoice
Billing Address	Miss. Stephanie Chin
	Attn: Miss. Stephanie Chin
Total	0.00 USD

RE: Permission to Use Copyrighted Material in a Doctoral Thesis (JBC Feedback Form)

Maria Pasho ▮▮▮▮▮▮▮▮▮▮▮▮▮▮▮▮

Thu 2018-04-12 1:33 PM

To:Stephanie Chin ▮▮▮▮▮▮▮▮▮▮▮▮▮▮▮▮

Please see http://www.jbc.org/site/misc/edpolicy.xhtml#copyright

Authors do not need to request permission to reuse their own work.

Best,
JBC

-----Original Message-----
From: Stephanie Chin ▮▮▮▮▮▮▮▮▮▮▮▮▮▮▮▮▮▮▮
Sent: Wednesday, April 11, 2018 6:39 PM
To: jbc-feedback@highwire.stanford.edu
▮▮▮▮▮▮▮▮▮▮▮▮▮▮▮▮▮
Subject: Permission to Use Copyrighted Material in a Doctoral Thesis (JBC Feedback Form)

Comments sent via JBC Feedback Page

  TO: jbc-feedback@highwire.stanford.edu
  NAME: Stephanie Chin USER NAME: (not signed in)
  EMAIL: ▮▮▮▮▮▮▮▮▮▮▮▮▮▮▮▮

▮▮▮▮▮▮▮▮▮▮▮▮▮▮▮▮▮▮▮▮▮▮▮▮▮▮▮▮▮▮▮▮

COMMENTS:
Hi there,

I am a University of Toronto graduate student completing my Doctoral???s thesis entitled "Insights on the structural and functional changes of CFTR induced by interactions at the cell surface".

I would like to inquire whether I have copyright permission to reuse my first author paper published in your journal. The paper is "Attenuation of Phosphorylation-dependent Activation of Cystic Fibrosis Transmembrane Conductance Regulator (CFTR) by Disease-causing Mutations at the Transmission Interface. Chin et al. 2017 Feb 3;292(5):1988-1999.

▮▮▮▮▮▮▮▮▮▮▮▮▮▮▮▮▮▮▮▮▮▮▮▮▮

October 25, 2018

Stephanie Chin

███████████████████████████
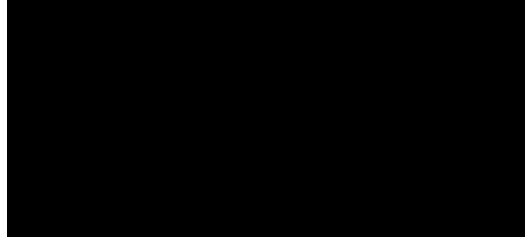
Dear Stephanie Chin:

This is to grant you permission to include the following article in your thesis entitled "Regulation of CFTR function and stability by phosphorylation and its membrane environment" for the University of Toronto:

S Chin, M Hung, A Won, Y-S Wu, S Ahmadi, D Yang, S Elmallah, K Toutah, CM Hamilton, RN Young, RD Viirre, CM Yip, and CE Bear (2018) Lipophilicity of the Cystic Fibrosis Drug, Ivacaftor (VX-770), and Its Destabilizing Effect on the Major CF-causing Mutation: F508del, *Mol Pharmacol*, 94: 917-925; DOI: https://doi.org/10.1124/mol.118.112177

On the first page of each copy of this article, please add the following:

Reprinted with permission of the American Society for Pharmacology and Experimental Therapeutics. All rights reserved.

In addition, the original copyright line published with the paper must be shown on the copies included with your dissertation.

Sincerely yours,

███████████████████████████
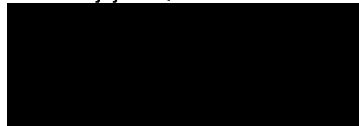
Richard Dodenhoff
Journals Director